AD NUMBER
AD913499
LIMITATION CHANGES

TO:

Approved for public release; distribution is unlimited.

FROM:

Distribution authorized to U.S. Gov't. agencies only; Test and Evaluation; SEP 1973. Other requests shall be referred to Air Force Armament Laboratory, Attn: DLTI, Eglin AFB, FL 32542.

AUTHORITY

AFATL ltr, 2 Oct 1875

O42

NOV 6 1931

REACTION JET CONTROL EFFECTS ON
THE AIR FORCE ADVANCED TACTICAL ROCKET
AT MACH NUMBERS 2, 3, 4, AND 5

W. T. Strike, Jr.

ARO, Inc.

September 1973

VON KÁRMÁN GAS DYNAMICS FACILITY
ARNOLD ENGINEERING DEVELOPMENT CENTER
AIR FORCE SYSTEMS COMMAND
ARNOLD AIR FORCE STATION, TENNESSEE

NOTICES

REACTION JET CONTROL EFFECTS ON THE AIR FORCE ADVANCED TACTICAL ROCKET AT MACH NUMBERS 2, 3, 4, AND 5

W. T. Strike, Jr.
ARO, Inc.

This document has been approved for public release
its distribution is unlimited. *Per TAB 76-4*
13 Feb., 1976

FOREWORD

The work presented herein was conducted by the Arnold Engineering Development Center (AEDC) under sponsorship of the Armament Development and Test Center, Air Force Armament Laboratory (AFATL), Air Force Systems Command (AFSC), under Program Element 63601F, System 670D.

The test results presented were obtained by ARO, Inc. (a subsidiary of Sverdrup & Parcel and Associates, Inc.), contract operator of AEDC, AFSC, Arnold Air Force Station, Tennessee. The test program was conducted on April 16 and 17, 1973, under ARO Project No. VA294, and the final data package was completed on May 11, 1973. The manuscript was submitted for publication on July 6, 1973.

The author wishes to express his appreciation to Jim Uselton, ARO, Inc., for providing the trajectory analysis results presented in Section IV.

This technical report has been reviewed and is approved.

JIMMY W. MULLINS
Lt Colonel, USAF
Chief Air Force Test Director, VKF
Directorate of Test

FRANK J. PASSARELLO
Colonel, USAF
Director of Test

ABSTRACT

This program is part of a study to provide the Advanced Tactical Rocket (ATR) under development by the Air Force Armament Laboratory with a jet reaction control system (RCS). This control system, consisting of four sets of six supersonic nozzle jets, will be used to make final corrections to the ATR trajectory. The wind tunnel study was conducted at Mach numbers 2, 3, 4, and 5 using a 4/7-scale model of the ATR with a set of six sonic nozzles to simulate, with air, the jet wake disturbance produced by the full-scale RCS. The tests were conducted with the RCS placed at two different axial positions along the model axis and at roll angles of 0 and -45 deg with respect to the vertical tail fins. The data consisted of 5-component force (excluding axial force) and moment data. The model angle of attack was varied from -12 to 12 deg, and model roll angle was varied from 0 to -90 deg. The disturbance generated by the RCS simulation produced significant rolling moments when the model was in a combined pitch and roll attitude. Also, the slope of the aerodynamic coefficients with angle of attack varied depending on the RCS jet conditions and model roll position.

Distribution limited to U.S. Government agencies only;
this report contains information on test and evaluation of
military hardware: September 1973; other requests for
this document must be referred to Air Force Armament
Laboratory (DLTI), Air Force Systems Command, Eglin
AFB, FL 32542.

CONTENTS

ILLUSTRATIONS

APPENDIXES

NOMENCLATURE

A	Reference area, $\pi D^2/4$, in.^{2}
A_j	Nozzle exit area, in.^{2}
A^*	Nozzle throat area, in.^{2}
C_ℓ	Rolling-moment coefficient, rolling moment/$(q_\infty AD)$
$C_{\ell,a}$	$\partial C_\ell/\partial a$ at $a = 0$, per deg
C_m	Measured pitching-moment coefficient (referenced to 0.421ℓ from the model nose), pitching moment/$(q_\infty AD)$
$C_{m,j}$	Pitching-moment coefficient produced by RCS reaction force ($C_{m,j} = C_{N,j} \times x_j/D$)
$C_{m,a}$	$\partial C_m/\partial a$ at $a = 0$, per deg
C_N	Measured normal-force coefficient, normal force/$(q_\infty A)$
$C_{N,j}$	Normal force produced by the RCS reaction force, total jet thrust/$(q_\infty A)$
$C_{N,a}$	$\partial C_N/\partial a$ at $a = 0$, per deg
C_n	Yawing-moment coefficient, yawing moment/$(q_\infty AD)$
$C_{n,\beta}$	$\partial C_n/\partial \beta$ at $\beta = 0$, per deg
C_Y	Side-force coefficient, side force/$(q_\infty A)$
$C_{Y,\beta}$	$\partial C_Y/\partial \beta$ at $\beta = 0$, per deg
D	Model diameter, 2.00 in.
d	Nozzle throat diameter, 0.188 in.
F_j	Resultant reaction force produced by the RCS, lbf
ℓ	Model length, 37.73 in.
M	Mach number
$\dot{m}$	Mass flow rate, lbm/sec

p	Static pressure, psia
p_o	Tunnel stilling chamber pressure, psia
$p_{o,J}$	RCS chamber pressure, psia
q	Dynamic pressure. psia
Re_ℓ	Reynolds number based on the model length, $(\rho_\infty U_\infty \ell)/\mu_\infty$
T_o	Tunnel stilling chamber temperature, °R
u	Velocity. ft/sec
x_J	Location of the geometric center of the array of nozzles in the RCS from the model moment reference point. in.
α	Angle of attack in rolling body axes, deg (see Fig. 1b)
β	Angle of sideslip in rolling body axes, deg (see Fig. 1b)
γ	Ratio of specific heats
$\Delta\phi_j$	Angular position of tail fins to pitch plane containing the array of jet nozzles of the RCS
δ	Initial turning angle of the jet plume boundary, $\delta = \nu_b - \nu_j + \theta_N$, deg
θ_N	Nozzle divergence angle. deg
ν	Prandtl-Meyer expansion angle, deg
ν_∞	Free-stream kinematic viscosity, ft²/sec
ϕ	Model roll angle, deg

SUBSCRIPTS

b	Conditions at jet plume boundary
j	Nozzle exit conditions
∞	Free-stream conditions

SECTION I
INTRODUCTION

The Advanced Tactical Rocket (ATR) is under development by the Air Force Armament Laboratory (AFATL) and, as originally conceived, is an unguided, fin-stabilized, air-launched missile. Currently, in the Phase II development program of this missile, the feasibility of making corrections to the missile's flight path using a reaction jet control system (RCS) is being investigated. Although computation of the jet reaction control forces and moments produced by the RCS is fairly straightforward, the expanding jet plume could have significant secondary effects, particularly on the stabilizing effectiveness of the vehicle's tail surfaces. Therefore, the purpose of this study was to define the effects of the RCS jet plume on the aerodynamic characteristics of an ATR missile configuration (N_2T_5 without roll tabs or N_2T_8 without fin cant; see Ref. 1).

The test program was planned and executed by the Aerodynamic Projects Branch, von Kármán Gas Dynamics Facility (VKF), of the Arnold Engineering Development Center (AEDC), for AFATL. This program included model design and fabrication (modification of the existing ATR model from Ref. 1) and the design and fabrication of a special balance to permit passage of the air supply for the RCS simulation. The tests were conducted in the Supersonic Wind Tunnel (A) at nominal Mach numbers of 2, 3, 4, and 5. The model RCS chamber pressure and the free-stream tunnel pressures were selected so that the model jets simulated the plumes of the RCS jets on the ATR missile at various pressure altitudes, including a sea-level condition. The tests were conducted at angles of attack from -12 to 12 deg and model roll angles of 0, 30, 45, 60, and 90 deg.

SECTION II
APPARATUS

2.1 WIND TUNNEL

Tunnel A is a continuous, closed-circuit, variable density wind tunnel with an automatically positioned, flexible-plate-type nozzle, a 40- by 40-in. test section, and a model injection system. The tunnel operates at Mach numbers from 1.5 to 6.0 at maximum stagnation pressures from 29 to 200 psia, respectively, and at stagnation temperatures up to 750°R ($M_\infty = 6$). The minimum operating pressures vary from about one-tenth to one-twentieth of the maximum pressure at each Mach number.

2.2 MODEL

The model, shown in Fig. 1, was an existing 4/7-scale version of the Phase II ATR missile modified by AEDC-VKF for this test. The model geometry consisted of a 3.0-caliber tangent ogive nose with a cylindrical center section about 13.5 calibers long and a cruciform tail section. The nose and tail section were fabricated of stainless steel. The forward section of the cylindrical centerbody, fabricated from stainless steel, contained a plenum chamber with a row of six equally spaced 0.188-in.-diam sonic orifices for simulation of the RCS

18.50R

1.905, Six Equally Spaced Sonic Orifices
with 0.188-in. Exit Diam

11 deg

4.00

17.00

0.196

1.21

6.00

15.87

¢ of Sonic Orifice Pattern

2.00 Diam

7.15

Moment Reference
at 15.89 in.

0.196   1.905

37.72

All Dimensions in Inches
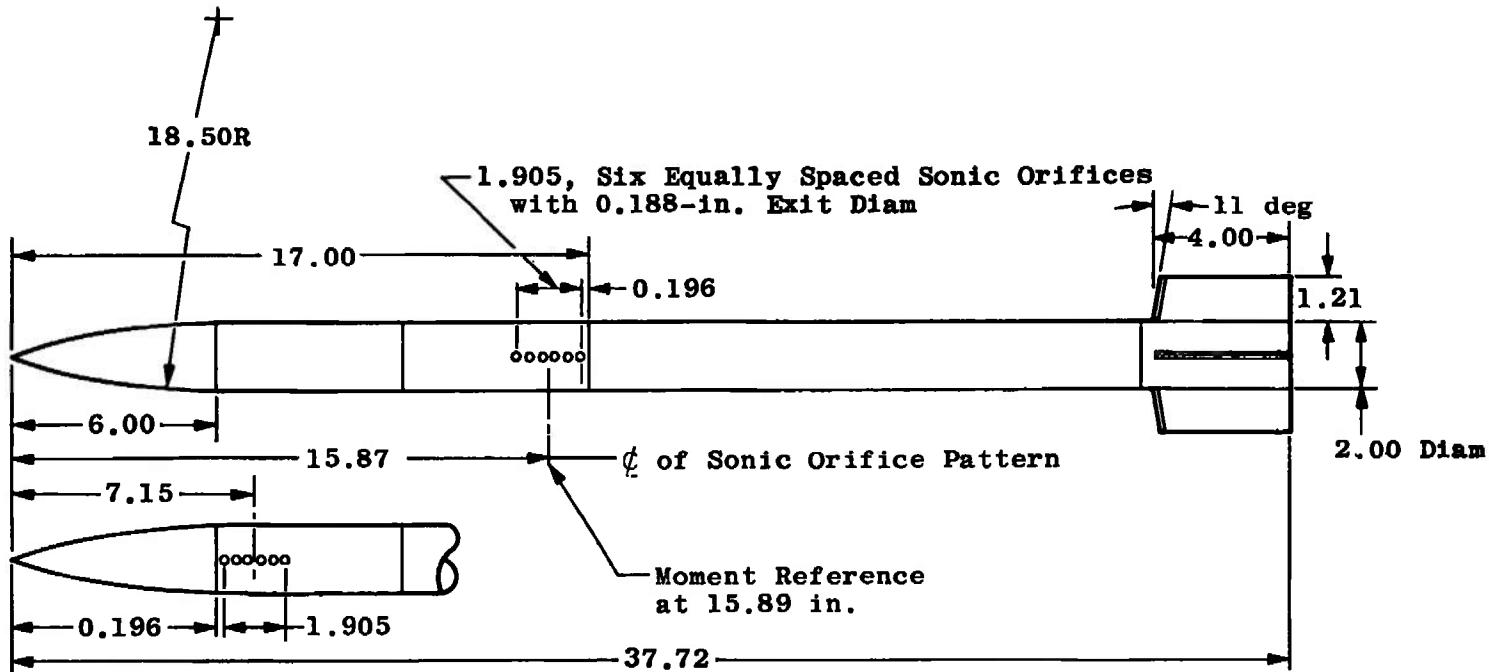
a. ATR Model
Fig. 1 ATR Phase II Model and Axis System
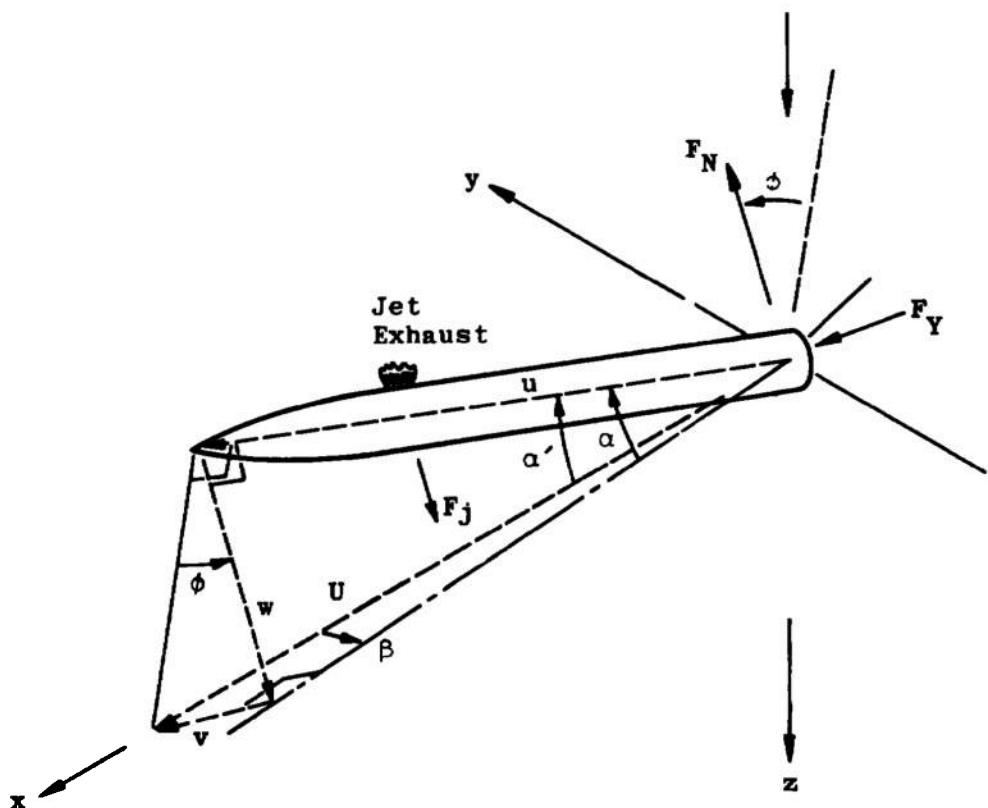
Figure Nomenclature

F_N	Normal force
F_Y	Side force
U	Resultant or tunnel velocity vector
u, v, w	Velocity components in the rolling body axes
x, y, z	Tunnel axis system
α	Angle of attack in the rolling body axes
α′	Total or tunnel sector angle
β	Angle of sideslip in the rolling body axes
φ	Model roll angle

b. Rolling Body Axes
Fig. 1 Concluded

jets (see Section 3.1.2). This forward section could be removed and rotated end-to-end so that the center of the sonic orifice pattern was located either 7.2 in. or 15.9 in. from the model nose. The aft section of the cylindrical body was fabricated from brass and housed the five-component (no axial-force element) gas balance. The tail section was designed so that it could be rotated 45 deg with respect to the model generatrix containing the row of sonic orifices. Some test results were obtained with this tail section removed, which decreased the model length from 18.9 calibers to 16.7 calibers as shown in Fig. 2. Additional details concerning the model geometry can be found in Ref. 1.
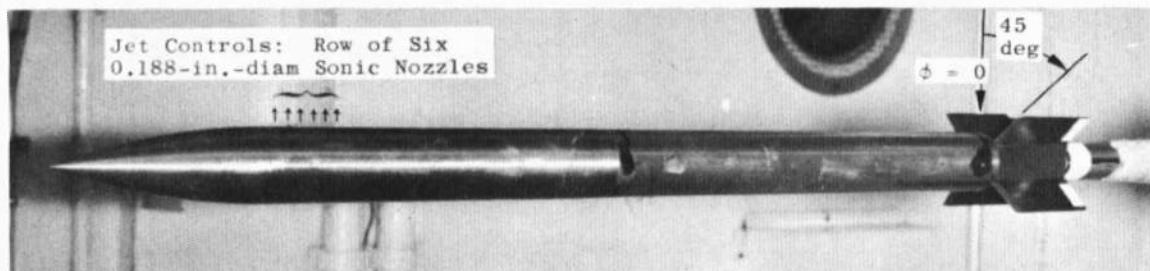
a. Tail-on Configuration, rotated 45 deg from the Jet Controls
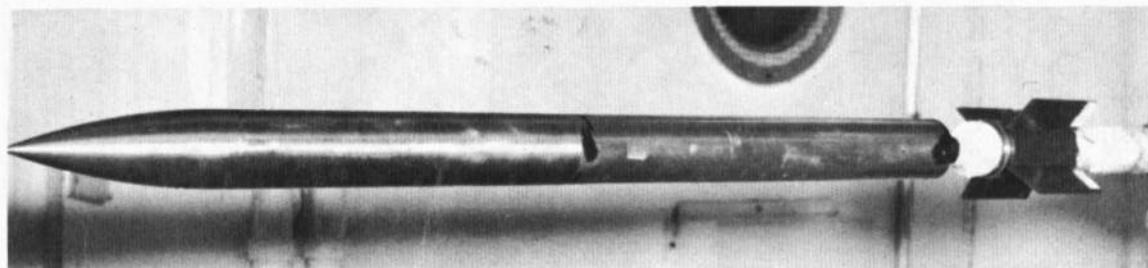
b. Tail-off Configuration
Fig. 2 Model Installation

The auxiliary air supply for the sonic nozzles passed through the model support sting and through a 0.65-in.-diam cylindrical cavity in the balance into a plenum chamber in the forward section of the model. Just before the flow entered the cavity in the balance, the total pressure of the air supply was monitored by means of a pressure tap located at the forward end of the sting cavity.

A fouling strip was attached to the sting near the model base to provide an indication when model deflections caused the model base to bottom out on the sting.

2.3 INSTRUMENTATION AND PRECISION OF DATA

Tunnel A stilling chamber pressure is measured with 15-, 60-, and 150-psid transducers having an estimated uncertainty of ±0.5 percent of the calibrated ranges of 10, 50, and 150 psid. Tunnel stilling chamber temperature is recorded with total temperature probes containing copper-constantan thermocouples with an estimated uncertainty of ±1°F. By taking into account the repeatability and uniformity of the test section flow (Mach number distribution) defined by the wind tunnel calibrations, the estimated uncertainty in the free-stream properties, using a Taylor series error propagation, is summarized as follows:

Nominal Mach No.	Re x 10^{-6}	Uncertainty, percent (±)				
		M_∞	p_o	p_∞	q_∞	Re_ℓ
2.0	5.1	0.5	1.2	1.9	1.3	1.2
	10.4	0.5	0.5	1.6	0.8	0.7
3.0	12.5	0.4	1.1	2.1	1.5	1.3
4.0	17.1	0.5	1.2	2.9	2.0	1.6
5.0	19.4	0.3	0.5	1.8	1.2	0.9

The pressure in the model cavity was recorded with a 2000-psid transducer calibrated for a pressure range of 500 psia. The mass flow rate through the model was measured using a standard ASME long radius venturi metering nozzle, installed according to ASME specifications, in the nozzle supply line located external to the tunnel test section. The supply line pressure was recorded with a vacuum-referenced 2000-psid transducer calibrated for 500 psia. The differential pressure between the venturi throat tap and the supply line pressure was recorded with a 200-psid transducer calibrated half-scale for 100 psia. Based on periodic comparisons with a secondary standard, the uncertainty of these transducers is estimated to be ±0.2 percent of the calibrated range of each transducer. The jet gas temperature was recorded with a copper-constantan thermocouple located near the venturi mass-flow meter. This thermocouple has an estimated uncertainty of ±1°F. A summary of the estimated uncertainty of the mass flow and jet pressure results, assuming a Taylor series error propagation, is given below.

m/A^*, lbm/sec-ft^2	Uncertainty, percent (±)		
	$\dot{m}$	$p_{o,J}$	p_J/p_∞
350	0.6	0.50	2.9
1310	0.3	0.13	2.9

5

A five-component, moment-type, strain-gage balance (AEDC-VKF Balance No. 4.00-Y-35-062) was designed, fabricated, and calibrated by AEDC-VKF. This balance was designed with a cylindrical cavity so that gas could be supplied through it to the nozzle cavity in the model without affecting the balance measurements. Before testing, single and combined static loads were applied to the balance to simulate the range of anticipated model loads (including jet reaction force and aerodynamic loading). Characteristics of the five-component balance are given below: the uncertainties shown represent the bands which bracket 95 percent of the measurement residuals, which represent the differences between the applied loads and the loads calculated from the balance calibration equations used in the final data reduction.

Balance Component	Design Load	Range of Static Loads	Measurement Uncertainty
Normal force, lbf	300	± 100	±0.19
Pitching moment*, in.-lbf	1485	± 1100	±0.51
Side force, lbf	200	± 40	±0.13
Yawing moment*, in.-lbf	870	± 160	±0.30
Rolling moment, in.-lbf	100	± 8	±0.17

*These moments are referenced to the forward-moment bridges. The transfer distance to the model reference point, which is known to within ±0.005 in., was 3.44 in.

The resulting propagated uncertainties in the force and moment coefficients, which include the uncertainties in the free-stream properties, are listed below for a typical set of coefficients. This list contains the maximum uncertainties, in percent (±), which occurred at the maximum values of the coefficients.

M_∞ (nominal)	Percent (±)				
	C_N	C_m	C_Y	C_n	C_ℓ
2	1.5	1.3	1.4	1.3	4.7
3	1.5	1.5	1.5	1.5	3.0
4	2.1	2.1	2.0	2.0	7.3
5	1.3	1.3	1.3	1.3	13.1

The model angle of attack, based on repeat calibrations of the sector pitching mechanism, was known to within ±0.05 deg. The model attitude correction, based on a combined sting and balance deflection, was incorporated in the evaluation of the final model attitude. This correction increased the uncertainty in the model attitude (i.e., in α and β) to about ±0.1 deg.

SECTION III
PROCEDURE

3.1 TEST PROCEDURE

3.1.1 General

The five basic model configurations investigated are listed below. (A complete test summary is given in Section 3.3.)

Configuration Number	x_j/D	$\Delta\phi$, deg	Tail Section
1	4.37	0	On
2	4.37	0	Off
3	0.00	0	On
4	4.37	45	On
5	0.00	45	On

At each test condition the sector was moved continuously at a nominal rate of one degree per second from 12 to -12 deg angle of attack while the force and moment measurements were recorded continuously. The five gage outputs from the strain-gage balance were scanned about 107 times per second. No axial-force measurements were made, but the change in base drag was recorded when the tail section was attached to the model. The aerodynamic coefficients were computed and tabulated for the angle-of-attack range in exactly 1-deg increments. Therefore, at any given angle of attack a direct comparison could be made between the jet-off and jet-on effects on the missile aerodynamic static stability coefficients.

3.1.2 RCS Simulation

High-pressure air was used to simulate the jet plume produced by the RCS on the full-scale ATR missile. The proposed RCS will consist of a row of six solid-propellant motors with supersonic nozzles which will be fired simultaneously for a time interval of at least 0.010 seconds. Some features of the plume produced by one RCS nozzle for a sea-level condition are listed below for a rocket exhaust gas and for air.

$$A_j/A^* = 4.0 \qquad\qquad p_{o,j} \approx 7500 \text{ psia}$$
$$d = 0.650 \text{ in.} \qquad\qquad p = 14.7 \text{ psia}$$
$$F_j \approx 5800 \text{ lbf (Total for 6 nozzles)}$$

γ_j (Estimated)	M_j	p_j, psia	p_j/p_∞ (minimum)	$\gamma_j p_j M_j^2/p_\infty$	M_b/γ_j	δ, deg ($\theta_N = 15$ deg)
1.25	2.70	294	15	183.0	3.56	52
1.40	2.95	220	20	182.5	3.55	43

As noted in Ref. 2, the effective spoiler height of a jet plume is proportional to the square root of the term $\gamma_j p_j M_j^2/p_\infty$, and as shown in Ref. 3, the initial size and shape of the jet plume are functions of the nozzle exit diameter, the ratio M_b/γ_j, and the initial turning angle of the plume boundary at the nozzle exit, δ. In the present test, sonic nozzles were used and jet chamber pressure was varied as shown below to simulate the jet plume conditions produced by the full-scale RCS.

$A_j/A^* = 1.0$	$M_j = 1.0$	$p_{o,j}$ — Varied	
$\underline{d} = 0.188$ in.	$\gamma_j = 1.4$	F_j — Varied	

M_∞	p_j/p_∞	$\gamma_j p_j M_j^2/p_\infty$	M_b/γ_j	δ, deg ($\theta_N = 0$)
2.0	90, 128, 190	126, 179, 266	2.91, 3.09. 3.34	67, 70, 74
3.0	123, 245	172, 343	3.09, 3.48	70, 76
4.0	132, 266	185, 372	3.13, 3.55	71, 77
5.0	265	371	3.55	77

A comparison of the two preceding summaries of jet plume parameters indicates that, in most respects, the full-scale and wind tunnel-generated plumes for the RCS on the ATR missile are quite similar. The primary difference between the plumes is in the initial turning angle, which for the simulated plumes is from 14 to 34 deg greater than that estimated for the full-scale RCS plumes. Therefore, the simulated plumes in the immediate vicinity of the missile will tend to be a little larger than the full-scale RCS plumes. However, considering the overall magnitude of the disturbance produced by these plumes, this difference in the initial geometry should have no significant effect on the simulation.

3.2 DATA REDUCTION

For most of the data presented in this report (Appendix I), the measured aerodynamic forces and moments have been modified by subtracting the jet reaction force effect from the normal-force and pitching-moment coefficients. The change in normal-force and pitching-moment coefficients attributed to the jet reaction force is defined as follows:

$$C_{N,j} = [p_j(1 + \gamma_j M_j^2) - p_\infty](A_j/A)/q_\infty \qquad (1)$$

In the case of a sonic nozzle using air at room temperature as the jet gas, this expression can be simplified to read

$$C_{N,j} = [1.268 - (p_\infty/p_{o,j})](p_{o,j}/q_\infty)(A_j^*/A) \qquad (2)$$

and

$$C_{m,j} = C_{N,j} \, x_j/D \qquad (3)$$

The jet controls produced a thrust force vector which rolled with the missile orientation and remained perpendicular to the missile axis, which, for $\phi = 0$, produced

a negative change in the missile's normal-force and pitching-moment coefficients. The test data indicate that the thrust vector passed through the model axis and did not produce any measurable amount of rolling moment. The changes in rolling moment, side force, and yawing moment obtained during the test program can be attributed to the orientation of the missile in the airstream (i.e., to the aerodynamic loading of the missile) and to the flow field produced by the interference of the jet plume with the external stream.

The results in this report are referenced to angles of attack and sideslip which are in the planes defined by a coordinate system which rotates with the missile orientation (a rolling body axis system).

3.3 TEST CONDITIONS

Most of the test was conducted at a fairly constant dynamic pressure of 4.6 to 4.9 psia with the free-stream Mach number varying from 2 to 5. One additional free-stream condition was run at Mach number 2 with the dynamic pressure reduced to 2.4 psia. A complete summary of the test program is given below.

Mach No.	p_o, psia	Re_l x 10^{-6}	$p_{o,j}$, psia	x_j/D 4.37	x_j/D 0.0	$\Delta\phi_1$, deg 0	$\Delta\phi_1$, deg 45	Tail Section On	Tail Section Off*	Model Roll Position, ϕ, deg 0	45	90
1.99	6.5	5.1	0	x		x		x	x	x	x	x [f]
1.99	6.5	5.1	0		x		x	x		x	x	x
1.99	6.5	5.1	150	x	x		x	x		x	x	x
1.99	6.5	5.1	150		x	x		x		x	x	x
1.99	6.5	5.1	210	x		x		x	x	x	x	x [†]
1.99	6.5	5.1	210	x	x		x	x		x	x	x
1.99	6.5	5.1	315	x	x	x	x	x	x	x	x	x
2.00	13.5	10.4	0	x	x	x		x		x	x	x
2.00	13.5	10.4	315	x	x	x	x	x	x	x	x	x
3.01	27.0	12.5	0	x	x	x	x	x	x	x	x	x
3.01	27.0	12.5	175	x	x	x		x	x	x	x	x
3.01	27.0	12.5	175		x		x	x		x	x	x
3.01	27.0	12.5	175	x			x	x		x	x	x
3.01	27.0	12.5	315		x	x	x	x		x	x	x
3.01	27.0	12.5	315	x			x	x		x	x	
3.01	27.0	12.5	350	x	x	x		x	x	x	x	x
3.01	27.0	12.5	350		x		x	x		x	x	x
4.03	64.0	17.1	0	x		x		x	x	x	x	x
4.03	64.0	17.1	105	x		x		x	x	x	x	x
4.03	64.0	17.1	210	x		x		x	x	x	x	x
5.04	144	19.4	0	x		x		x	x	x	x	x
5.04	144	19.4	135	x		x		x	x	x	x	x

*The tail-off configuration was always tested with the jet in the forward position (x_j/D = 4.37).

[†]Tests also conducted at ϕ = 30 and 60 deg.

9

SECTION IV
RESULTS

4.1 EXPERIMENTAL DATA

In general, the forces and moments imposed on an aerodynamic shape with lateral jet controls can be viewed as the sum of three types of loading, or forces. First, in the absence of the RCS jet, there is simply the aerodynamic loading on the vehicle, which varies with the vehicle attitude and free-stream conditions. Second, there is the jet interaction force (loading), which is the change in the missile loading resulting from the flow-field interference between the RCS jet plume and the external stream. The third component of force is simply the RCS jet reaction force.

The basic aerodynamic coefficients are presented in graphical form in Appendix I as a function of model attitude, with the normal-force and pitching-moment coefficients modified by subtracting the increments in these coefficients attributed to the RCS jet reaction force. The jet thrust does not directly affect the side force or the yawing and rolling moments of the missile, but the surface loading generated by the jet interaction influences all the experimentally defined force and moment coefficients.

The variations in the measured normal-force and pitching-moment coefficients at a = 0 with changes in the RCS conditions (that is, in the jet reaction thrust coefficient, $C_{N,j}$) are summarized in Fig. 3. These results show that the normal force, C_N, varied linearly with the calculated jet thrust coefficient, $C_{N,j}$, for both axial positions of the RCS and for both roll positions (RCS in line with vertical fin, $\Delta\phi_j = 0$, and top fins at 45 deg from the RCS, $\Delta\phi_j = 45$ deg). Furthermore, the ratio $C_{N,j}/C_N < 1.0$ (exact value varied from about 0.75 to 0.85 for all cases), which indicates that the net jet interaction loading along the model opposed the jet reaction force. Figures 3a and b also show that the measured pitching moment varied linearly with $C_{N,j}$ for the forward RCS location, but for the mid-body location (Figs. 3c and d), which was essentially centered on the moment reference point, small moments were measured which varied nonlinearly with $C_{N,j}$.

As noted previously, the jet interaction loading opposed the force produced by the jet thrust. This is represented in Fig. I-1 (Appendix I) by the fact that, with the RCS control on, the normal-force coefficient minus the jet thrust coefficient (i.e., $C_N - C_{N,j}$) exceeded the aerodynamic normal-force coefficient obtained with the RCS off. This reduction in the effectiveness of the jet control reaction force existed for all the test conditions and for all the model configurations tested in this program, including the tail-off missile configuration. At the higher free-stream Mach numbers at the higher angles of attack, the opposing jet interaction loading was significantly smaller so that the change in normal force produced by the RCS was nearly equal to the jet thrust [i.e., $C_N - C_{N,j}$ approached C_N ($p_{o,j} = 0$) for $a > 0$] as shown in Figs. I-1k and I-1n of Appendix I.
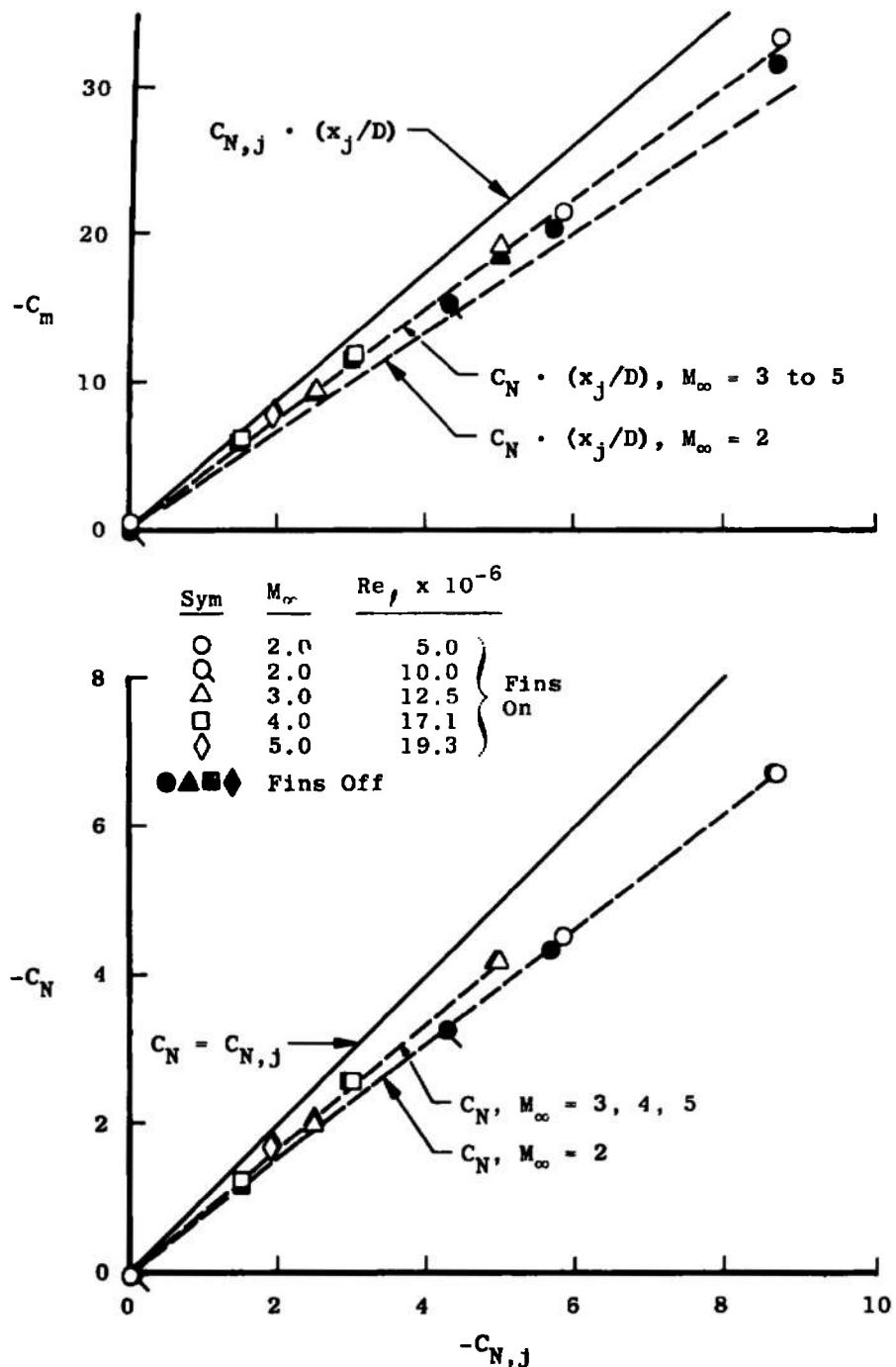
a. $x_j/D = 4.37$, $\Delta\phi_j = 0$

Fig. 3 Variation in the Normal-Force and Pitching-Moment Coefficients as Functions of $C_{N,J}$, $\phi = 0$

11
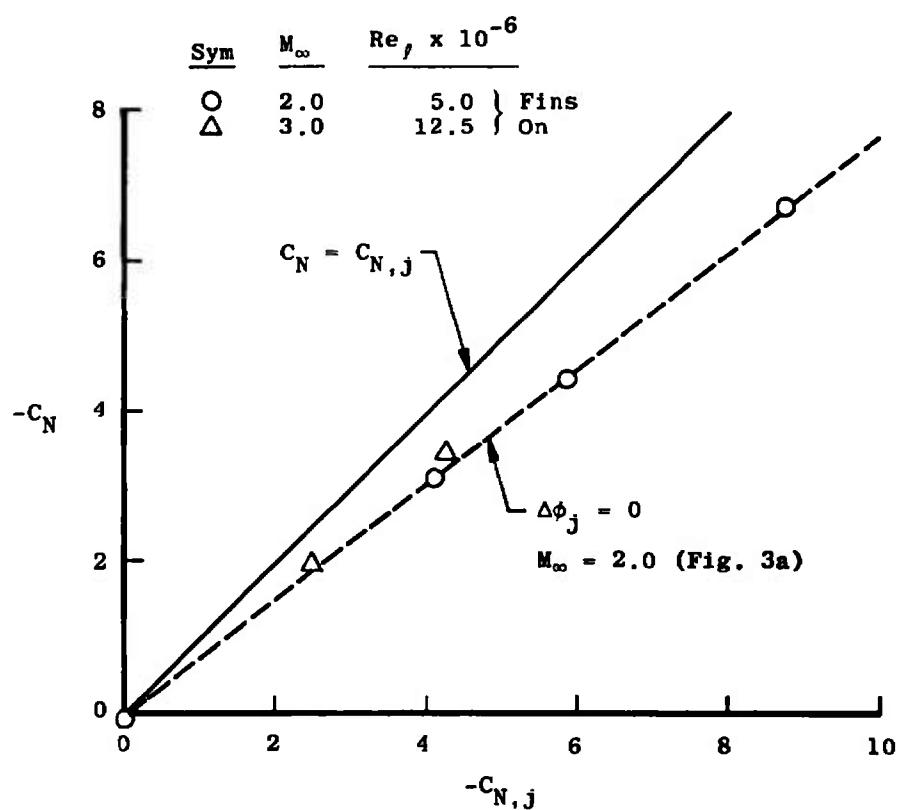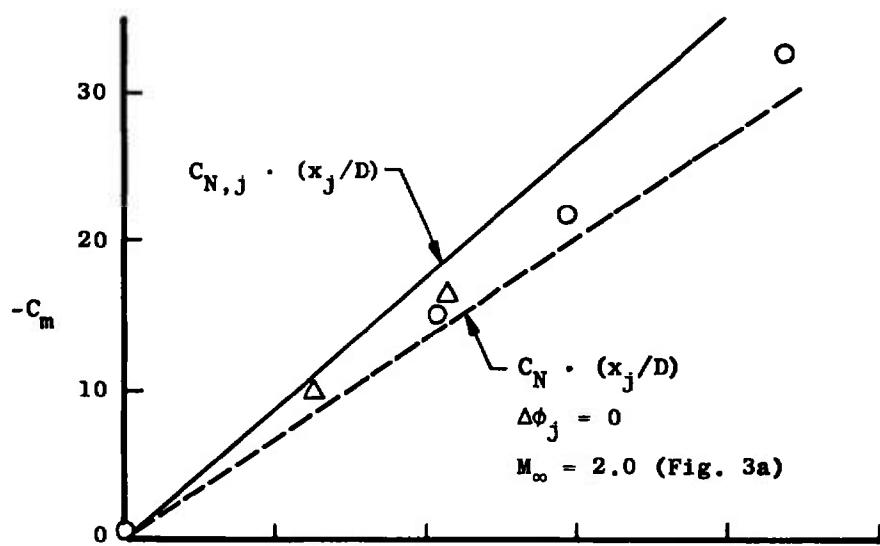
b. $x_j/D = 4.37$, $\Delta\phi_j = 45$ deg
Fig. 3 Continued
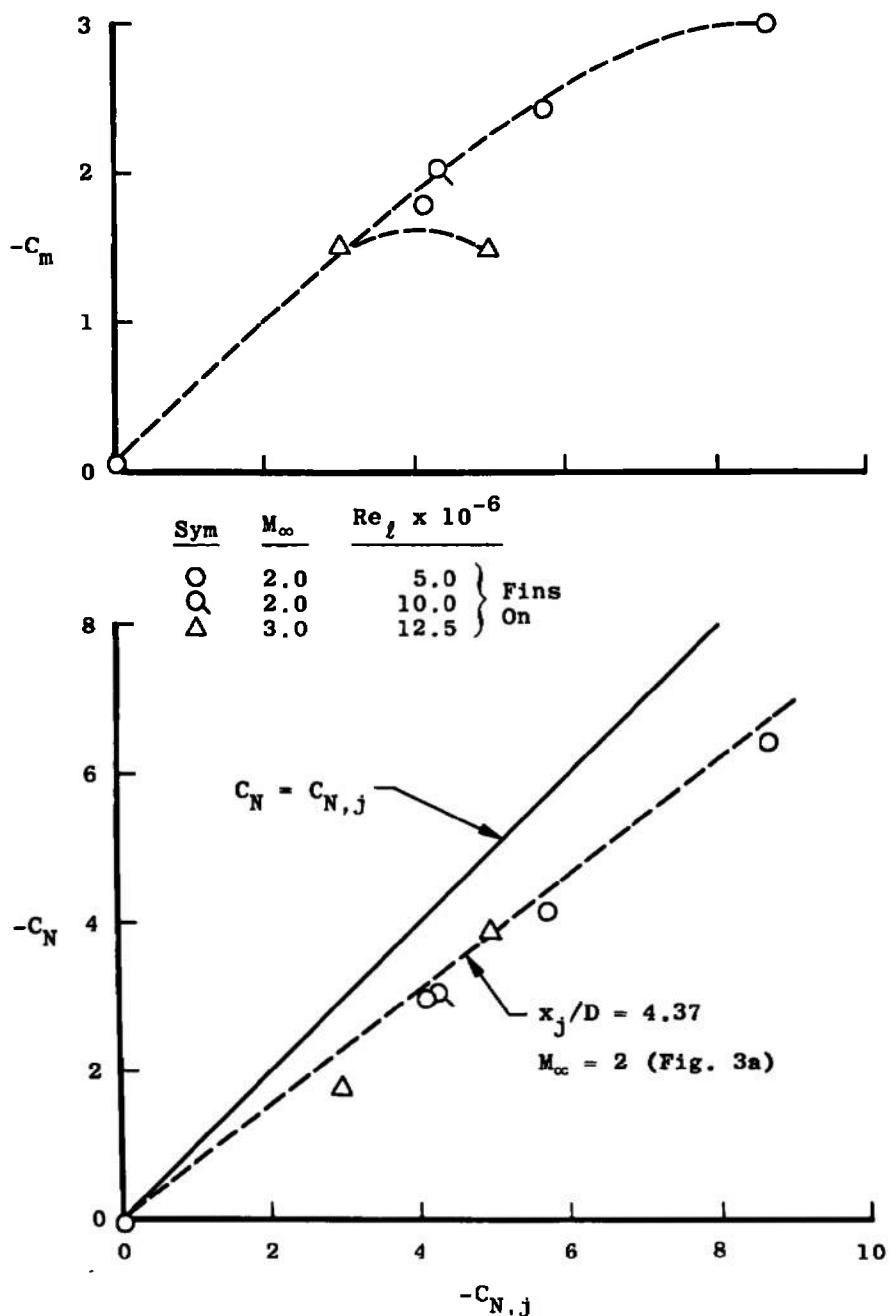
c. $x_j/D \approx 0.0$, $\Delta\phi_j = 0$
Fig. 3 Continued

13
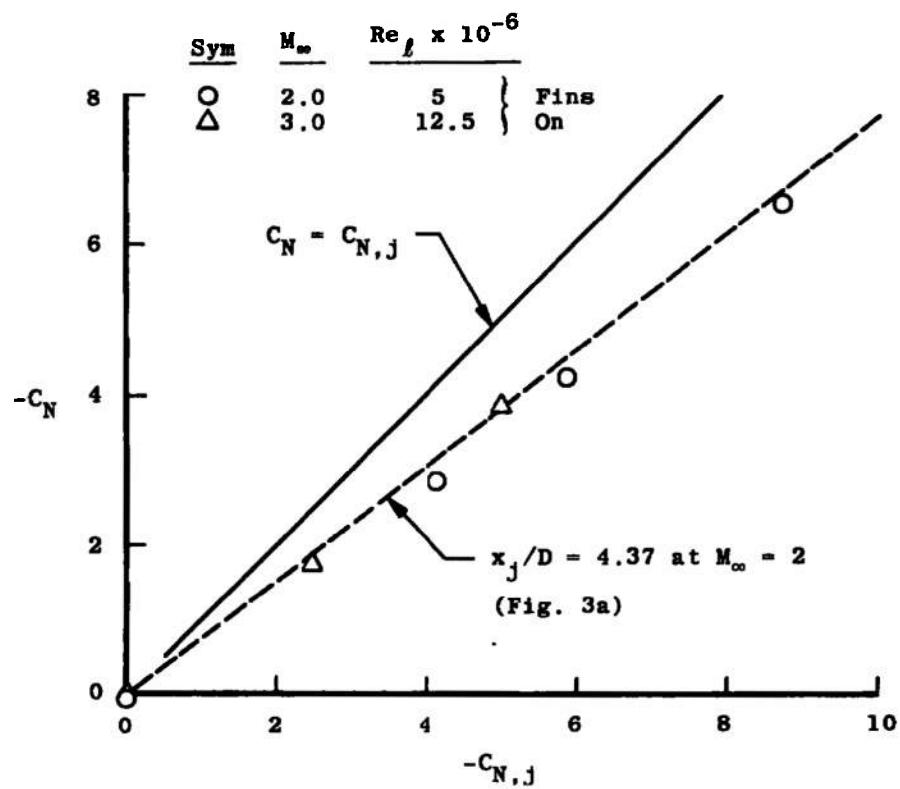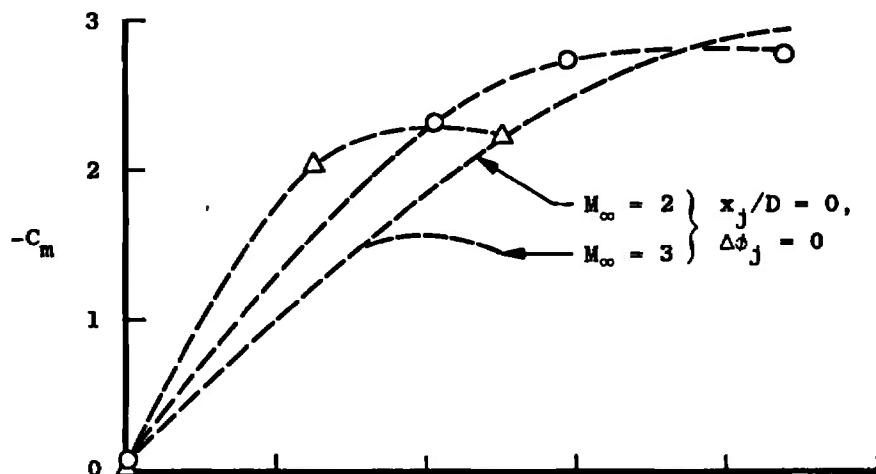
d. $x_j/D \approx 0.0.$, $\Delta\phi_j = 45$ deg
Fig. 3 Concluded

There were also test conditions where the jet interaction loading produced a moment which complemented (augmented) the moment attributed to the jet thrust. For example, in Fig. I-1a, for angles of attack less than -4 deg, the pitching moment less the moment produced by the jet thrust ($C_m - C_{m,j}$) was less than the C_m value obtained with the RCS off. Thus, the moment produced by the jet thrust and the moment attributed to the jet interaction loading were in the same direction. In general, the results in Appendix I indicate that at any given angle of attack not only will the RCS produce an incremental change in the aerodynamic coefficients, but the interaction loading will change the slope and variation of the coefficients with angle of attack and sideslip.

The variations in $C_{N,\alpha}$, $C_{m,\alpha}$, and $C_{\ell,\alpha}$ with the jet thrust coefficient, $C_{N,j}$, are given in Figs. 4 and 5. The results in Fig. 4 include the effects of (1) missile roll angle, (2) a moderate change in free-stream Reynolds number (at $M_\infty = 2$), and (3) the presence (or absence) of the tail section on the static stability of the ATR missile. In pitch, with the tail section on, increasing $C_{N,j}$ caused a reduction in the magnitude of $C_{m,\alpha}$ and $C_{N,\alpha}$. With the tail section removed, the RCS did not significantly affect the slope of the pitching-moment curve, but did increase $C_{N,\alpha}$. The RCS had essentially no effect on the rolling-moment coefficient slope, $C_{\ell,\alpha}$, when aligned in the pitch plane ($\phi = 0$), but when $\phi \neq 0$, the plume interference produced rolling moments which increased with the magnitude of ϕ. The negative $C_{\ell,\alpha}$ produced for negative model roll angles indicates that the rolling moment is caused primarily by the blanketing effect of the RCS wake on the aligned fin. Removing the tail section of the missile eliminated the induced rolling moment.

As shown in Fig. 5, for $M_\infty = 2$ and 3, rotating the missile tail section -45 deg from the plane containing the RCS row of jet nozzles (see Fig. 2) increased the RCS effects on $C_{N,\alpha}$ and $C_{m,\alpha}$ but had generally smaller and mixed effects on $C_{\ell,\alpha}$. The most noticeable effect of moving the RCS jets aft toward the model moment reference location on these stability parameters was to reduce the effects of model roll position.

The variations of $C_{N,\alpha}$ and $C_{m,\alpha}$ with Mach number are summarized in Fig. 6. A fairly good comparison between the present jet-off results and those obtained previously and reported in Ref. 1 is included in the figure. In the present test, when the tail section of the model was removed the overall length of the model was 2 calibers shorter than the tail-off configuration reported in Ref. 1, but the agreement between the two sets of data obtained is good. Although the present tail configuration had not been tested previously, a model with a similar tail configuration designated as $N_2 T_8$ in Ref. 1 had produced results which agree well with the present pitch data.

For the full configuration, the RCS jets reduced the slope of the normal-force curve and reduced the magnitude of the slope of the pitching-moment coefficient so that at Mach number 4 with $C_{N,j} = 4$, $C_{m,\alpha}$ was nominally zero for the roll positions of zero and -45 deg, as shown in Fig. 6b. With the tail section off, the RCS jets increased $C_{N,\alpha}$ at the lower free-stream Mach numbers, but at Mach number 5 they had little effect. For this tailless configuration, the RCS jets also had a relatively small effect on $C_{m,\alpha}$ over the Mach number range.
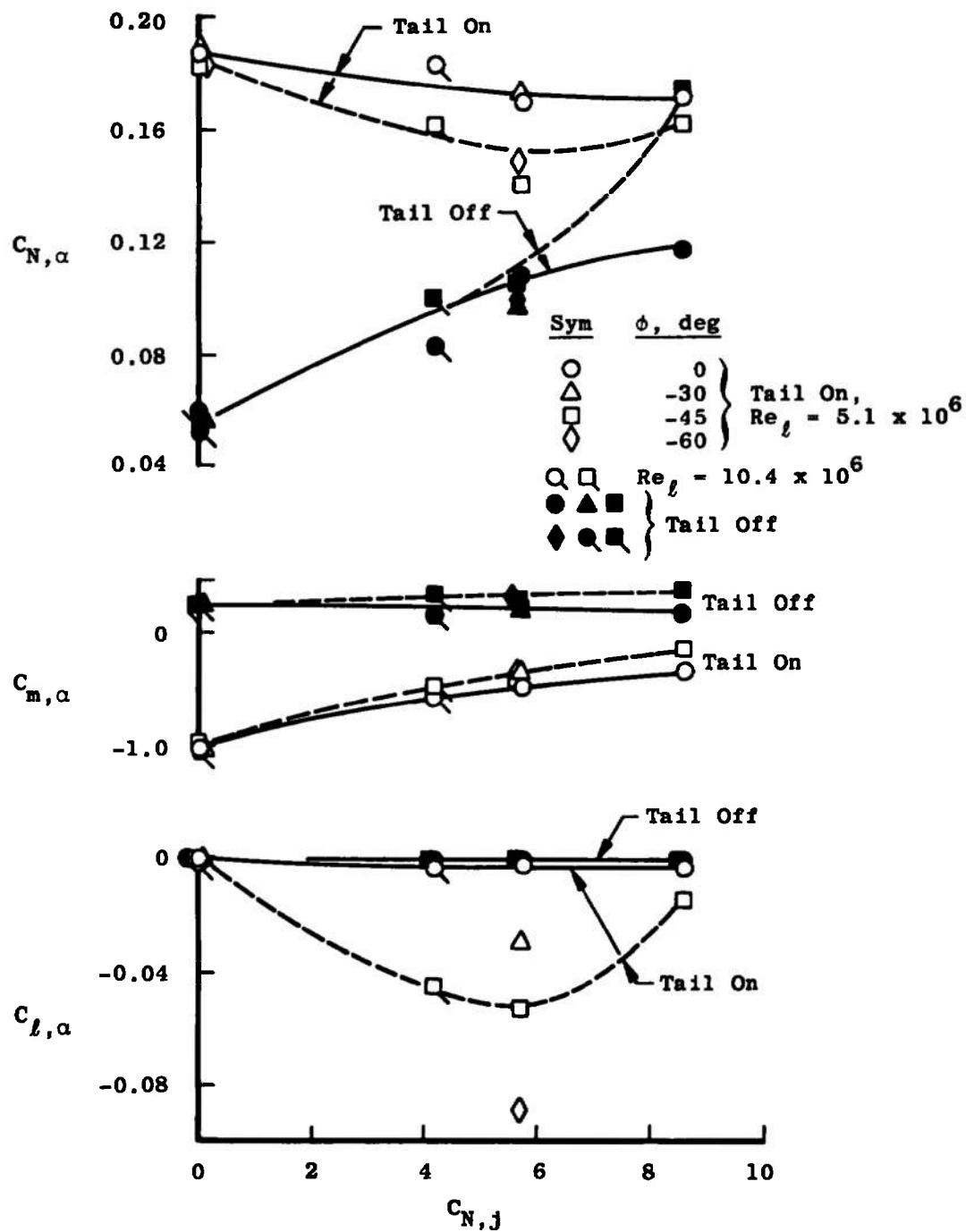
a. $M_\infty = 2.0$
Fig. 4 Effects of $C_{N,j}$, Roll Angle, and Tail Section on $C_{N,\alpha}$, $C_{m,\alpha}$, and $C_{\ell,\alpha}$ ($X_j/D = 4.37$, $\Delta\phi_j = 0$)

b. M_∞ = 3.0

c. M_∞ = 4.0 and 5.0
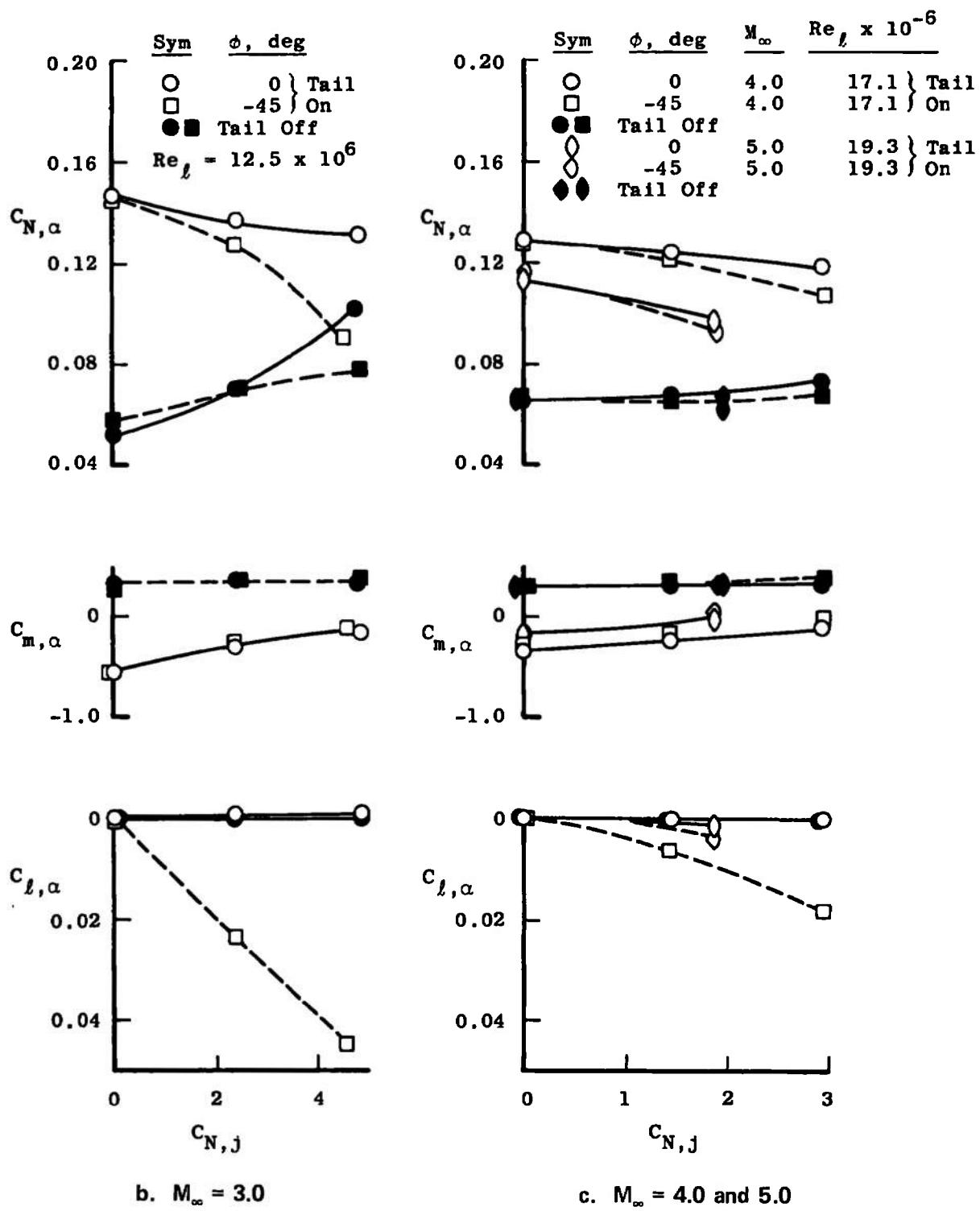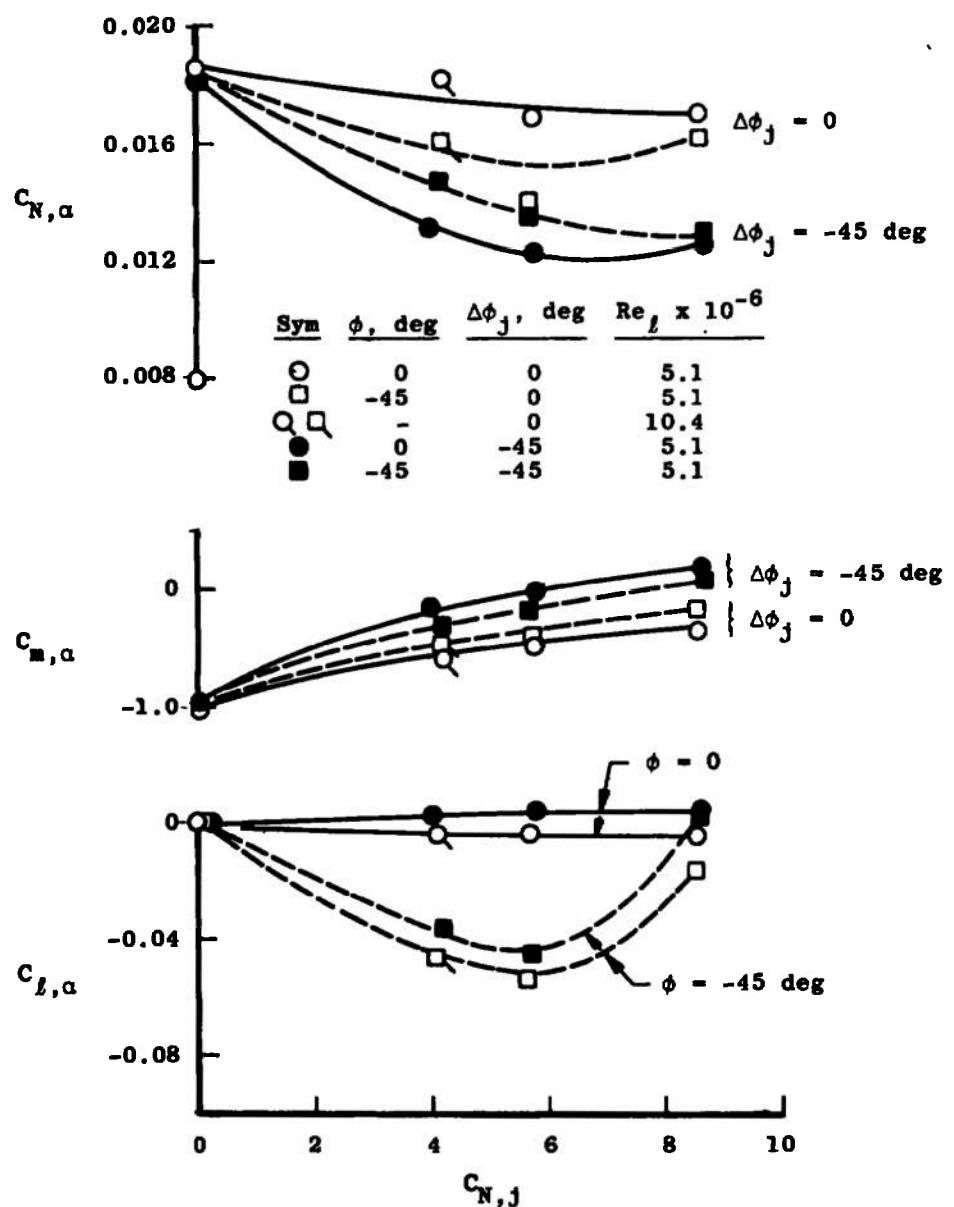
Fig. 4 Concluded

a. $x_j/D = 4.37$, $M_\infty = 2.0$

Fig. 5 Effects of the RCS Location and Thrust Vector Orientation ($\Delta\phi_j$) on $C_{N,a}$, $C_{m,a}$, and $C_{\ell,a}$
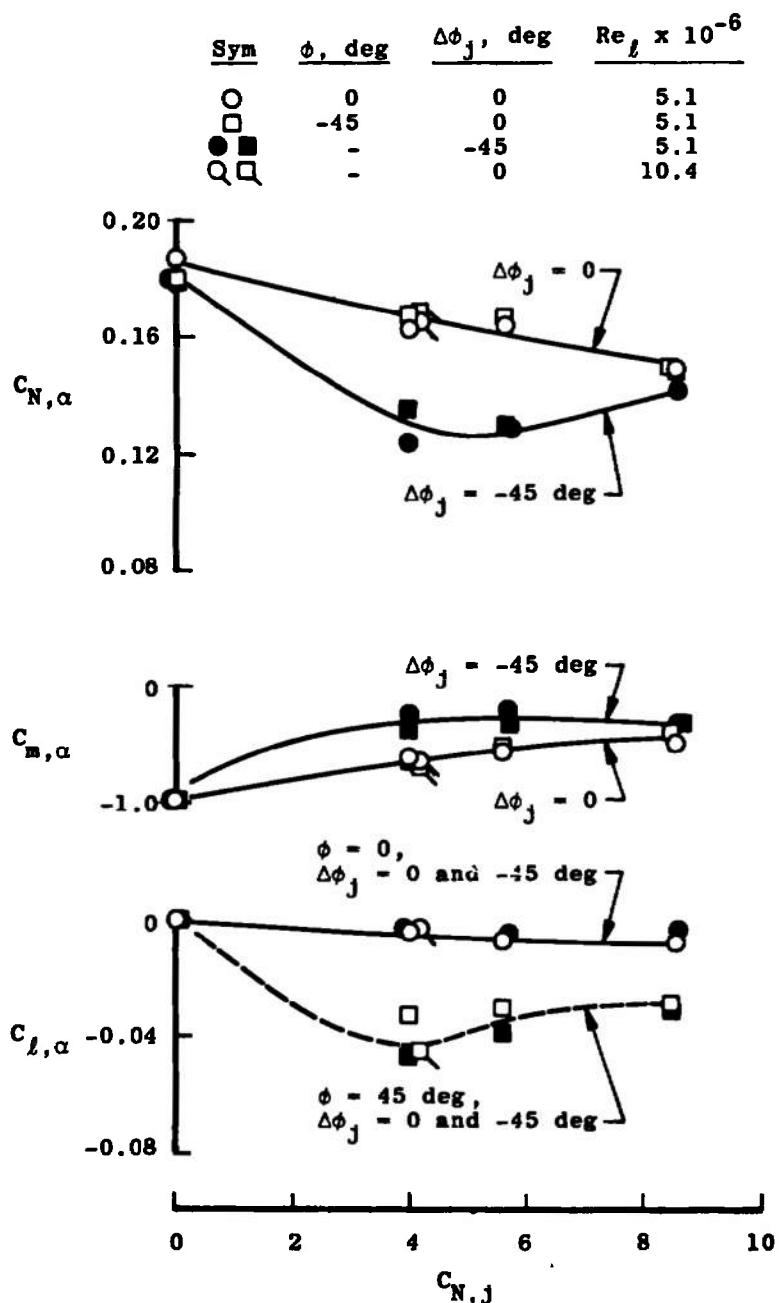
b. $x_j/D = 0.0$, $M_\infty = 2.0$
Fig. 5 Continued

19

Sym	ϕ, deg	$\Delta\phi_j$, deg
○	0	0
□	−45	0
●■	−	−45

c. $x_j/D = 4.37$, $M_\infty = 3.0$, $Re_\ell = 17.1 \times 10^6$

d. $x_j/D = 0.0$, $M_\infty = 3.0$, $Re_\ell = 19.3 \times 10^6$

Fig. 5 Concluded

20
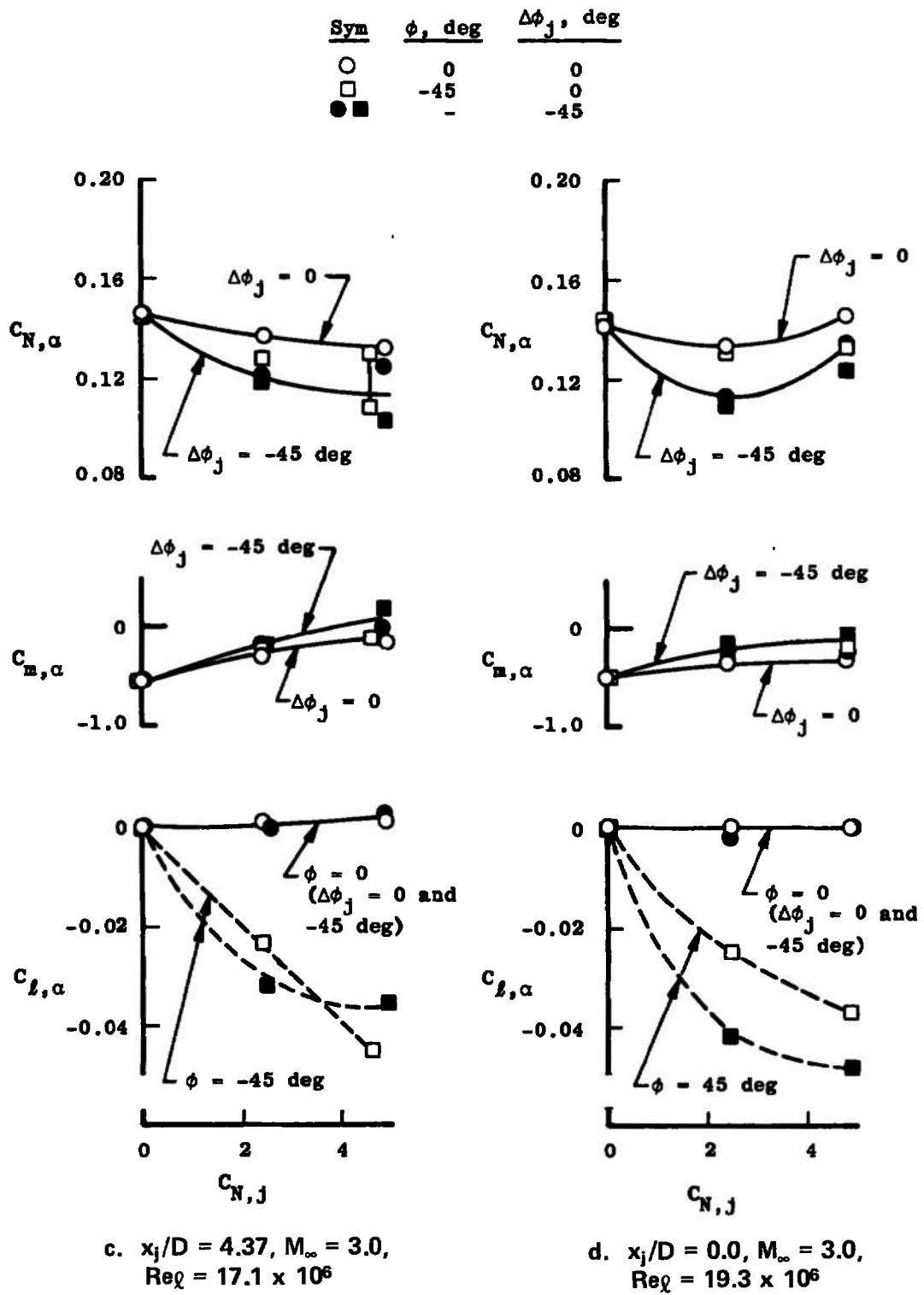
The rolling moment was zero for the tailless configuration for nearly all angles of attack and model roll positions. However, as shown in Fig. 6c and as noted previously, with the tail on and the model rolled (ϕ = -45 deg), the RCS jet disturbance produced significant rolling moments at the lower Mach numbers. The magnitude of $C_{\ell,\alpha}$ decreased markedly as Mach number increased. The RCS jet disturbance effects on the lateral stability parameters $C_{Y,\beta}$ and $C_{m,\beta}$ are shown in Figs. 6d and e. The effects on $C_{Y,\beta}$ also decreased with Mach number increase.

a. $C_{N,\alpha}$ versus M_∞

b. $C_{m,\alpha}$ versus M_∞
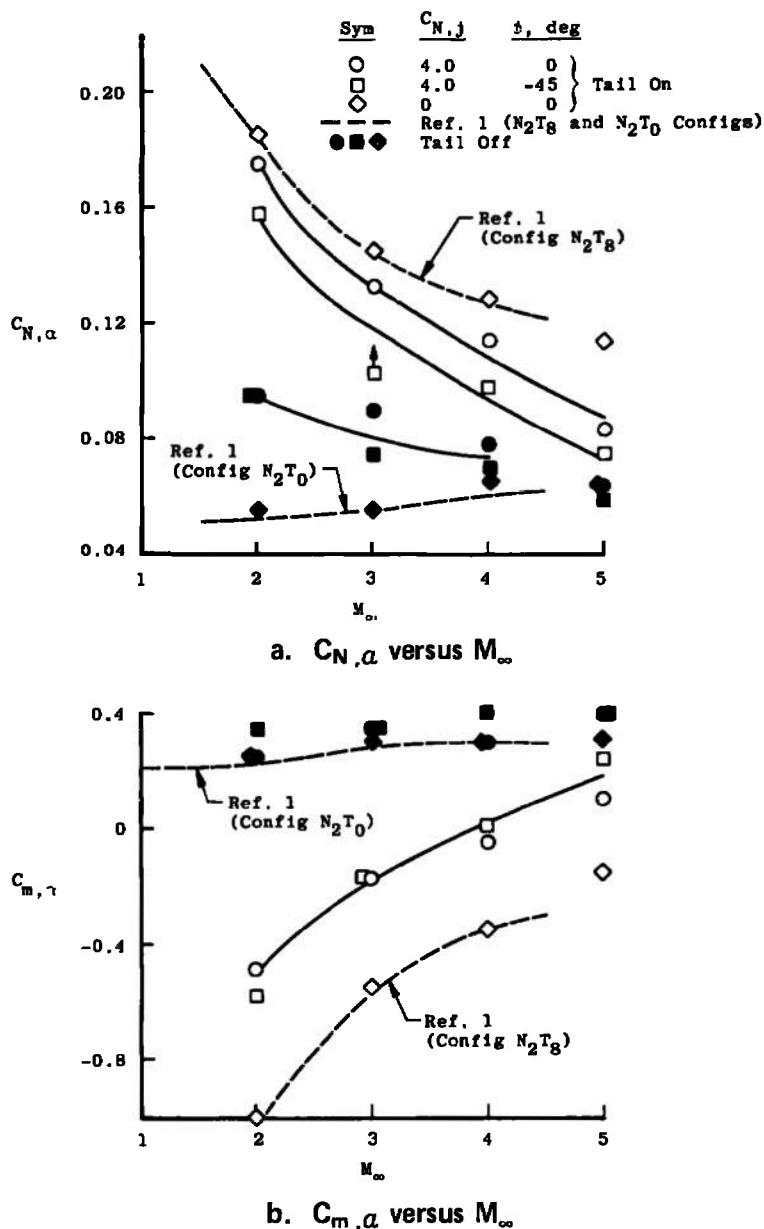
Fig. 6 Tail and Jet Control Effects on the Aerodynamic Static Stability of the ATR Missile ($C_{N,j}$ = 0 and 4.0)

Sym	$C_{N,j}$	$\pm$, deg	
O	4.0	-90	}
□	4.0	-45	} Tail On
◇	0.0	-90	}
——	Ref. 1 (N_2T_8 and N_2T_0 Configs)		
●■◆	Tail Off		
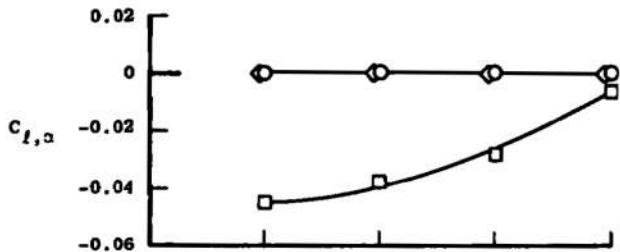
c. $C_{\ell,a}$ versus Mach Number
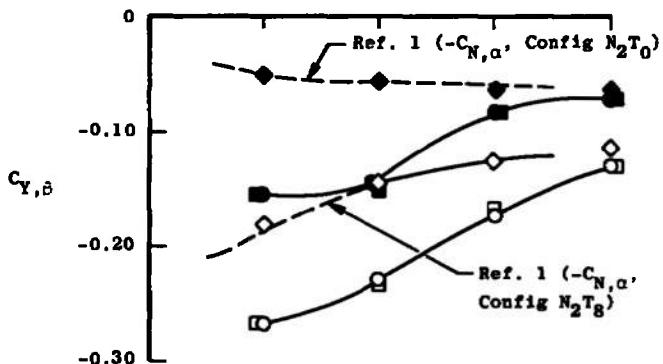
d. $C_{Y,\beta}$ versus M_∞
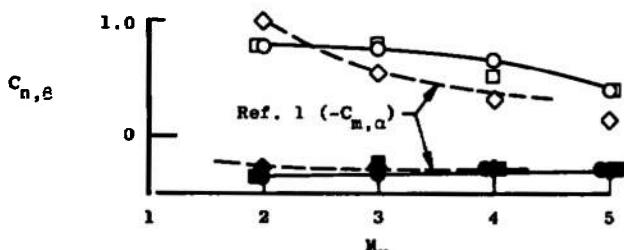
e. $C_{n,\beta}$ versus M_∞

Fig. 6 Concluded

22

Some of the variations in the static stability coefficients are suggested by the type of disturbance produced by the RCS. Typical shadowgraphs of the RCS disturbance are presented in Appendix II. The general characteristics of the flow field are sketched in Fig. 7. The jet plume produced by the row of six nozzles is indicated by the shaded region, and as the plume expands, the jet flow passes through a strong shock or set of terminal shocks in the jet plume. Downstream of these terminal shocks a turbulent jet plume wake is formed which, in general, moves parallel to the free-stream direction,

α – 10 deg

α ≈ 0

α – -10 deg

α – -10 deg
α – 0
α – 10 deg

① Jet Plume

② Jet Wake

③ Jet Wake Recompression Shock

④ Jet/Free-Stream Bow Wave

⑤ Separated Flow Ahead of Jet Disturbance

⑥ Separated Flow Region

⑦ Nose Bow Wave
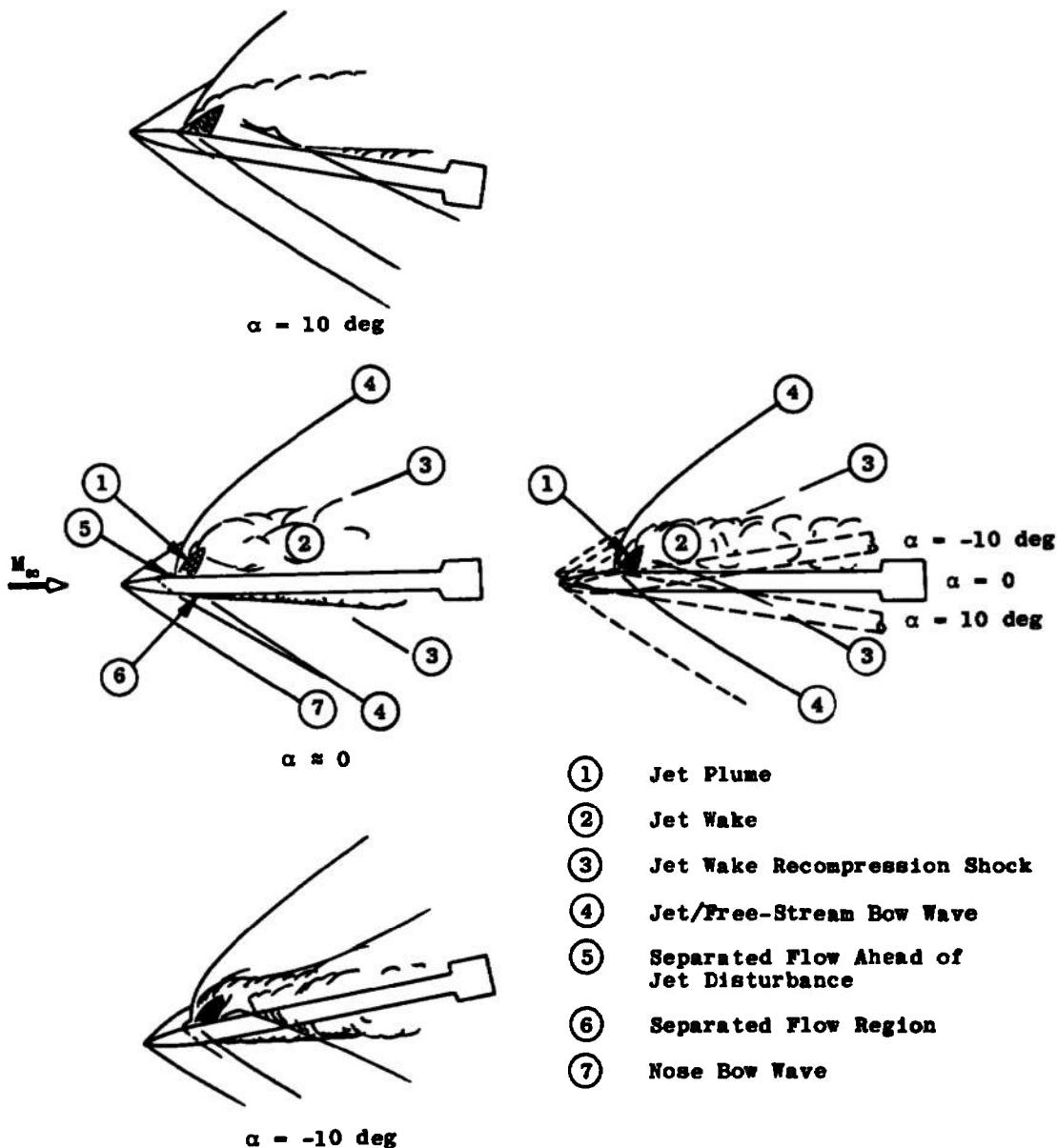
Fig. 7 Sketch of the RCS Jet Flow-Field Disturbance, $\phi = 0$

independent of the model angle of attack. Generally, the missile tail section passes through a different portion of the jet plume wake, depending upon the attitude of the missile. This, in part, explains the nonsymmetrical variations from negative to positive angles of attack in the static stability coefficients with the RCS on (see Appendix I).

Just immediately upstream of the jet/free-stream bow wave, there is a small region of separated flow producing high surface pressures which expand around the RCS nozzle jets on the model surface. Immediately aft of the jets is a low-pressure region followed by a region of high pressure produced by the jet wake impinging on the missile body and tail surfaces. On the opposite side of the RCS jets, particularly at the higher free-stream Mach numbers (see Figs. II-3, -4, and -5) there is a region of separated flow produced by the jet plume disturbance, which propagates circumferentially around the missile. Most of these comments on the pressure loading produced in and around the jet disturbance are based on previous lateral jet pressure tests, as for example, Ref. 4.

The composite sketch in Fig. 7 simply illustrates the fact that the orientation and shape of the jet/free-stream bow wave and the jet wake do not vary significantly with the angle of attack of the body. Similar results were obtained whether the entire model was rolled -30, -45, -60, or -90 deg. The missile and the missile tail section simply were pitched into different portions of the expanding jet wake.

4.2 RCS TRAJECTORY CORRECTION RESULTS

The potential trajectory corrections produced by the ATR's jet controls were examined by using the six-degree-of-freedom (6-DOF) flight path computer program described by Vorwald in Ref. 5. This program was manipulated to permit the aerodynamic coefficients to be perturbed at a particular point in the trajectory by an amount equal to the change in the aerodynamic coefficient equal to the firing of the RCS jet controls. These coefficient changes accounted not only for the direct effect of the jet thrust but also for the effects resulting from the jet wake's interfering with the external flow over the missile body and tail surfaces.

In this analysis, the missile was assumed to have the optimum nose and tail configuration selected by Uselton in Ref. 1 (namely the $N_2 T_5$ configuration). The ATR missile was assumed to begin its trajectory at an altitude of 7000 ft with an initial velocity of 884 ft/sec, an initial elevation angle of -30 deg, and an initial roll rate of 500 rpm. The main engine of the missile was assumed to fire for 2.25 sec at a constant thrust of 2200 lbf. From the initial point in the trajectory, the missile travels downrange about 11,400 ft to an impact point.

At an altitude of 2608 ft, when the flight speed of the missile theoretically reached Mach number 4.1, the jet thrusters in the RCS were fired for 10 msec at a thrust level of 5800 lbf. During this firing time, the missile will roll through an angle of 30 deg. The change in normal-force coefficient ($C_{N,j}$) produced by the thruster is nominally 4, and the change in the pitching-moment coefficient ($C_{m,j}$) is nominally 17.5. The present

24

test results indicate that the actual change in these coefficients is reduced by 15 percent because of the jet wake interference effects produced on the missile surfaces. At these flight conditions ($M_\infty \approx 4$, $C_{N,j} = 4.0$, and $C_{m,j} = 17.5$), the trajectory was computed for the following static stability aerodynamic coefficients as influenced by the RCS jet wake interference effects:

Nominal ϕ, deg	$C_{N,\alpha}$	$C_{m,\alpha}$	$C_{\ell,\alpha}$	$C_{Y,\beta}$	$C_{n,\beta}$
0	0.108	0.0	0.000	0.170*	0.500*
-45	0.093	0.0	-0.028	0.170	0.500
-90	≈ 0.0*	0.0*	-0.056	0.170	0.650
-180	0.108	0.0	0.000	0.170*	0.650*

*Estimated for small roll angles close to the nominal roll angle, ϕ.

The impact footprint produced by the missile with these RCS effects on the missile static stability is almost equal to an ellipse with semi-major and -minor axes of 77 and 39 ft, respectively. Besides the direct jet thrust effects of the RCS, the computed results show that the changes in rolling moment produced by the jet wake on the missile tail surfaces had a significant effect on the vehicle flight path. Since the actual missile would have four sets of these RCS thrusters, the net overall change in the impact footprint could consist of an ellipse with semi-major and -minor axes of 308 and 156 feet, respectively. This would amount to a net change in the flight path angle of 1.6 to 1.9 deg. Of course, an increase in the length of the RCS firing, an increase in the altitude at which the RCS is fired, or a decrease in the magnitude of the initial flight path elevation angle—any of these—would tend to increase the change in the impact point location.

SECTION V
SUMMARY

This preliminary experimental study of the change in the aerodynamic static performance of an Advanced Tactical Rocket (ATR) vehicle by its reaction jet controls was conducted in Tunnel A at nominal Mach numbers of 2, 3, 4, and 5. Some of the more significant observations made during this study follow.

1. The expanding jet wake from the jet reaction control system (RCS) thrusters located near the model nose produced a surface loading which opposed the forces and moments produced by the jet thrust. This jet interaction flow field disturbance reduced the RCS reaction force effectiveness by nearly 15 percent at zero angle of attack.

2. The rolling-moment coefficient was strongly affected by the jet wake from the RCS when the model was at a combined pitch and roll attitude. The induced jet interaction rolling-moment coefficient was negative and would

oppose the rolling moment used to stabilize the missile flight path. The full-scale missile will have canted fins or roll tabs to maintain a stabilizing roll rate.

3. The induced jet interaction effects on a tail configuration with deflected surfaces or roll tabs may also change the rolling-moment coefficient at zero angle of attack. Therefore, the final development of an RCS to control the ATR missile's trajectory should include an experimental program to evaluate the jet interaction effects on the selected missile tail fin configuration.

4. An analytical study of the jet effects on the missile impact point shows that the impact point can be evaluated in terms of the changes in forces and moments produced by the RCS jet thrust. Including jet wake interaction, effects on the missile aerodynamic coefficients for this 10-msec firing of the RCS changed the impact point by less than 10 percent. Obviously, a longer firing of the RCS will increase the error in predicting the missile impact point if the jet interaction effects are neglected.

REFERENCES

1. Uselton, James C. "Results of an Air Force Advanced Tactical Rocket Development Program." AEDC-TR-71-141 (AD885643L), AFATL-TR-71-73, July 1971.

2. Werle, M. J., Driftmyer, R. T., and Shaffer, D. G. "Two-Dimensional Jet Interaction with a Mach 4 Mainstream." NOLTR 70-50, May 1970.

3. Herron, R. D. "Investigation of Jet Boundary Simulation Parameters for Underexpanded Jets in a Quiescent Atmosphere." AEDC-TR-68-108 (AD675211), September 1968.

4. Strike, W. T. and Best, J. T., Jr. "NASA-Convair ACS Space Shuttle Study at Mach Number 8.0." AEDC-TR-73-40 (AD759578), May 1973.

5. Vorwald, R. F. "Six-Degree-of-Freedom Flight Path Study Generalized Computer Program." FDL-TDR-64-1, Part II, Vol. I, October 1964.

APPENDIX I
VARIATION OF THE BASIC AERODYNAMIC COEFFICIENTS
WITH ANGLE OF ATTACK AND SIDESLIP
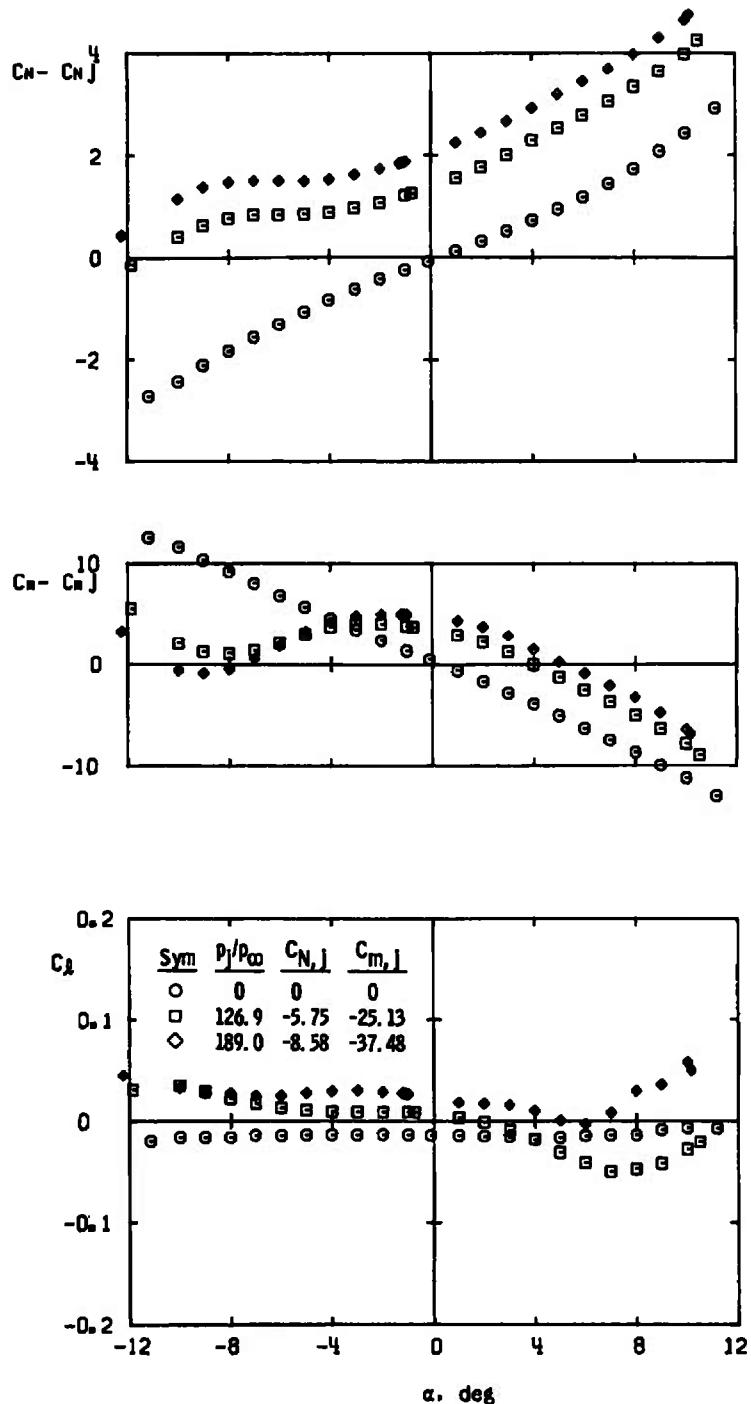
a. $\phi = 0$, $M_\infty = 2.0$, $Re_\ell = 5.1 \times 10^6$

Fig. I-1 Control Jet Effects on the ATR Missile with the Nozzle Jets at $x_j/D = 4.37$ and Aligned with the Fins
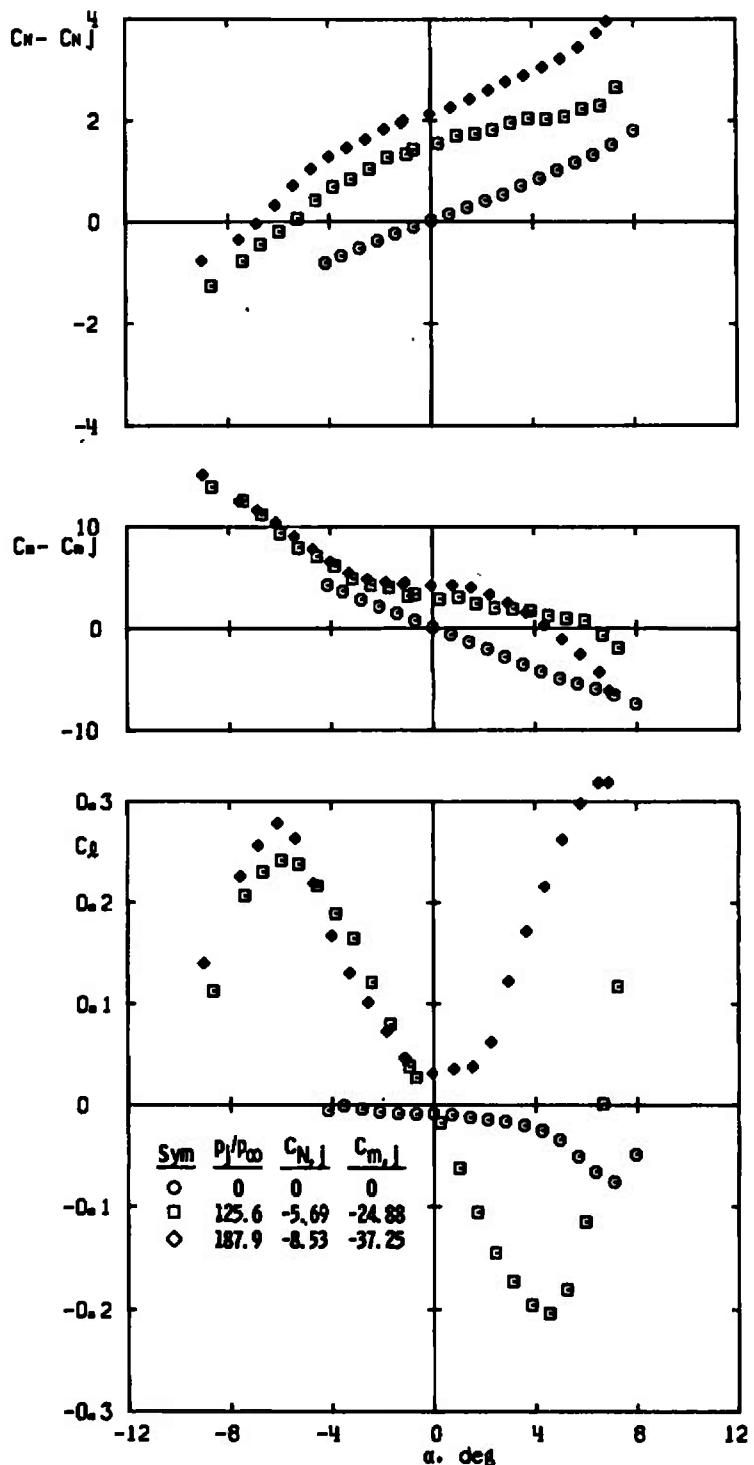
b. $\phi = -45$ deg, $M_\infty = 2.0$, $Re_\ell = 5.1 \times 10^6$

Fig. I-1 Continued

30
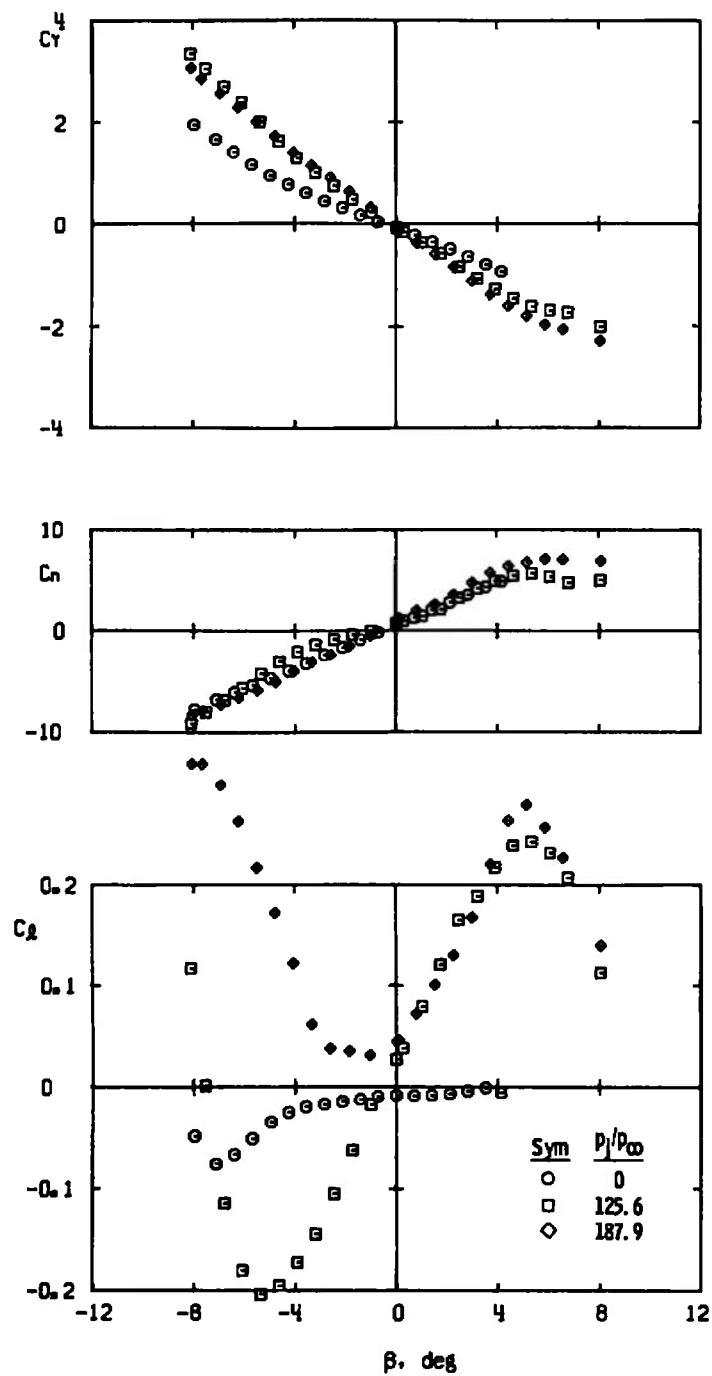
b. Concluded
Fig. I-1 Continued

c. ϕ = -90 deg, M_∞ = 2.0, $Re\ell$ = 5.1 x 10^{6}
Fig. I-1 Continued

32
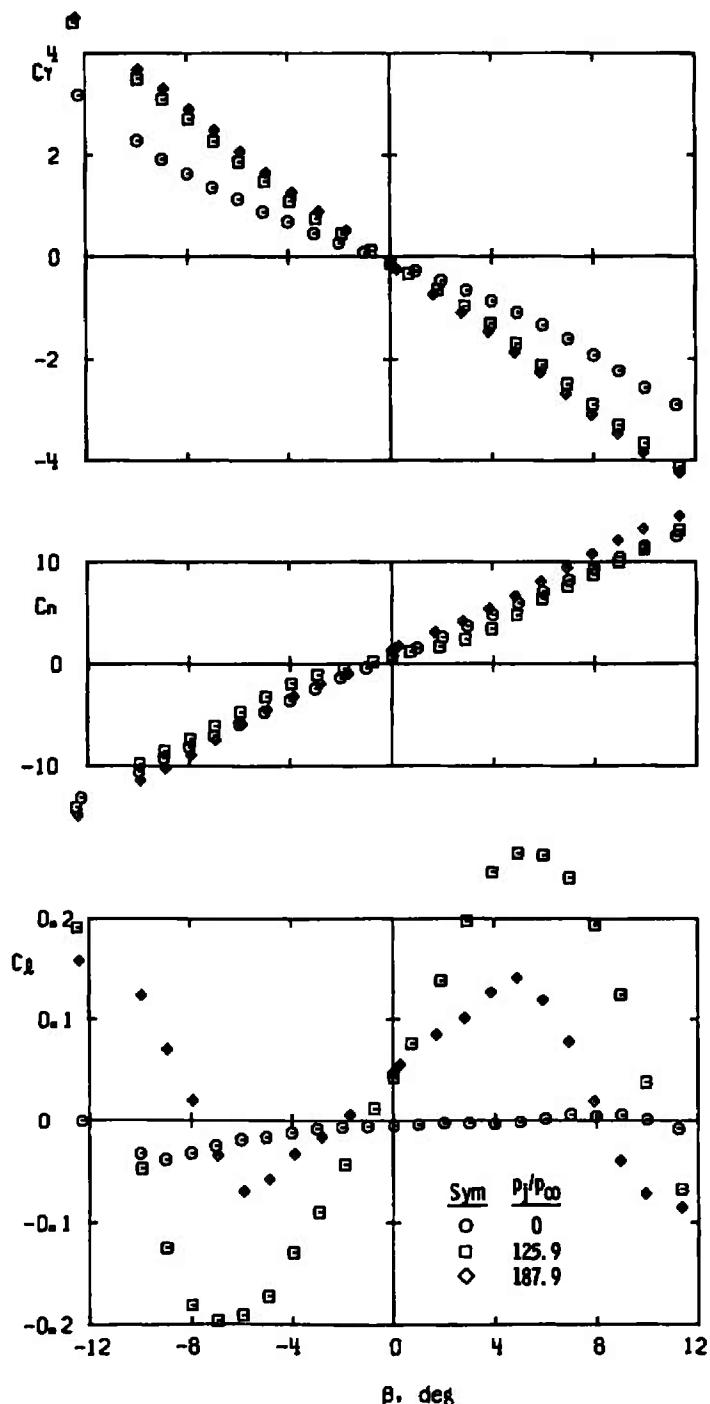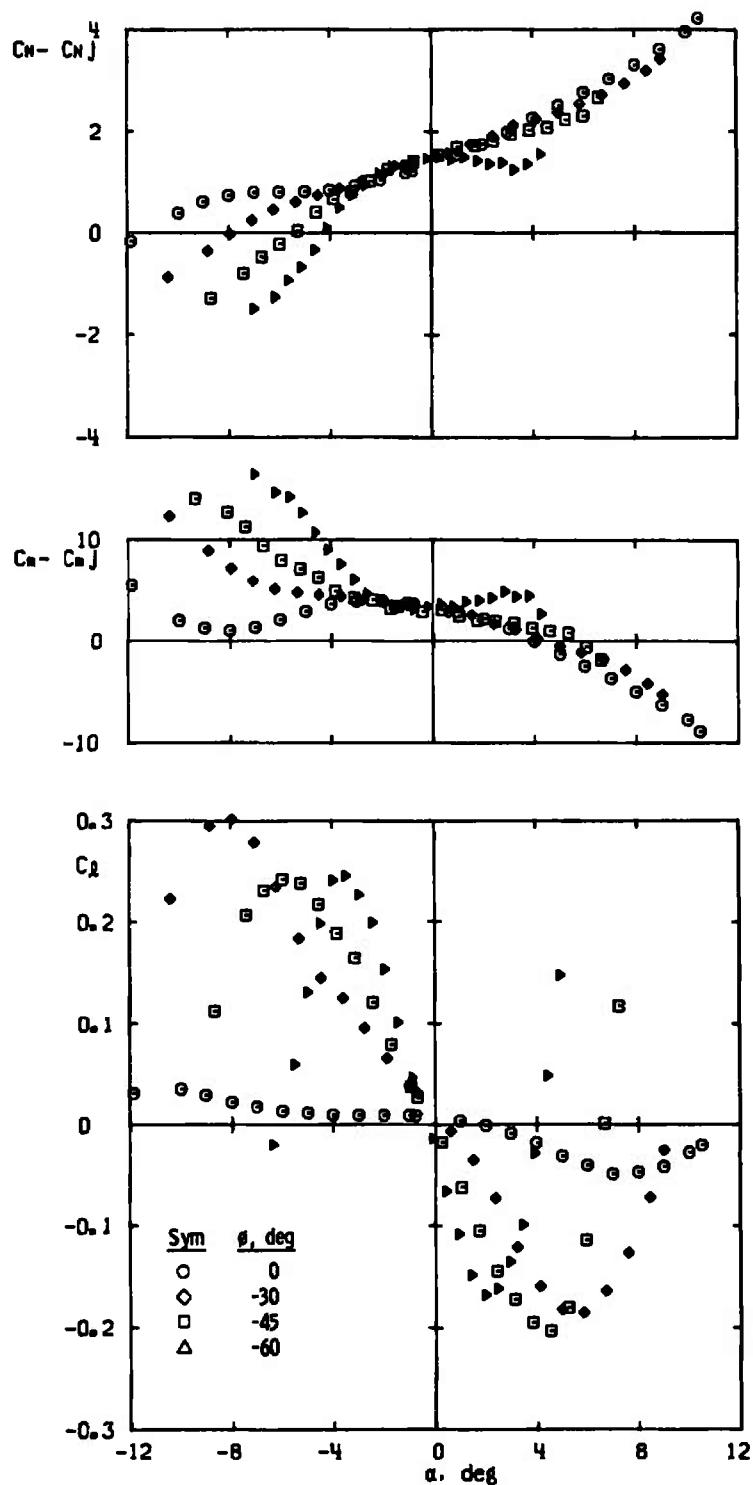
d. Variable ϕ, p_j/p_∞ = 188, M_∞ = 2.0, Re_ℓ = 5.1 x 10^6
Fig. I-1 Continued
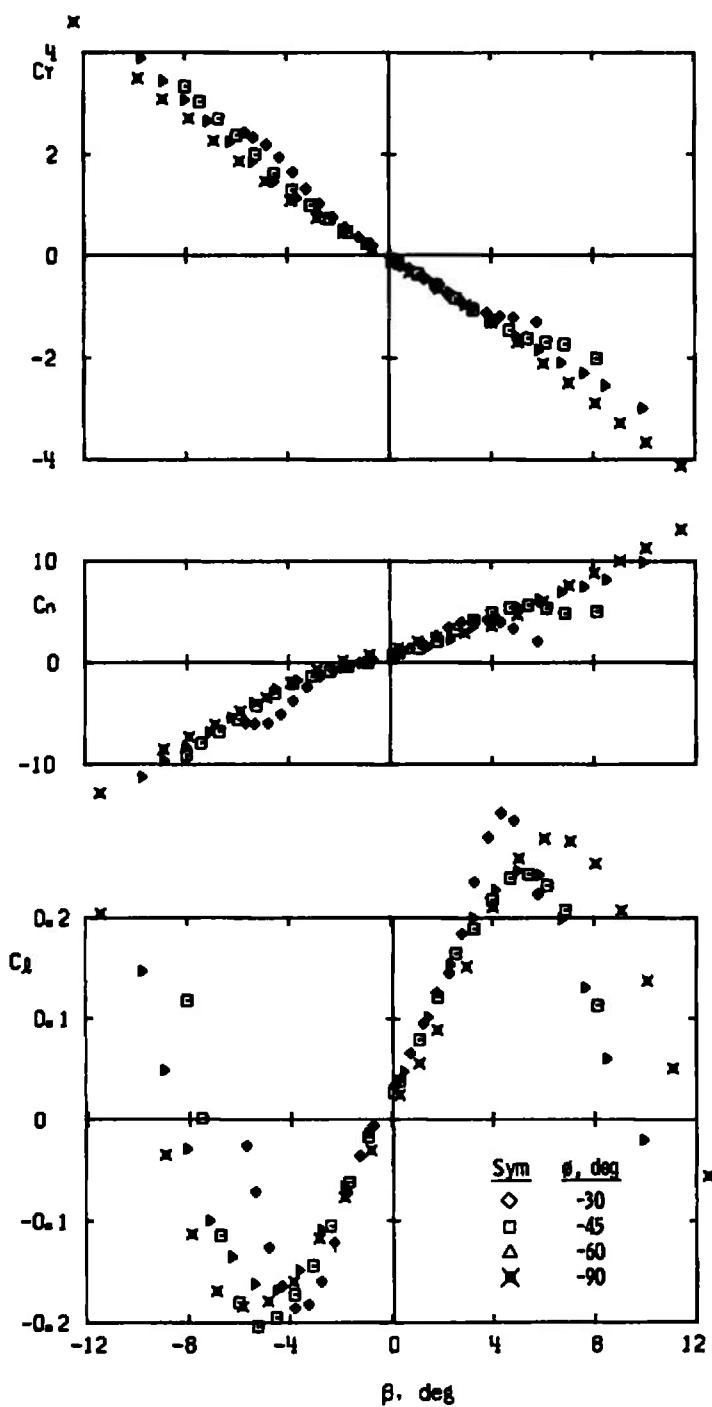
d. Concluded
Fig. I-1 Continued
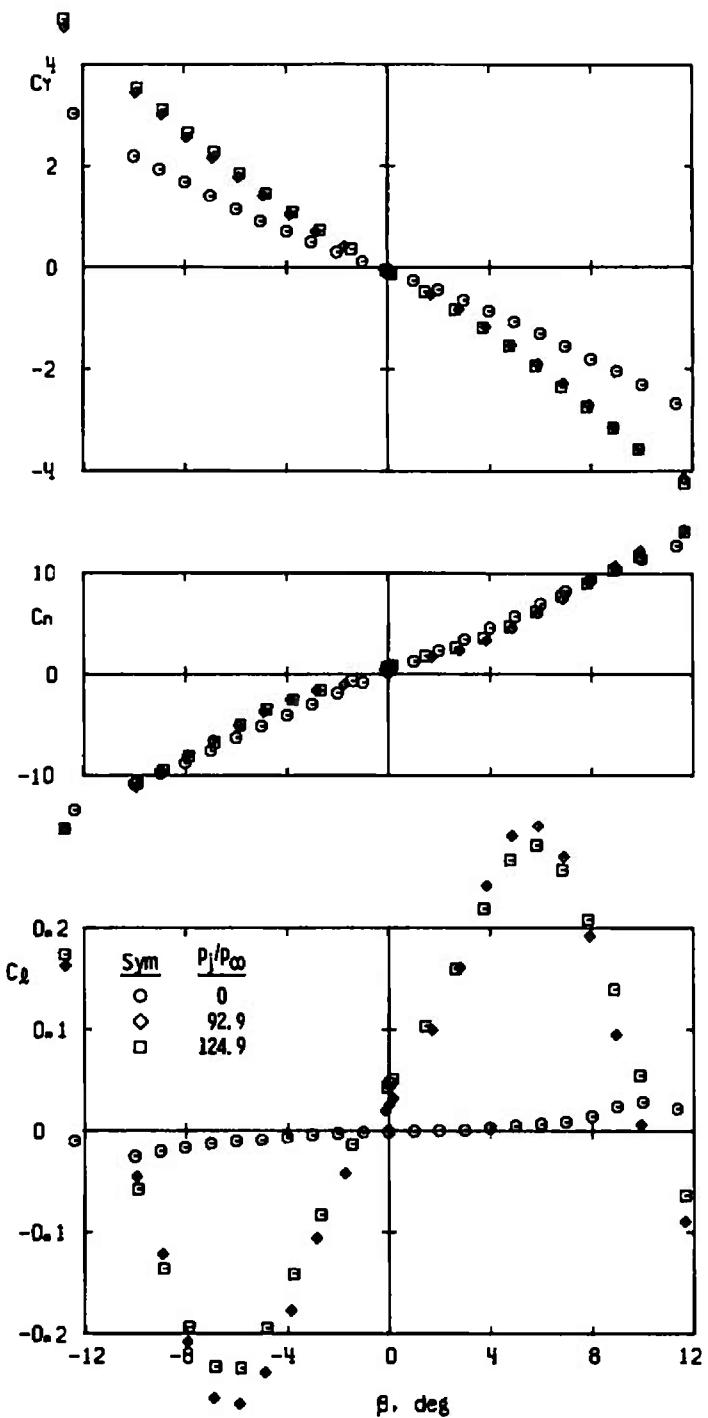
e. $\phi = -90$ deg, $M_\infty = 2.0$, $Re_\ell = 10.4 \times 10^6$
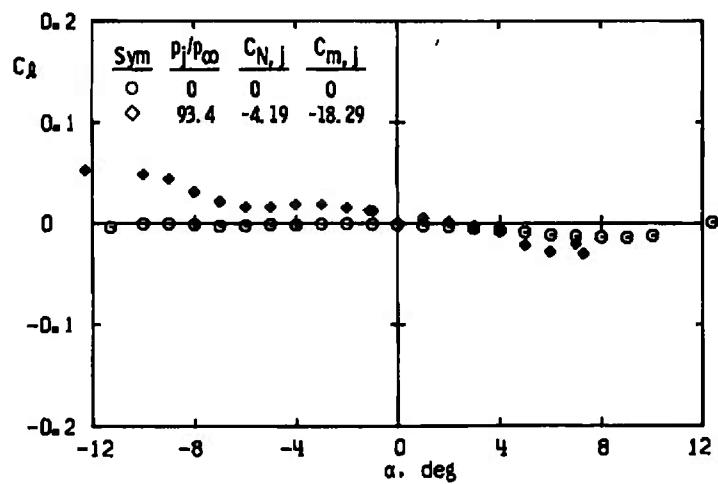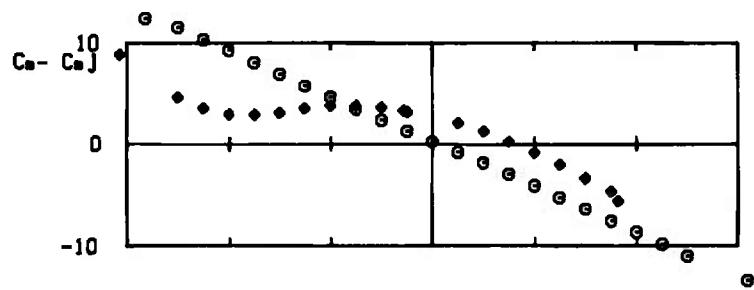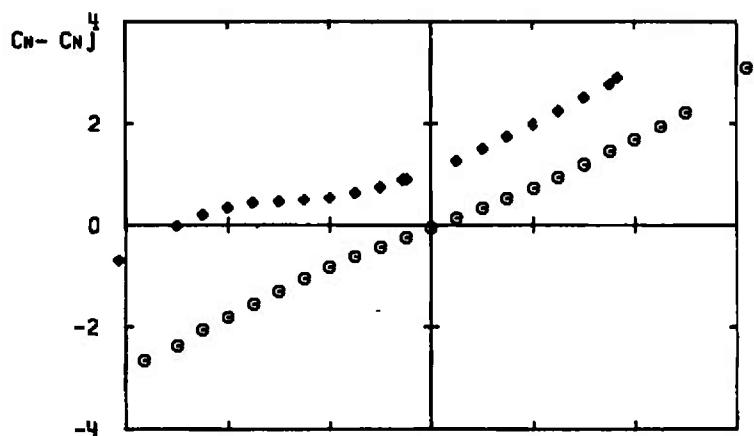
Fig. I-1 Continued

f. $\phi = 0$, $M_\infty = 2.0$, $Re_\ell = 10.4 \times 10^6$
Fig. I-1 Continued
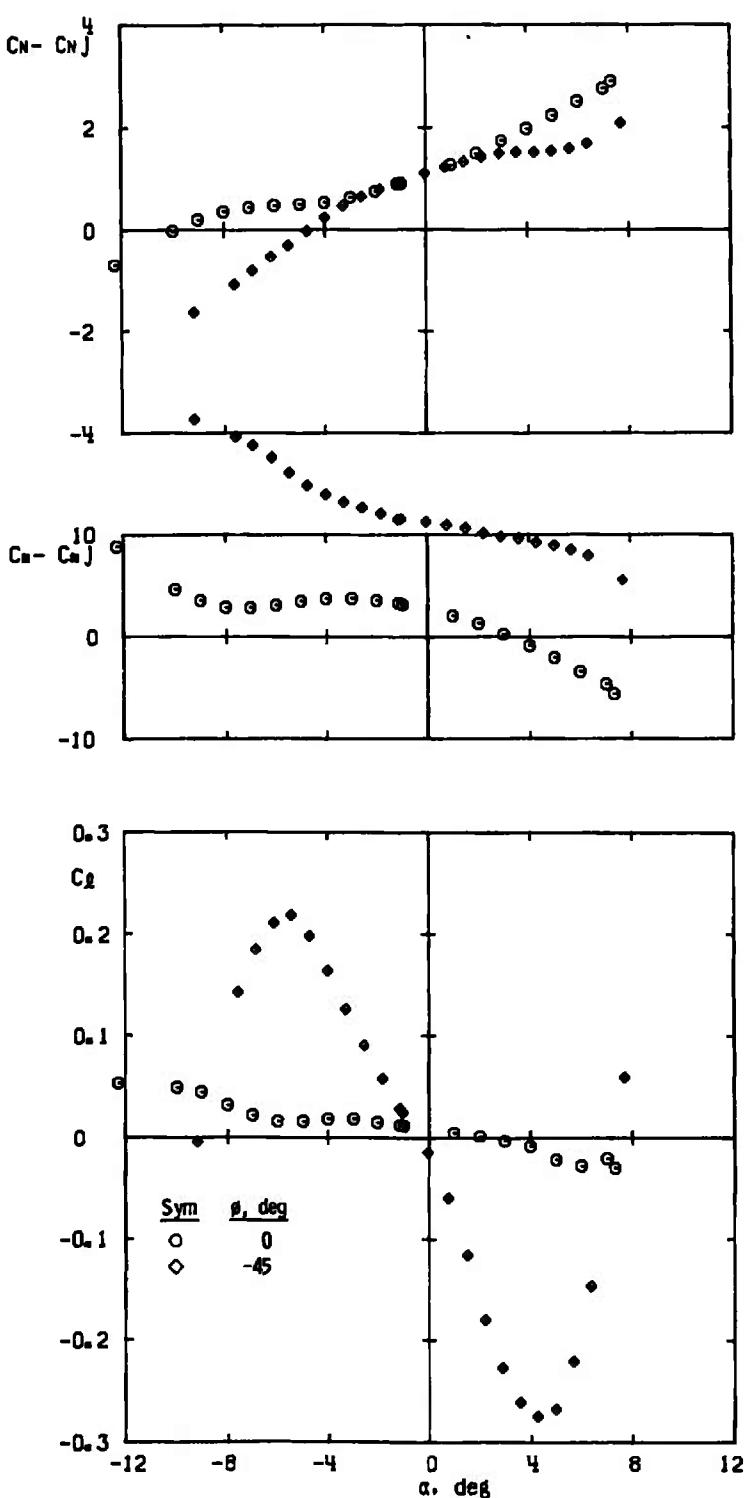
g. Variable ϕ, $p_j/p_\infty = 93$, $M_\infty = 2.0$, $Re_\ell = 10.4 \times 10^6$
Fig. I-1 Continued
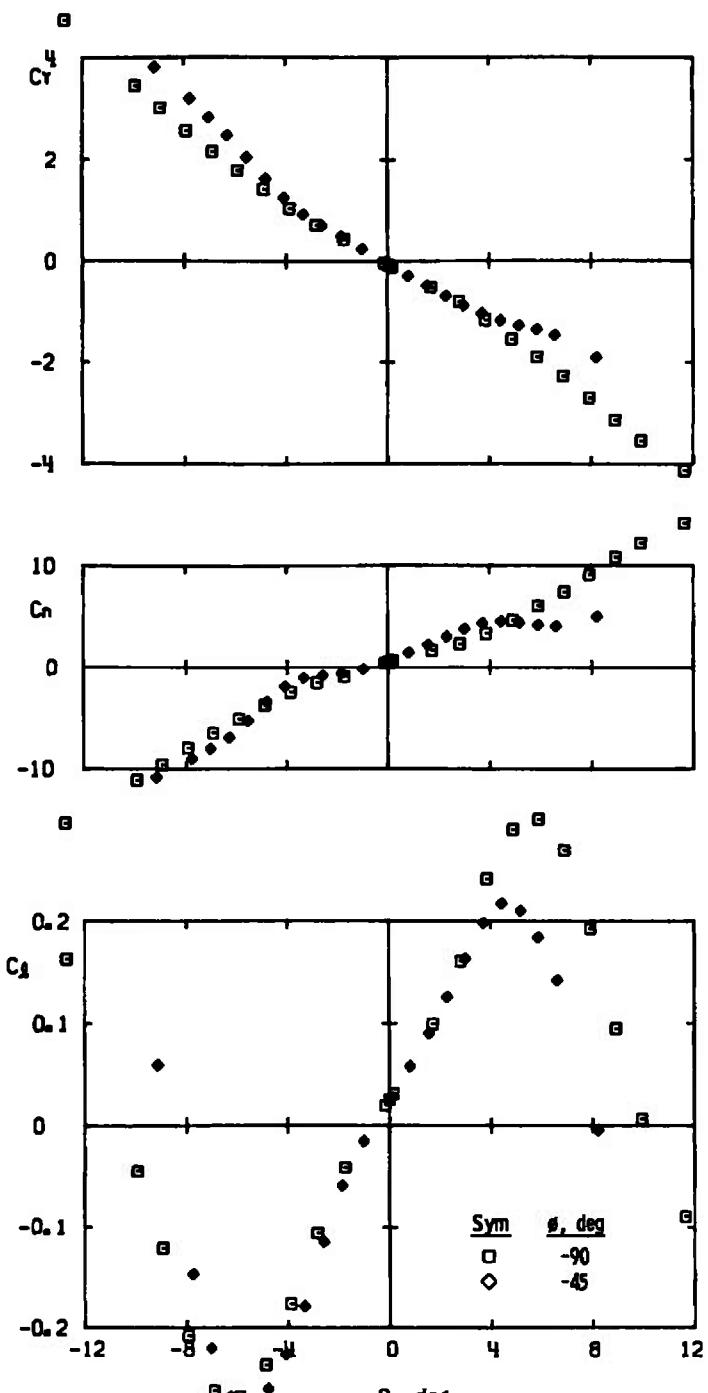
g. Concluded
Fig. I-1 Continued

38
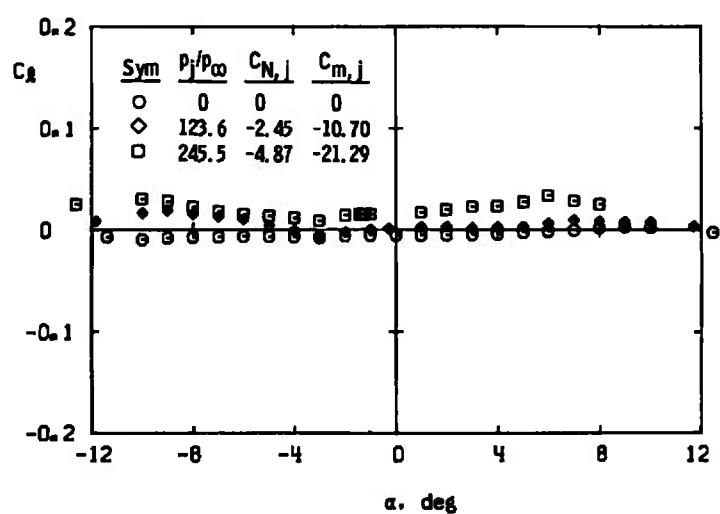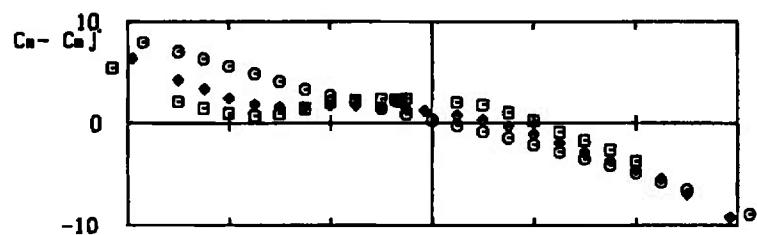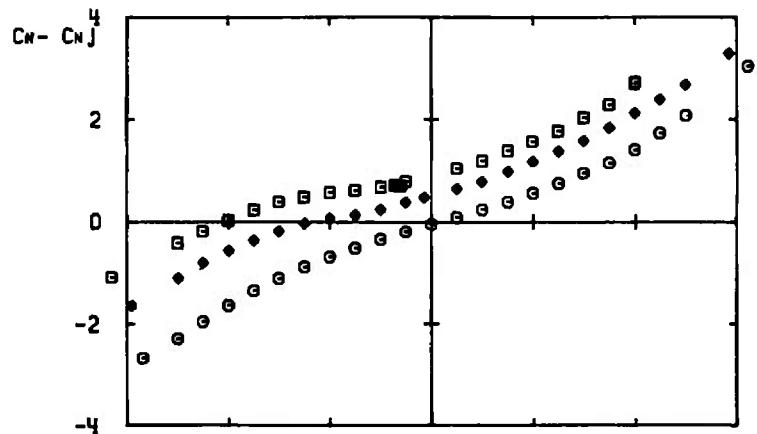
h. $\phi = 0$, $M_\infty = 3.0$, $Re_\ell = 12.5 \times 10^6$
Fig. I-1 Continued
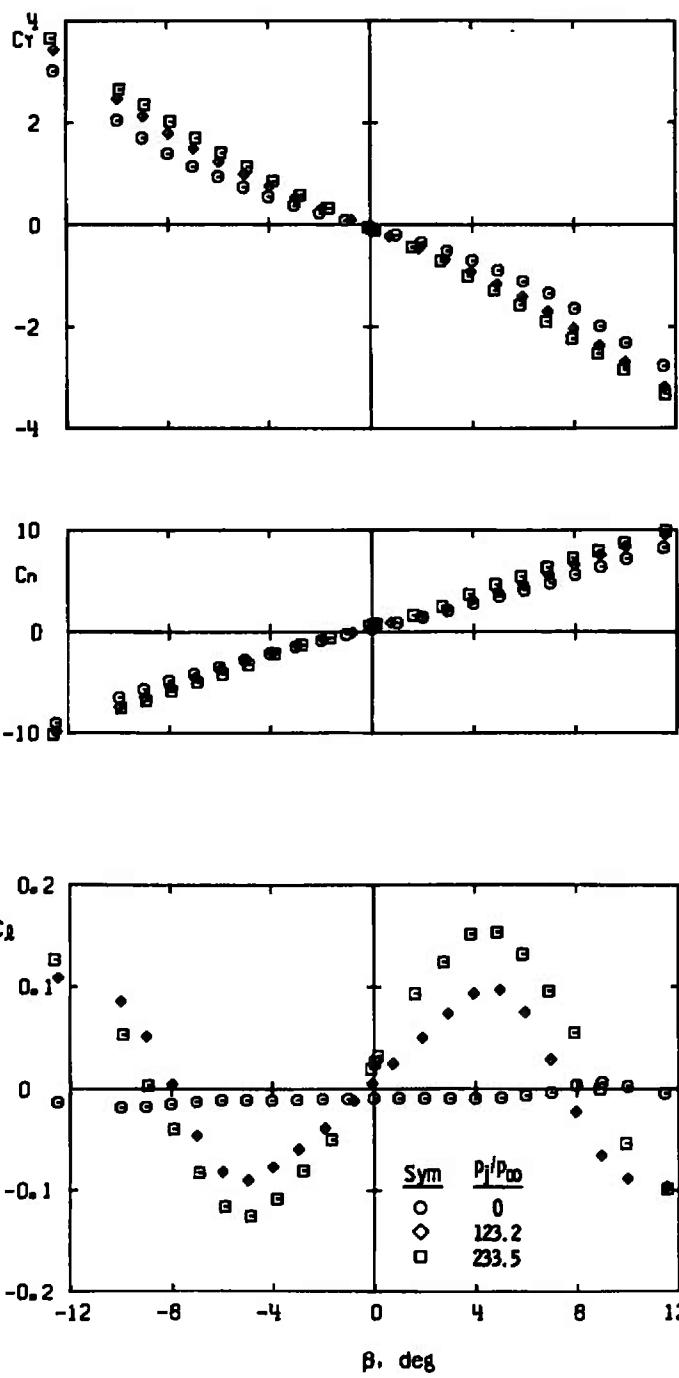
i. ϕ = -90 deg, M_∞ = 3.0, Re_ℓ = 12.5 x 10^6
Fig. I-1 Continued
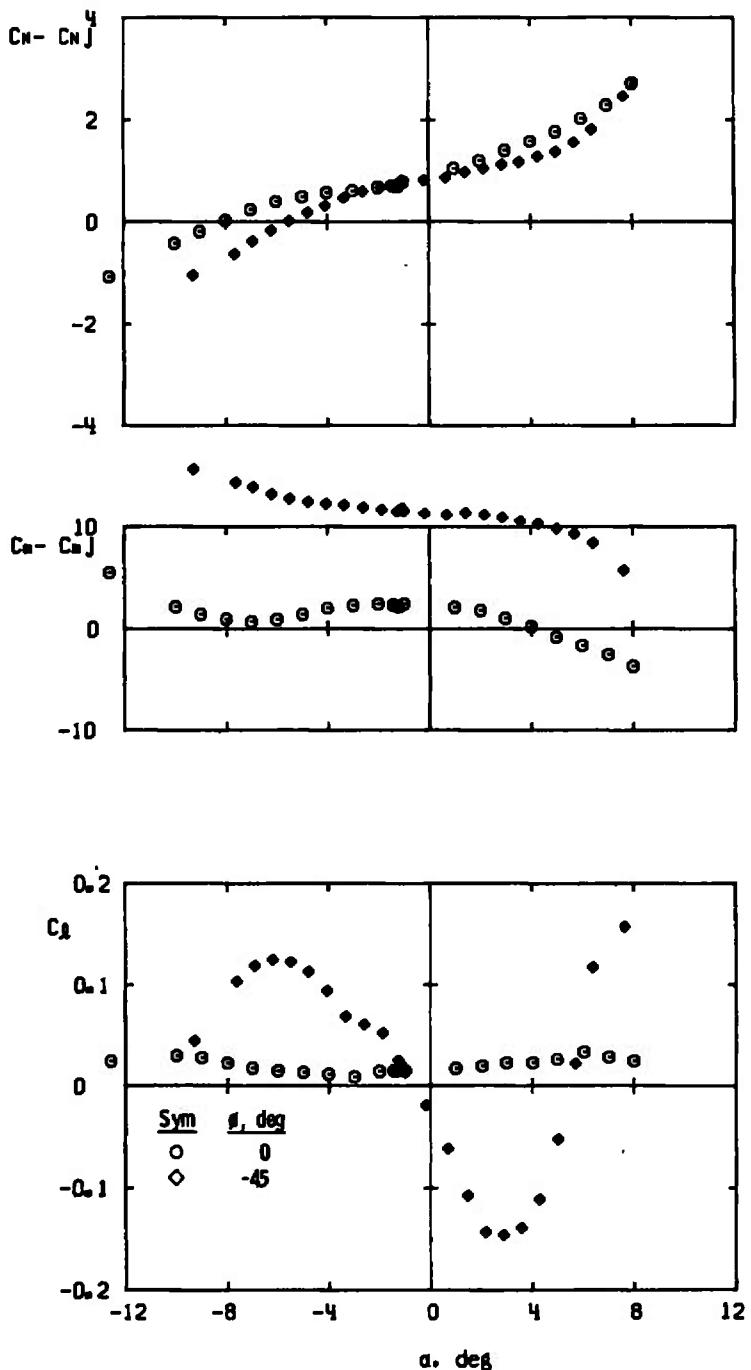
j. Variable ϕ, $p_j/p_\infty = 246$, $M_\infty = 3.0$, $Re_\ell = 12.5 \times 10^6$
Fig. I-1 Continued
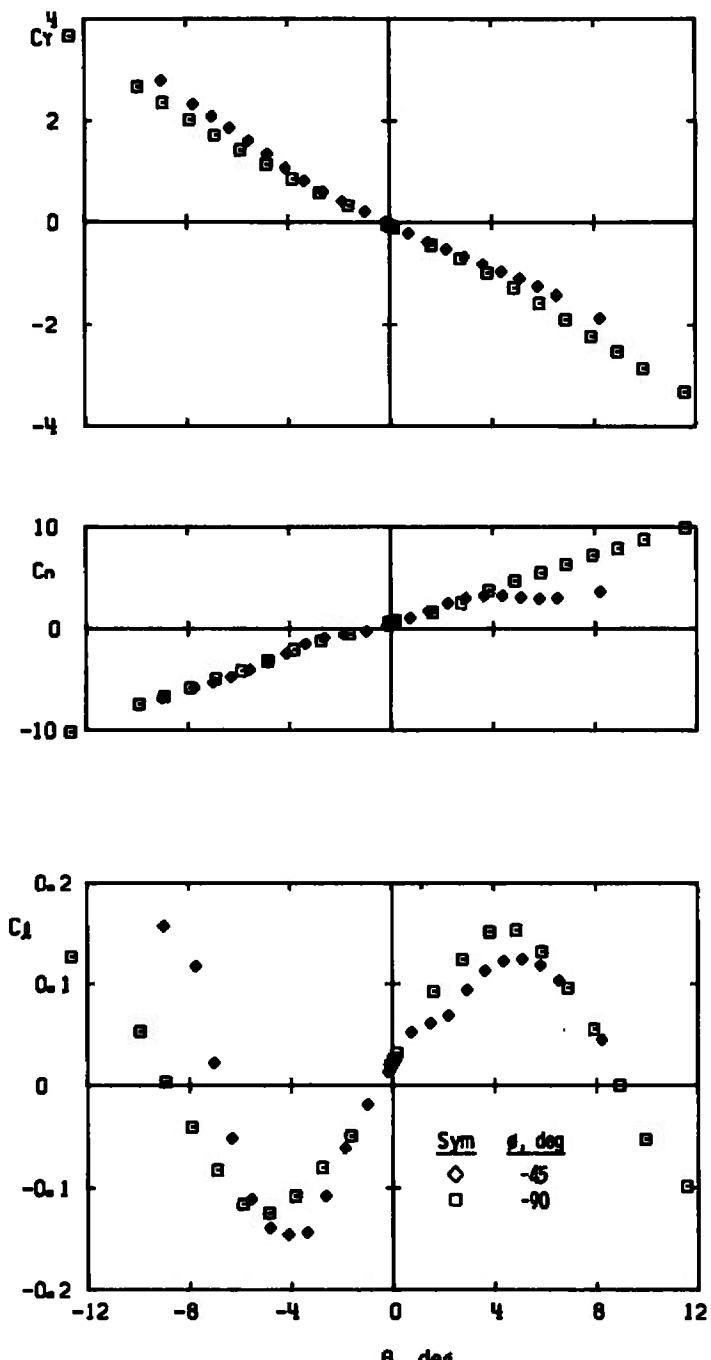
j. Concluded
Fig. I-1 Continued
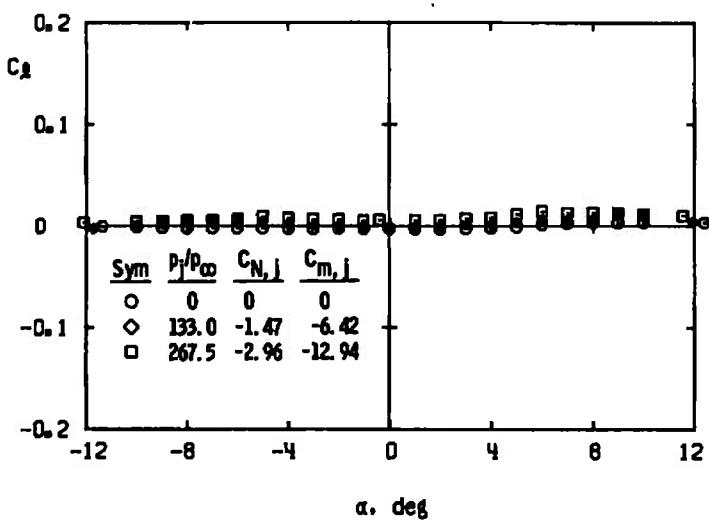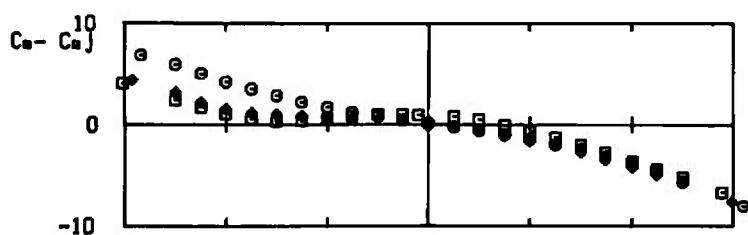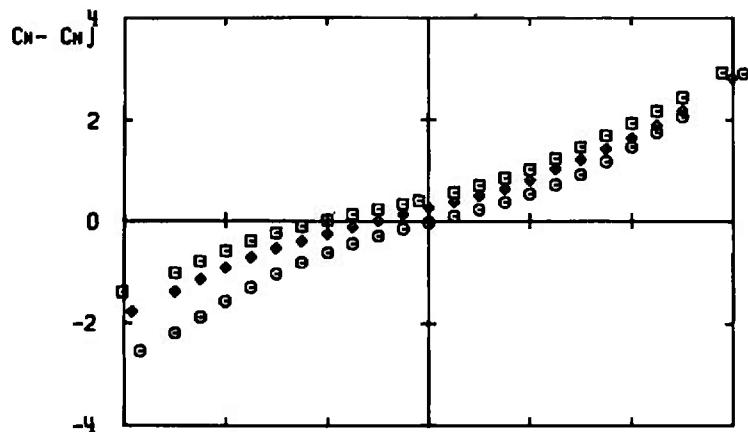
k. $\phi = 0$, $M_\infty = 4.0$, $Re_\ell = 17.1 \times 10^6$
Fig. I-1 Continued
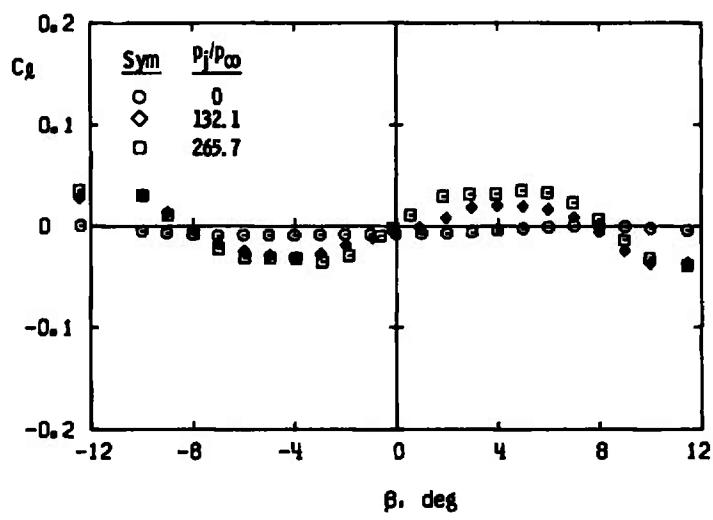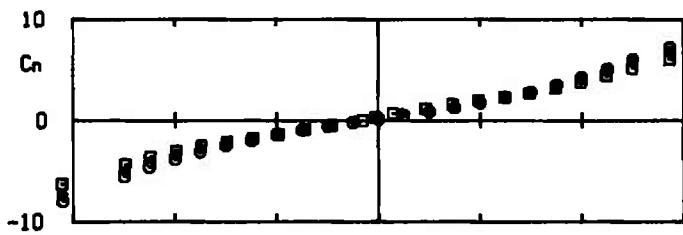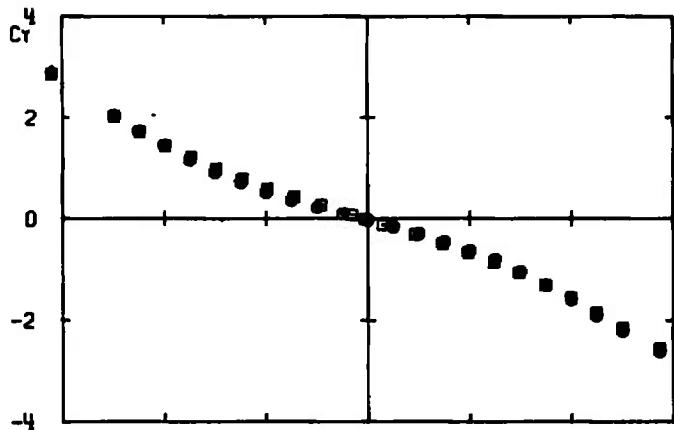
I. ϕ = -90 deg, M_∞ = 4.0, $Re\ell$ = 17.1 x 10^{6}
Fig. I-1 Continued
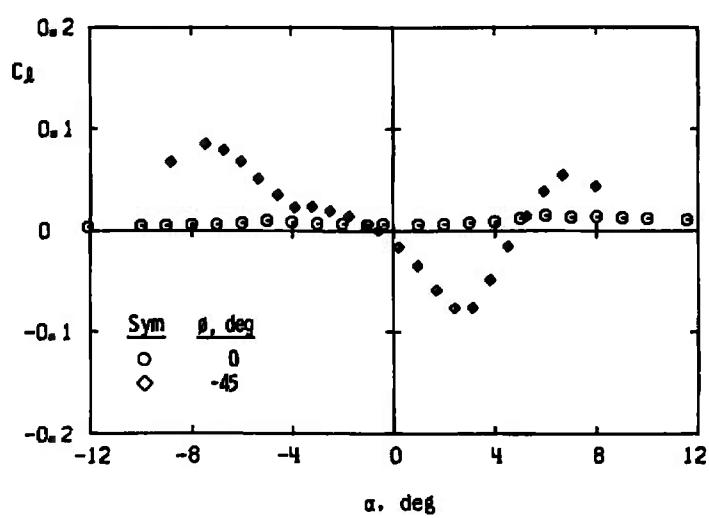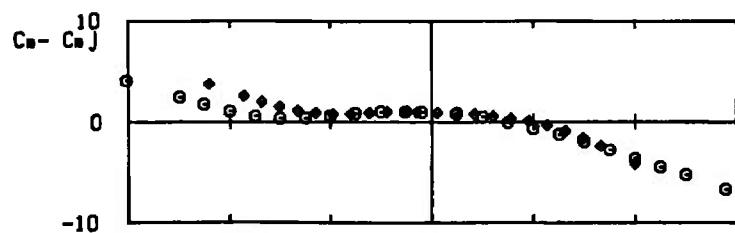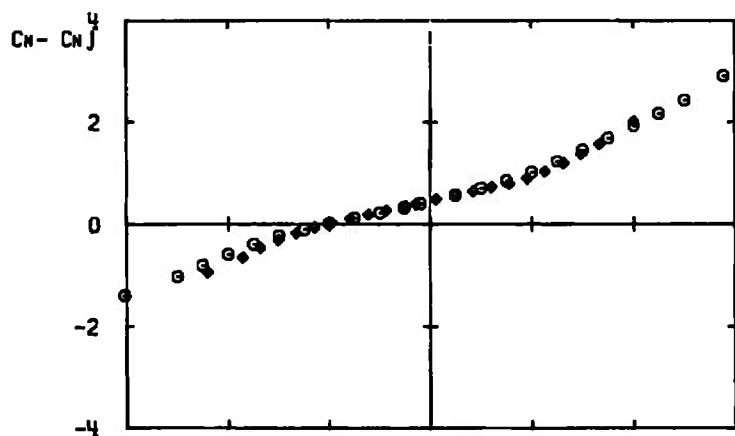
m. Variable ϕ, $p_j/p_\infty = 268$, $M_\infty = 4.0$, $Re_\ell = 17.1 \times 10^6$
Fig. I-1 Continued

m. Concluded
Fig. I-1 Continued

$C_N - C_{N,j}$

$C_m - C_{m,j}$

C_{ℓ}

Sym	p_j/p_∞	$C_{N,j}$	$C_{m,j}$
◯	0	0	0
◇	265.4	-1.88	-8.21

$\phi = 0$

α, deg
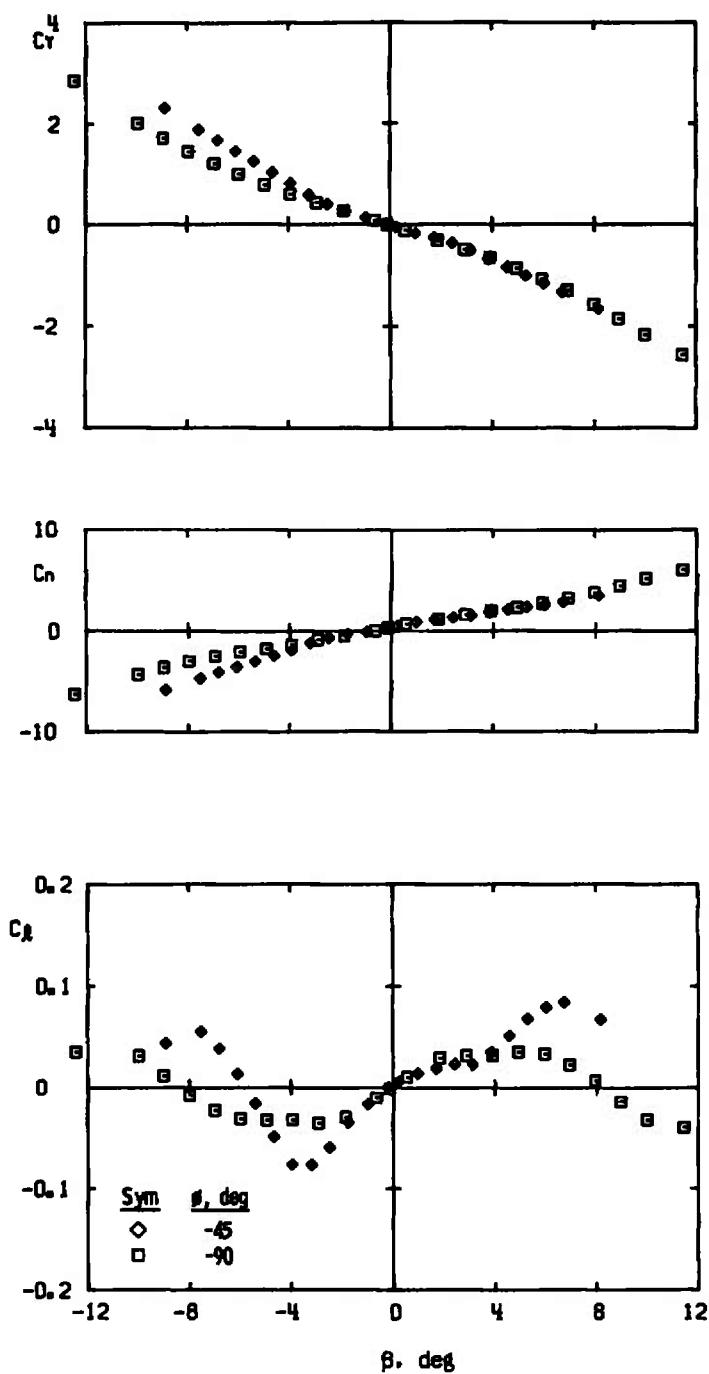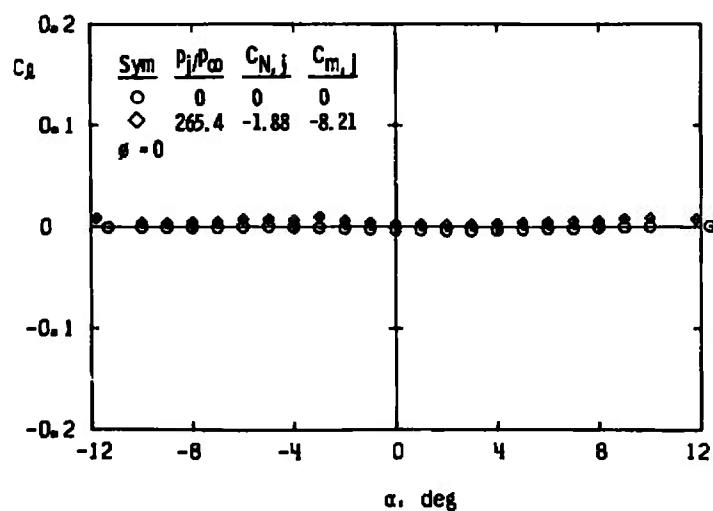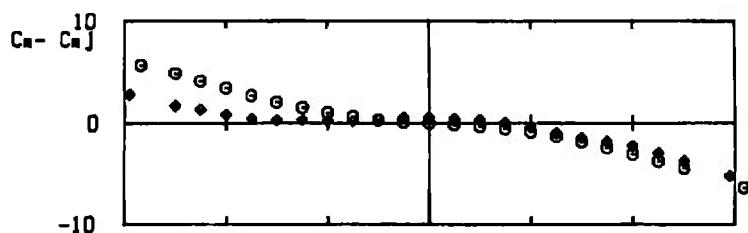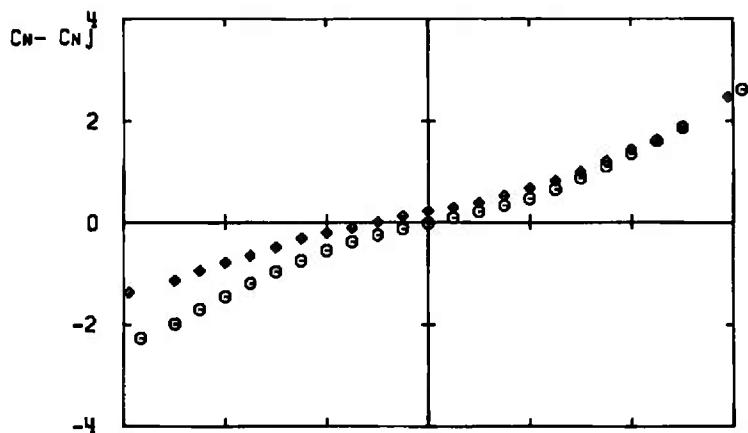
n. $M_\infty = 5.0$, $Re_\ell = 19.3 \times 10^6$
Fig. I-1 Continued
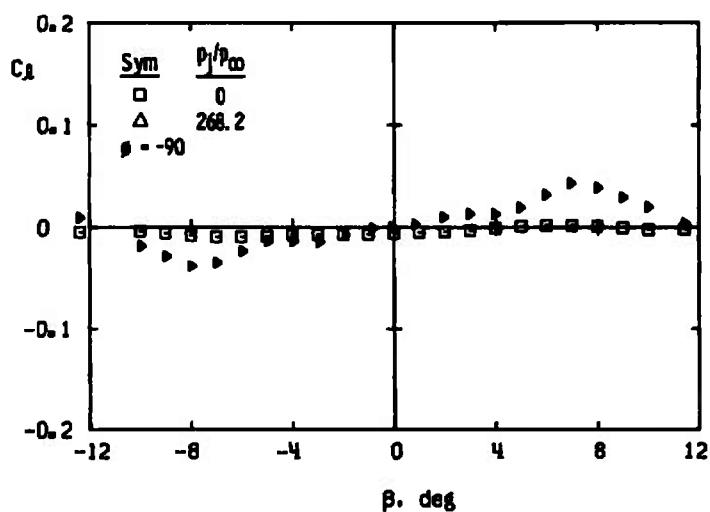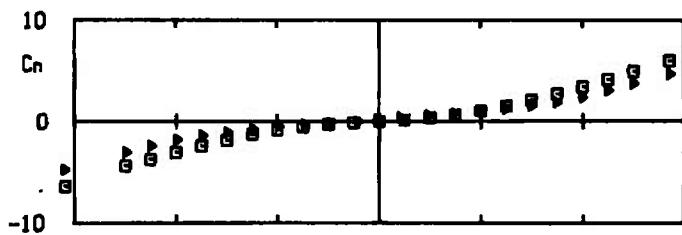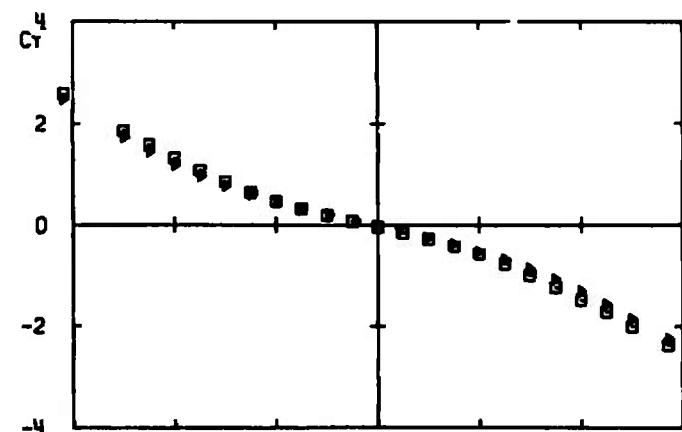
n. Concluded
Fig. I-1 Continued
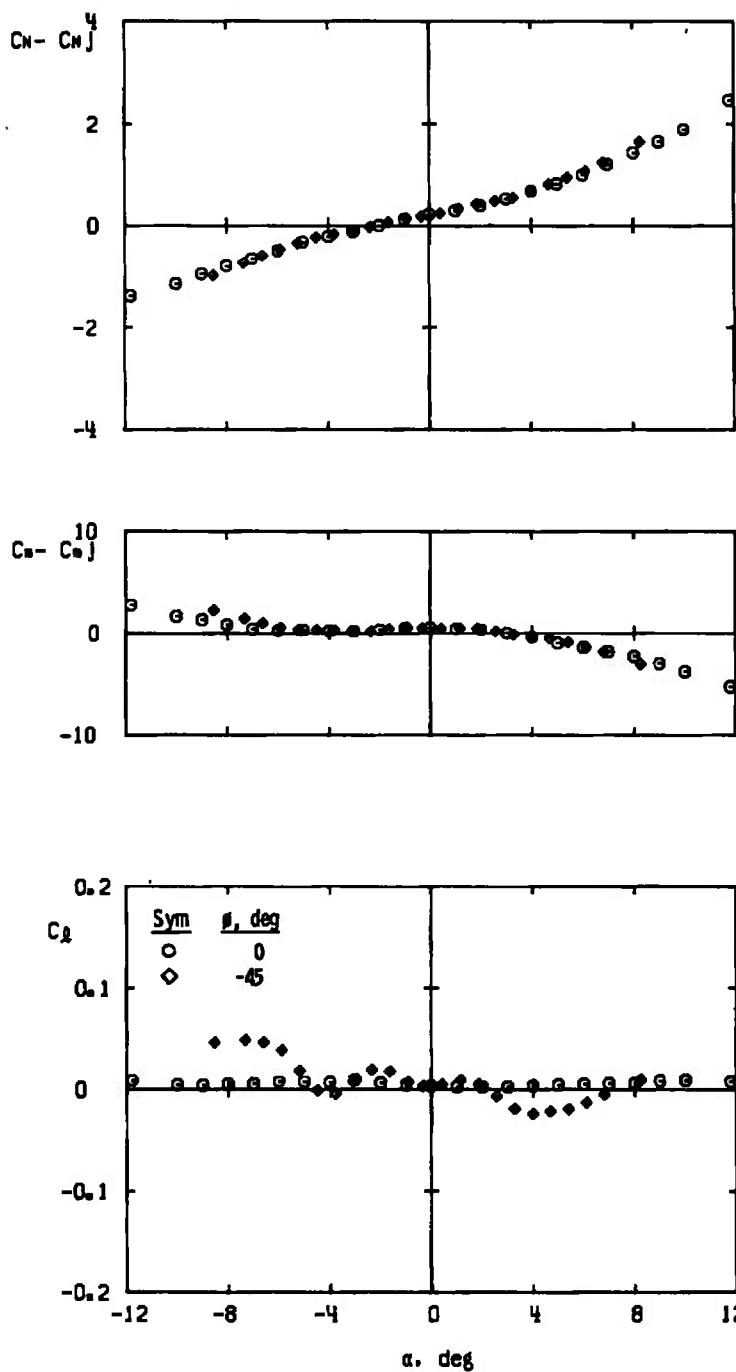
o. Variable ϕ, $p_j/p_\infty = 268$, $M_\infty = 5.0$, $Re\ell = 19.3 \times 10^6$
Fig. I-1 Continued

49
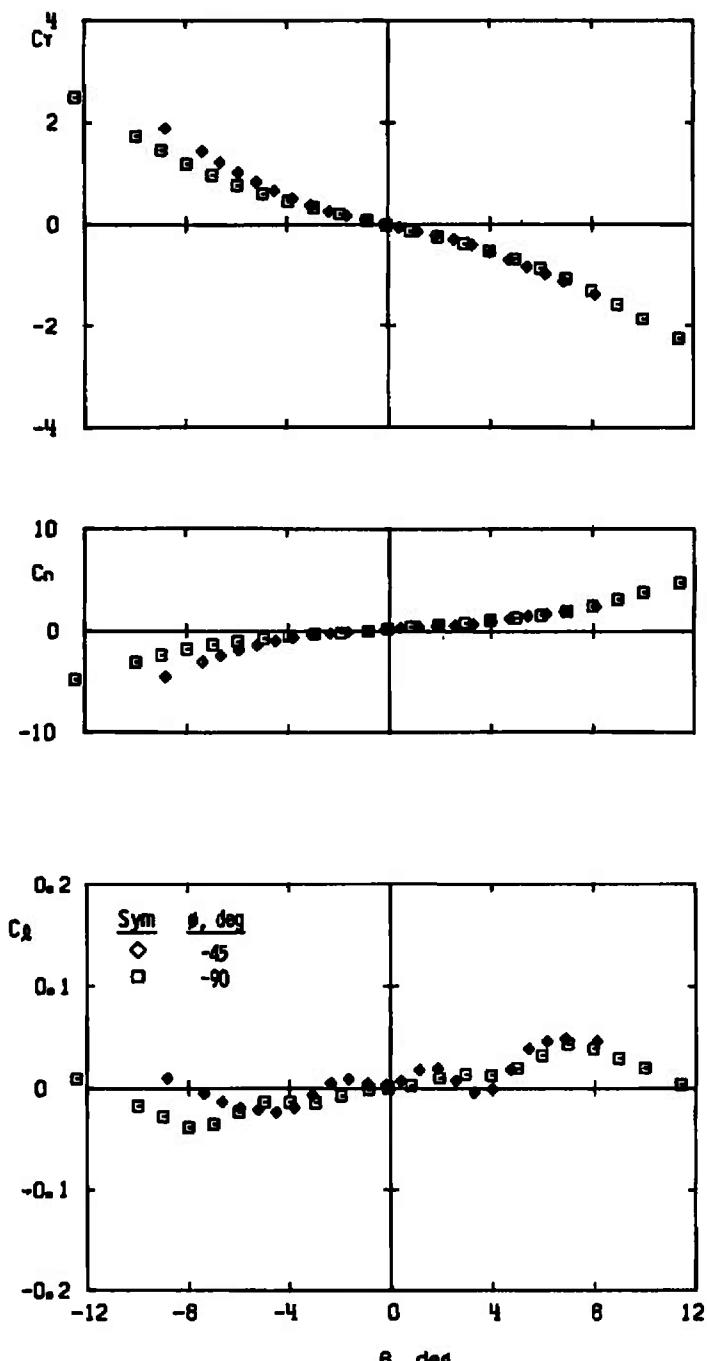
o. Concluded

Fig. I-1 Concluded
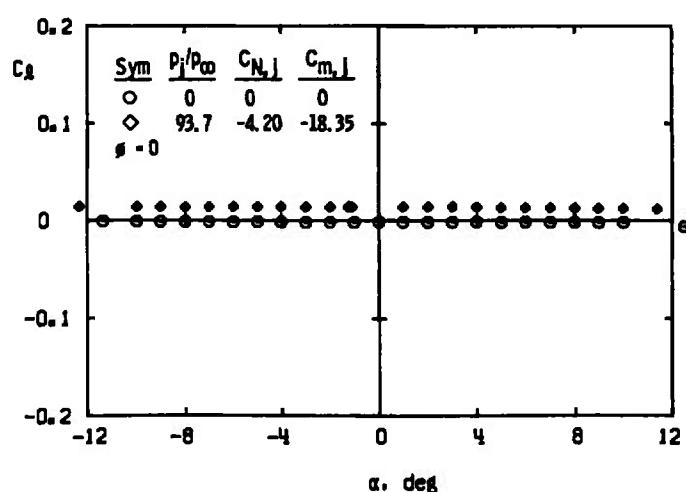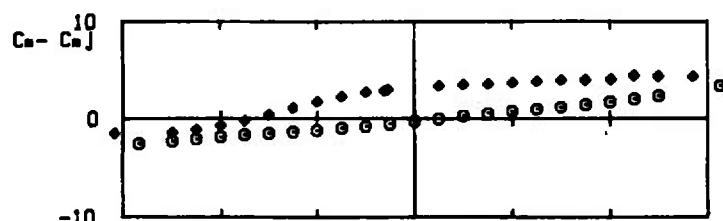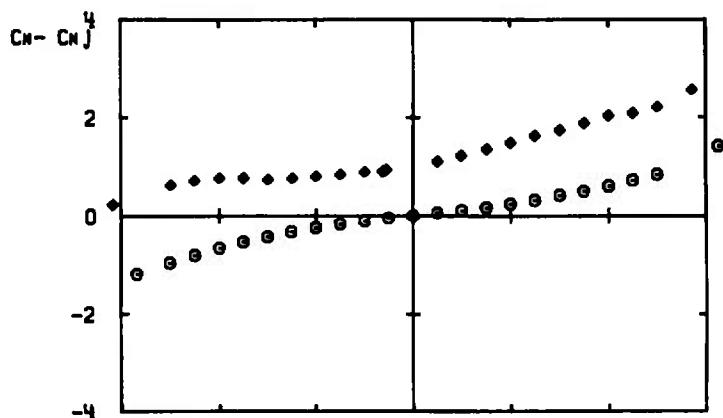
a. $\phi = 0$ and -90 deg, $M_\infty = 2.0$, $Re_\ell = 10.4 \times 10^6$

Fig. I-2 Control Jet Effects on the ATR Missile with the Nozzle Jets at $x_j/D = 4.37$ and the Missile Fins Off
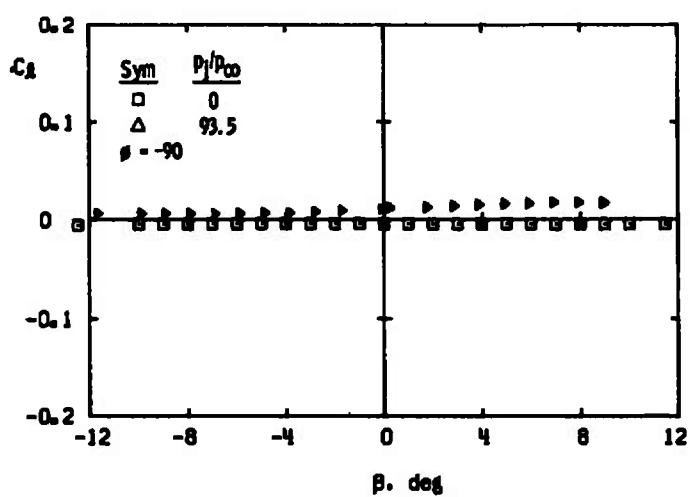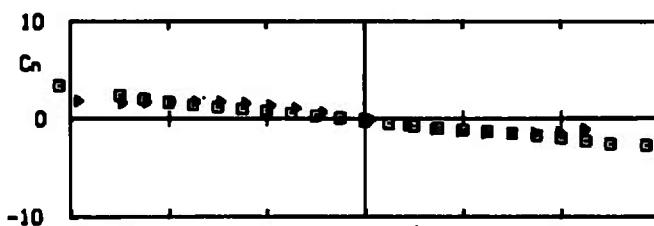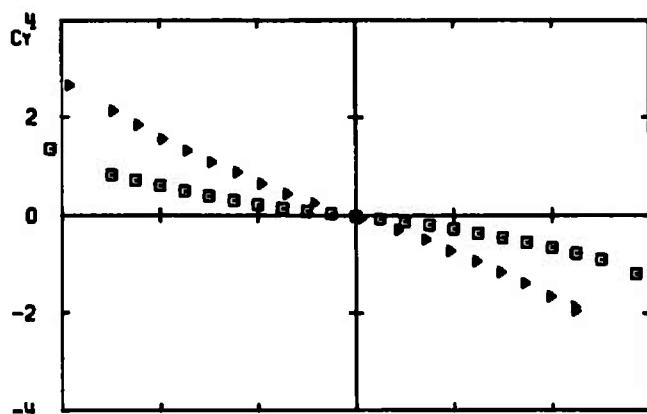
a. Concluded
Fig. I-2 Continued
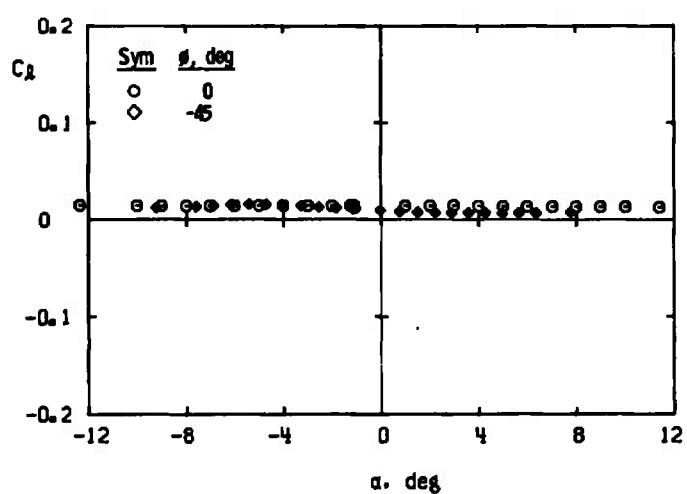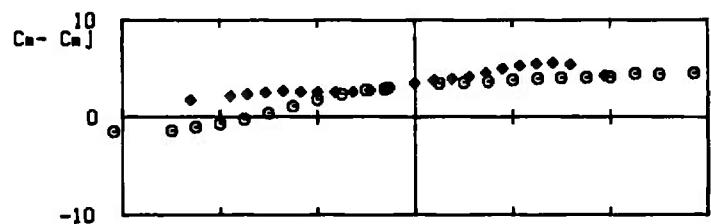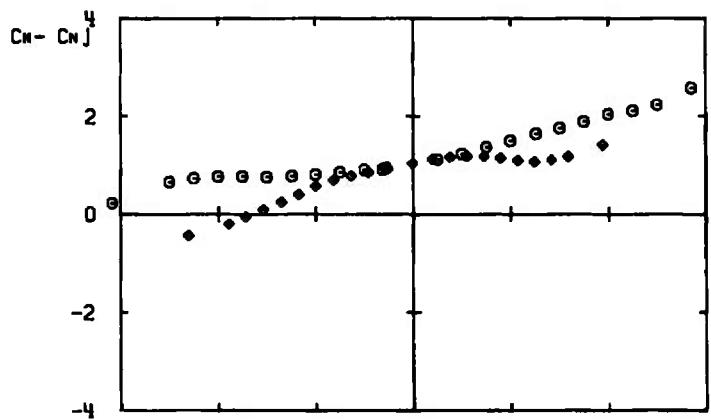
b. Variable ϕ, $p_j/p_\infty = 93.0$, $M_\infty = 2.0$, $Re_\ell = 10.4 \times 10^6$
Fig. I-2 Continued
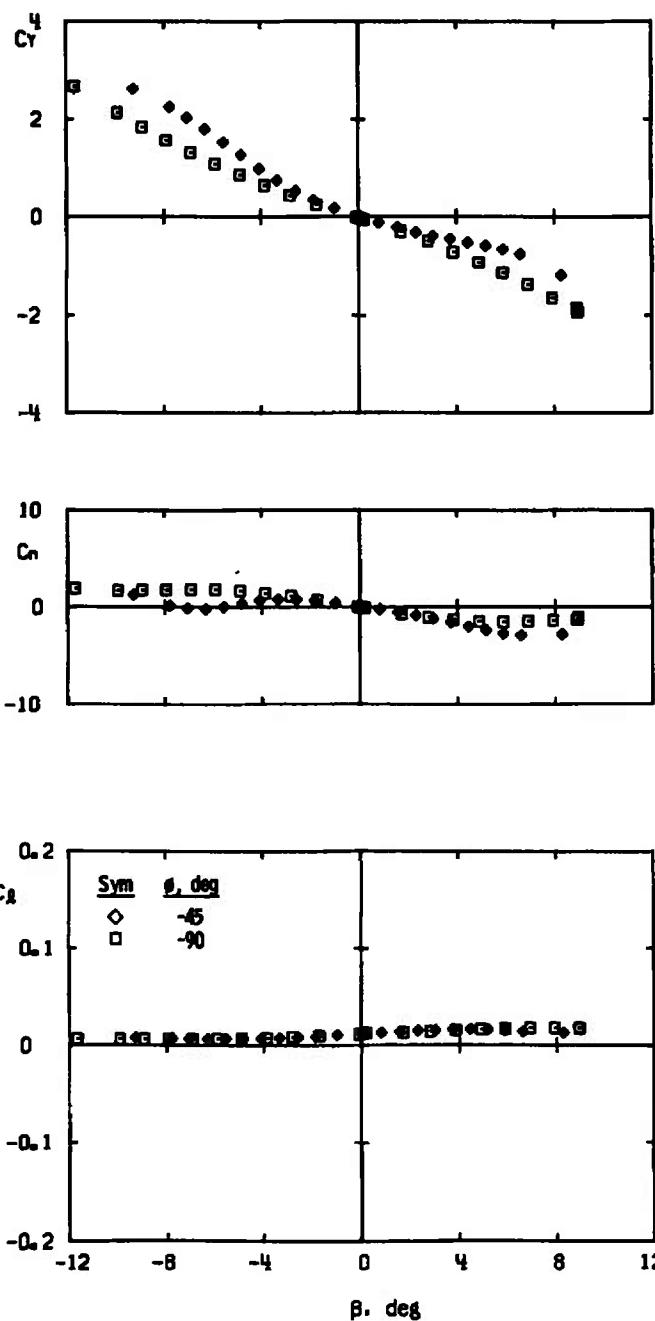
b. Concluded
Fig. I-2 Continued
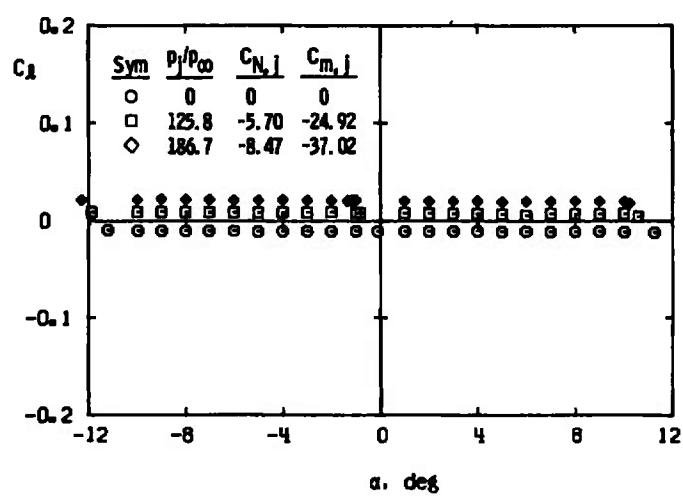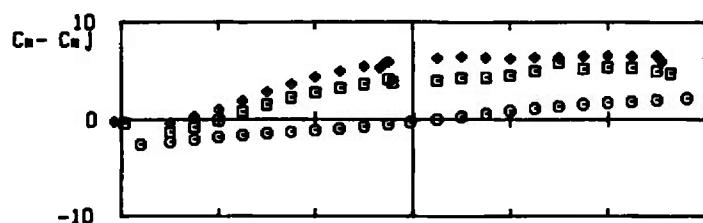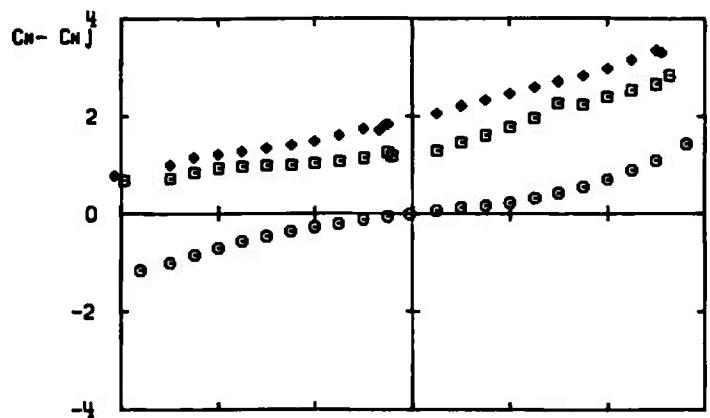
c. $\phi = 0$, $M_\infty = 2.0$, $Re_\ell = 5.1 \times 10^6$
Fig. I-2 Continued
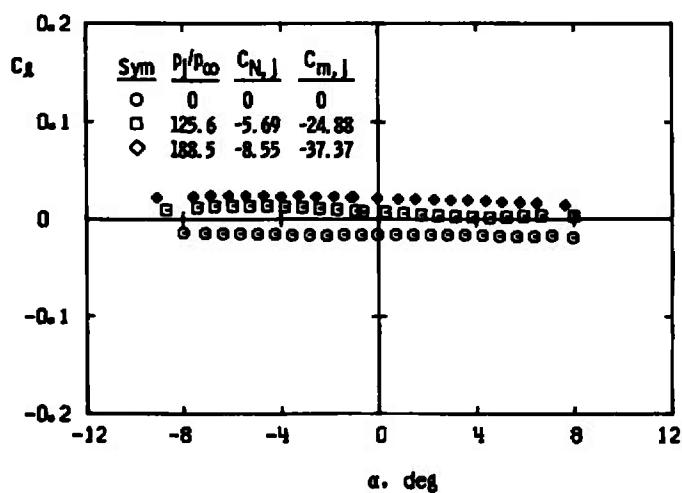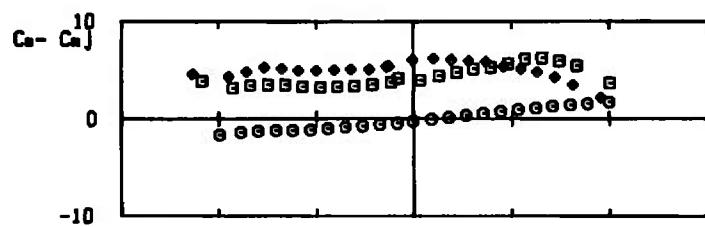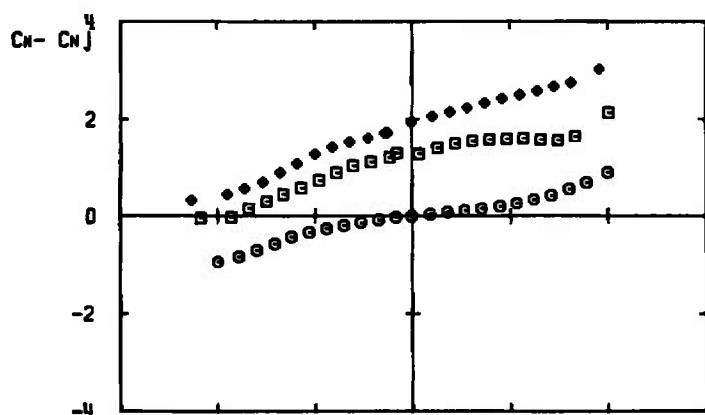
d. $\phi = -45$ deg, $M_\infty = 2.0$, $Re_\ell = 5.1 \times 10^6$
Fig. I-2 Continued
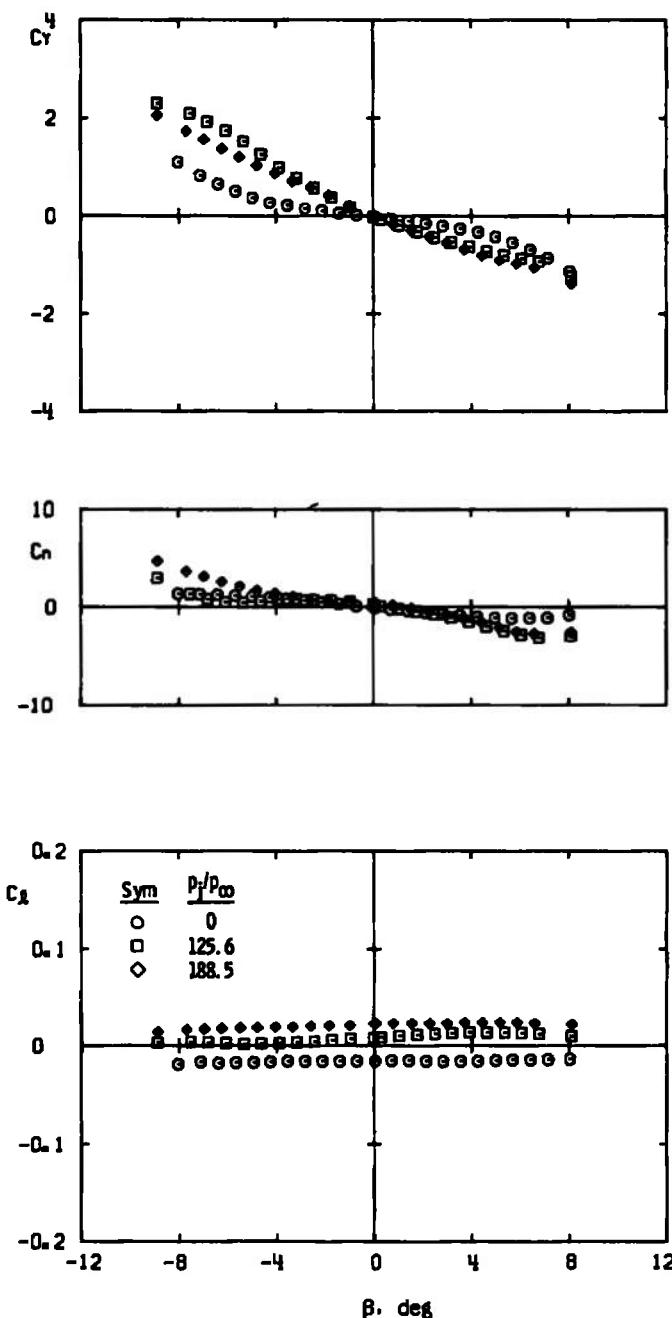
d. Concluded
Fig. I-2 Continued

57
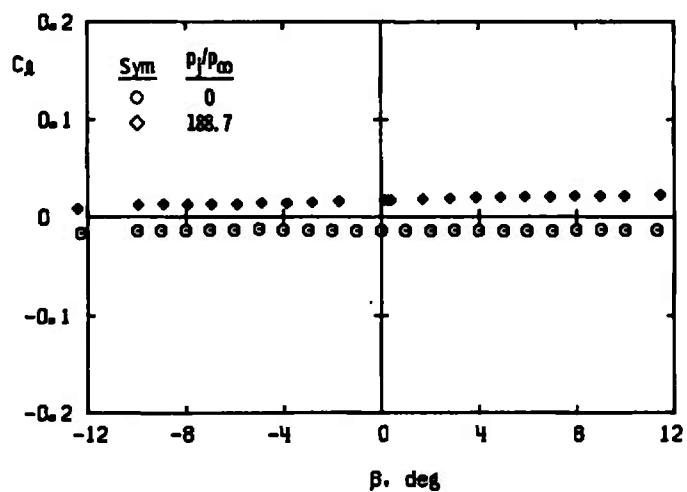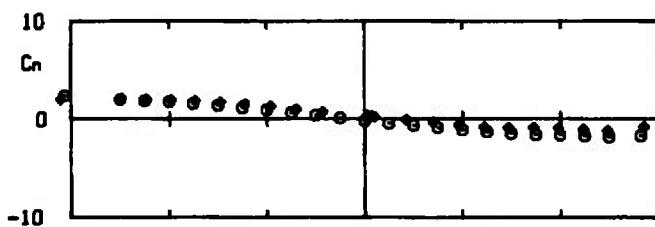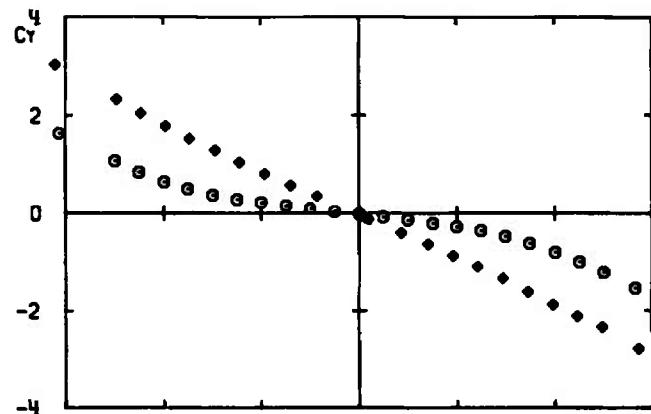
e. ϕ = -90 deg, M_∞ = 2.0, Re_ℓ = 5.1 x 10⁶
Fig. I-2 Continued
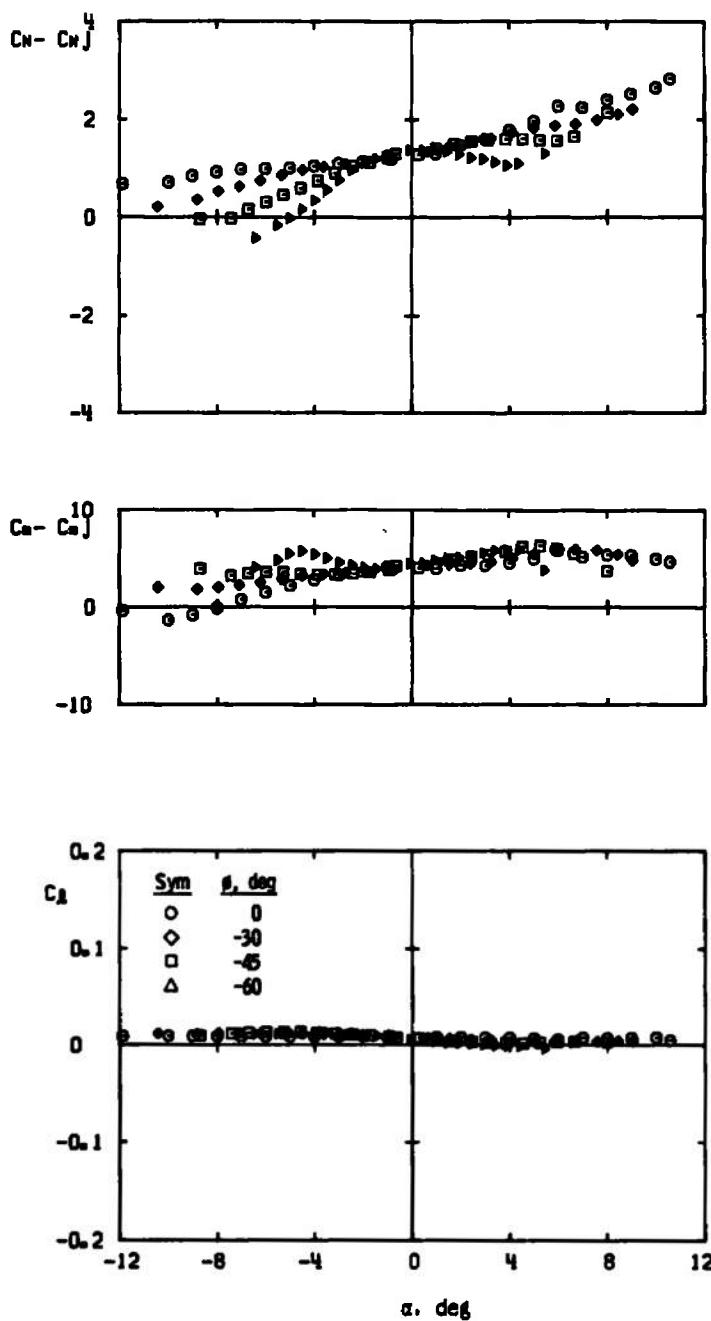
f. Variable ϕ, $p_j/p_\infty = 275$, $M_\infty = 2.0$, $Re\ell = 5.1 \times 10^6$
Fig. I-2 Continued
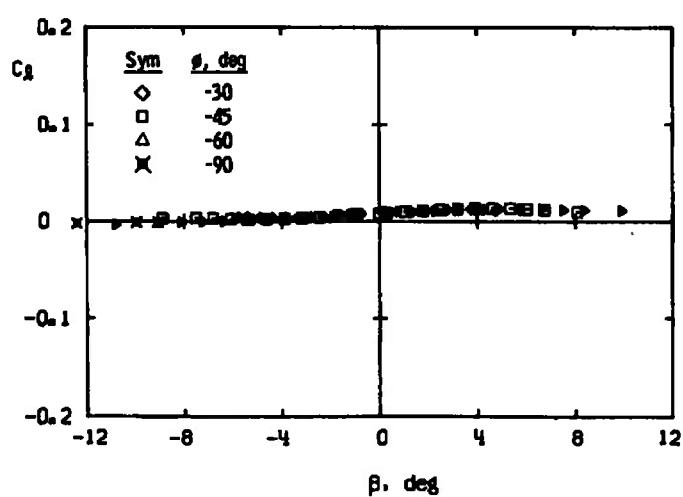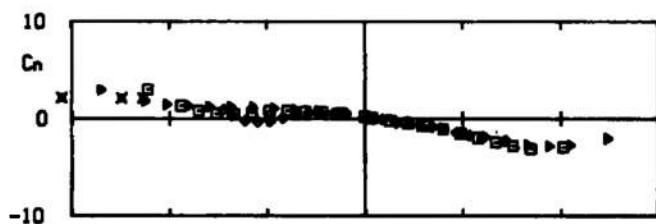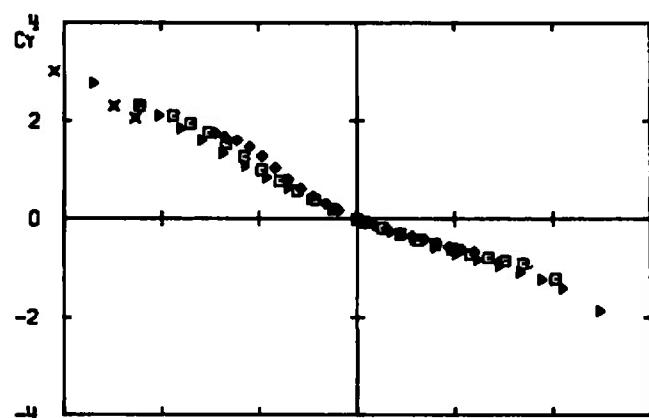
f. Concluded
Fig. I-2 Continued
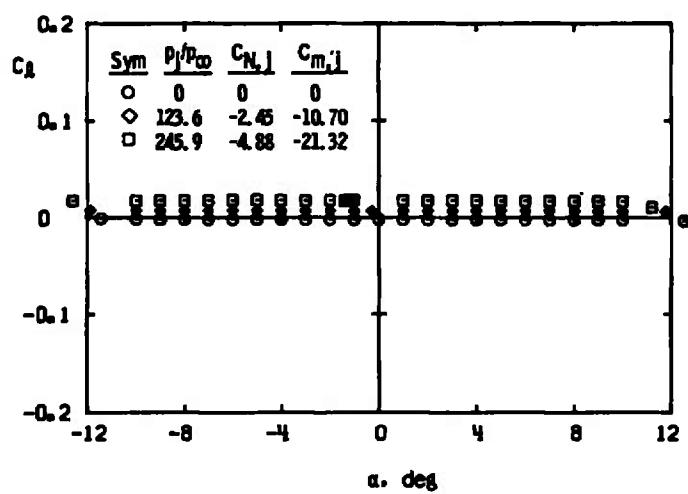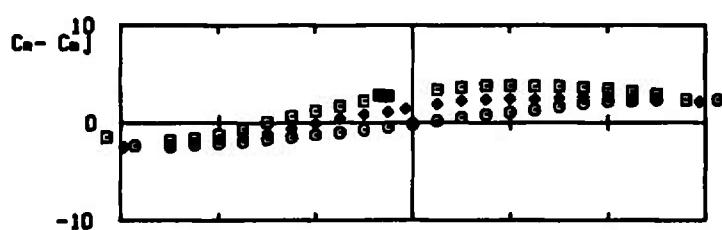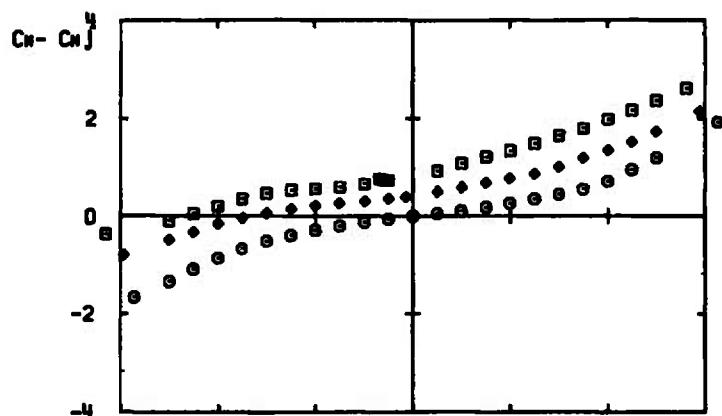
g. $\phi = 0$, $M_\infty = 3.0$, $Re_\ell = 12.5 \times 10^6$
Fig. I-2 Continued
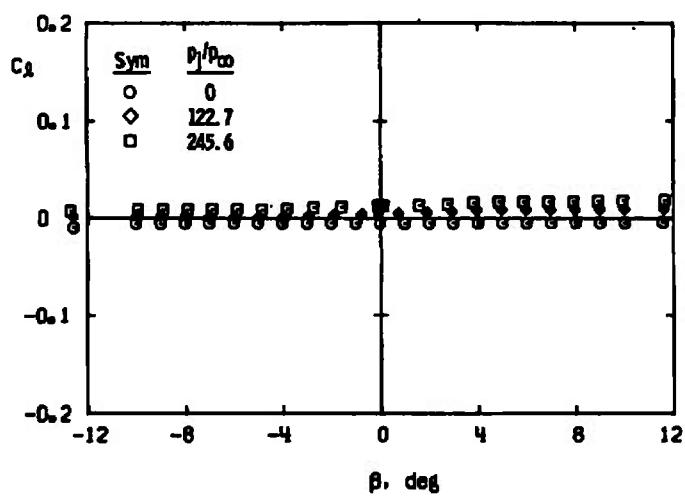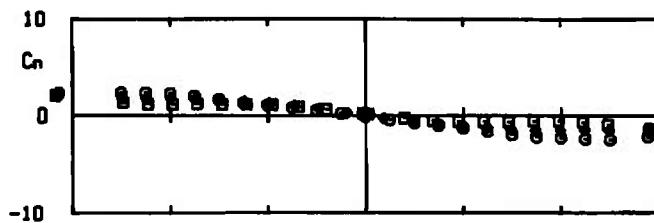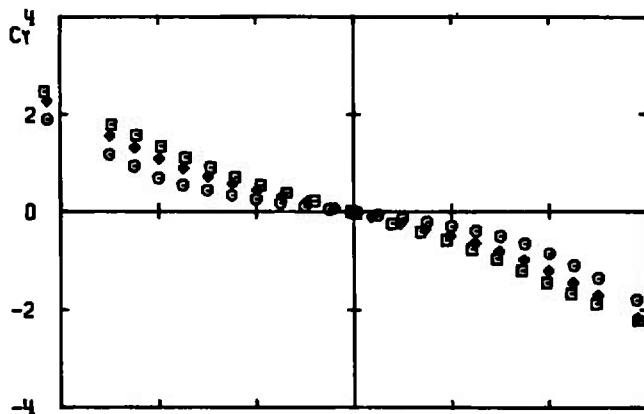
h. ϕ = -90 deg, M_∞ = 3.0, Re_ℓ = 12.5 x 10^6
Fig. I-2 Continued

i. Variable ϕ, $p_j/p_\infty = 246$, $M_\infty = 3.0$, $Re_\ell = 12.5 \times 10^6$
Fig. I-2 Continued

i. Concluded
Fig. I-2 Continued

j. $\phi = 0$, $M_\infty = 4.0$, $Re_\ell = 17.1 \times 10^6$
Fig. I-2 Continued
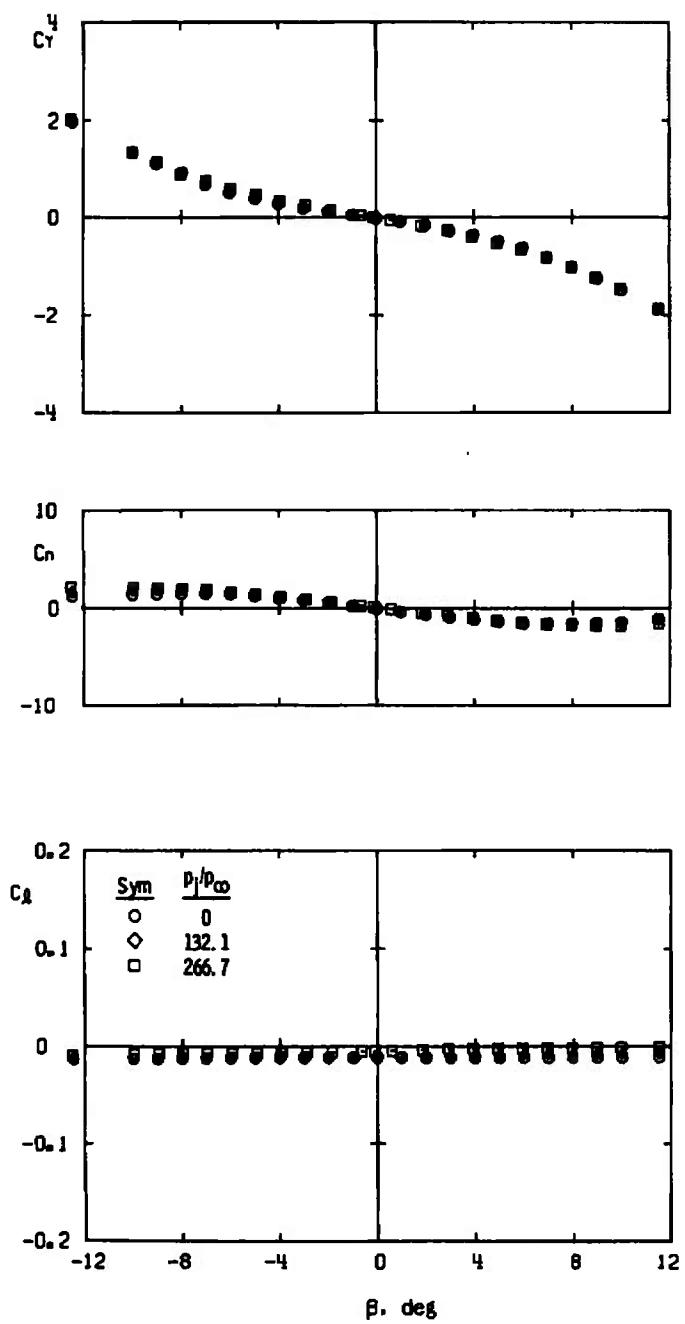
k. ϕ = -90 deg, M_∞ = 4.0, Reℓ =17.1 x 10^6
Fig. I-2 Continued
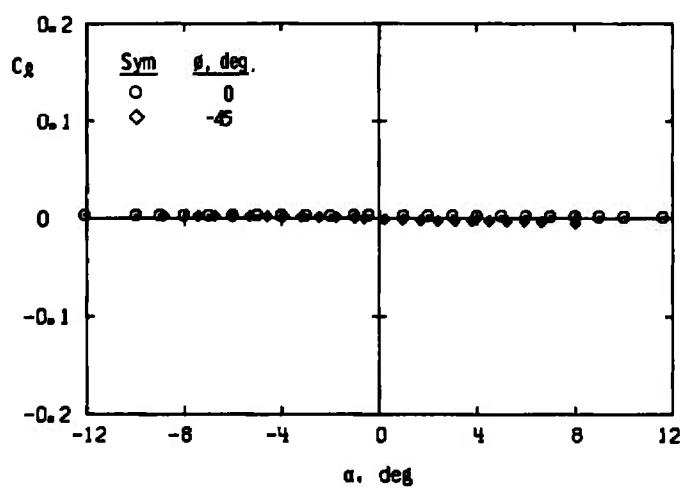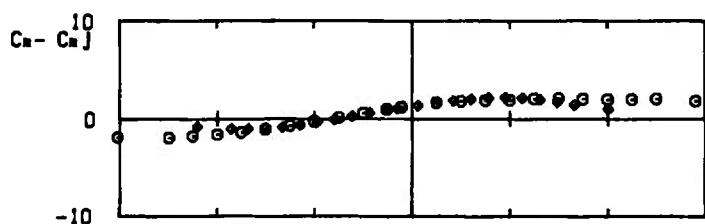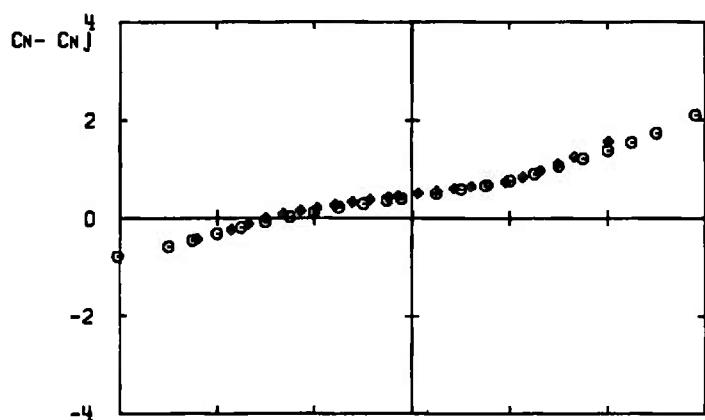
I. Variable ϕ, $p_j/p_\infty = 268$, $M_\infty = 4.0$, $Re_\ell = 17.1 \times 10^6$
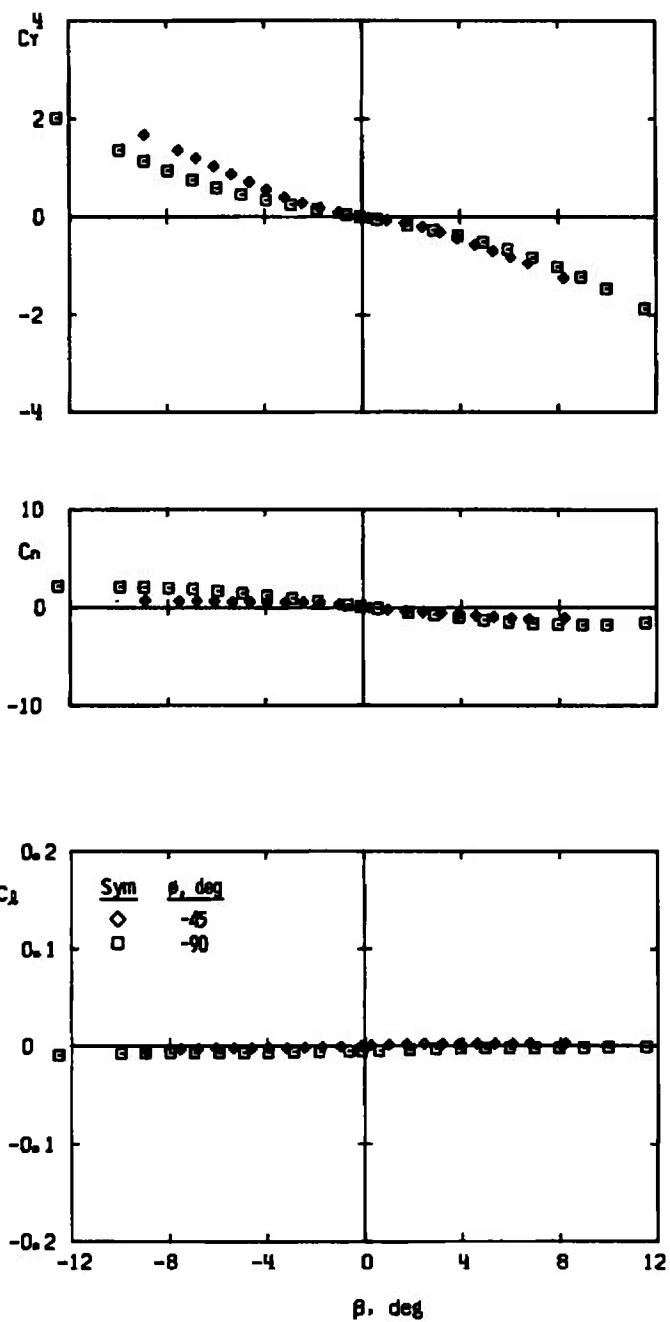
Fig. I-2 Continued

I. Concluded
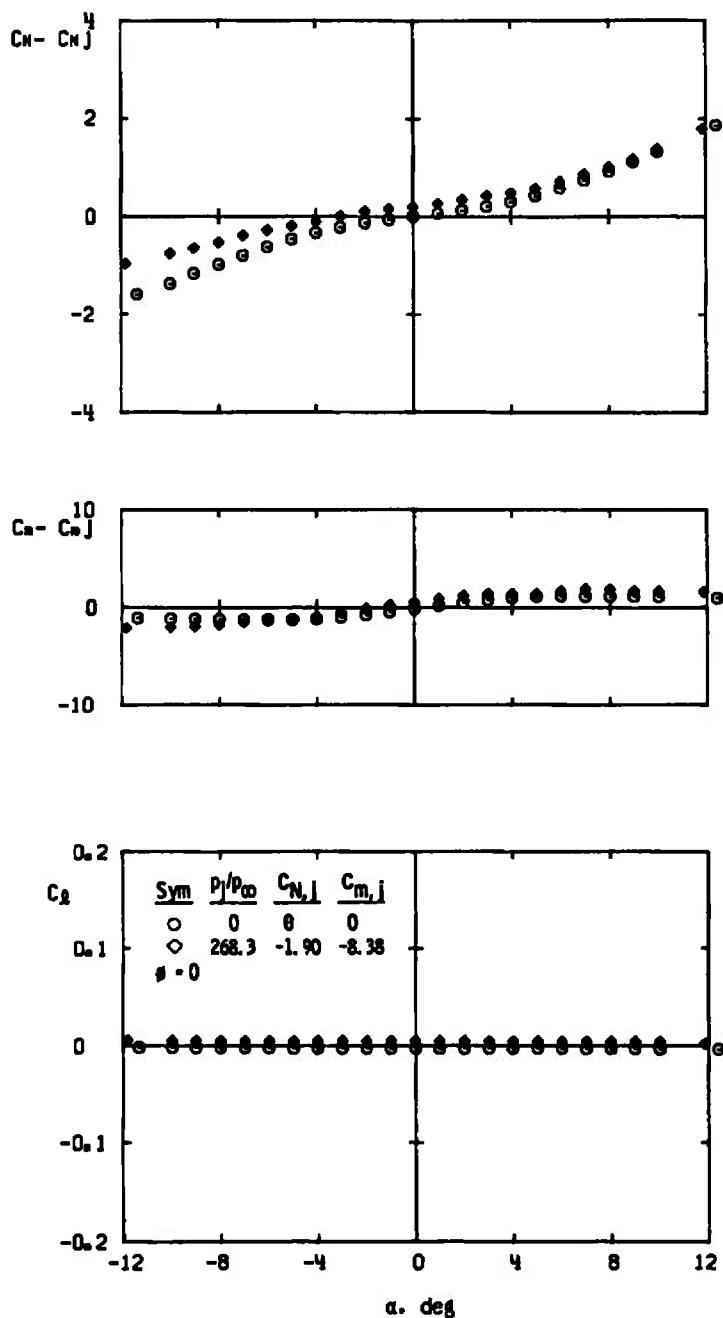
Fig. I-2 Continued

m. $\phi = 0$ and -90 deg, $M_\infty = 5.0$, $Re_\ell = 19.4 \times 10^6$
Fig. I-2 Continued
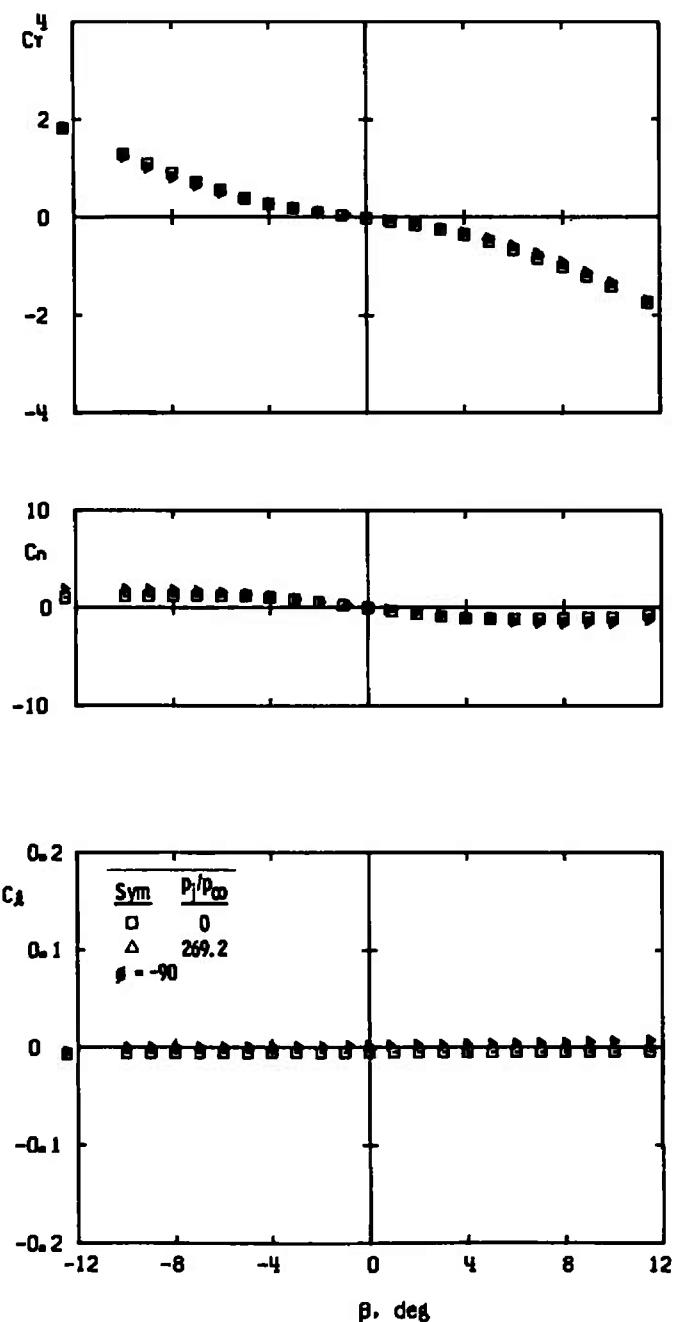
m. Concluded
Fig. I-2 Continued

n. Variable ϕ, p_j/p_∞ = 268, M_∞ = 5.0, $Re\ell$ = 19.4 x 10^6
Fig. I-2 Continued
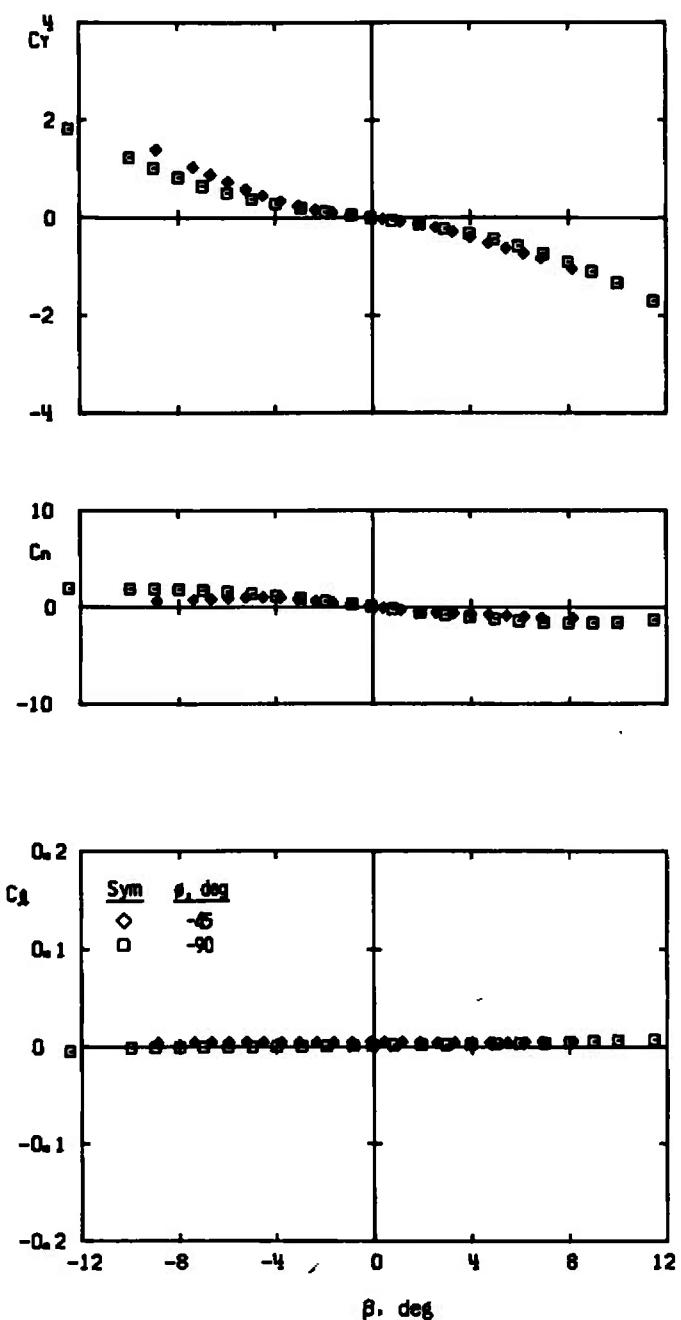
n. Concluded
Fig. I-2 Concluded
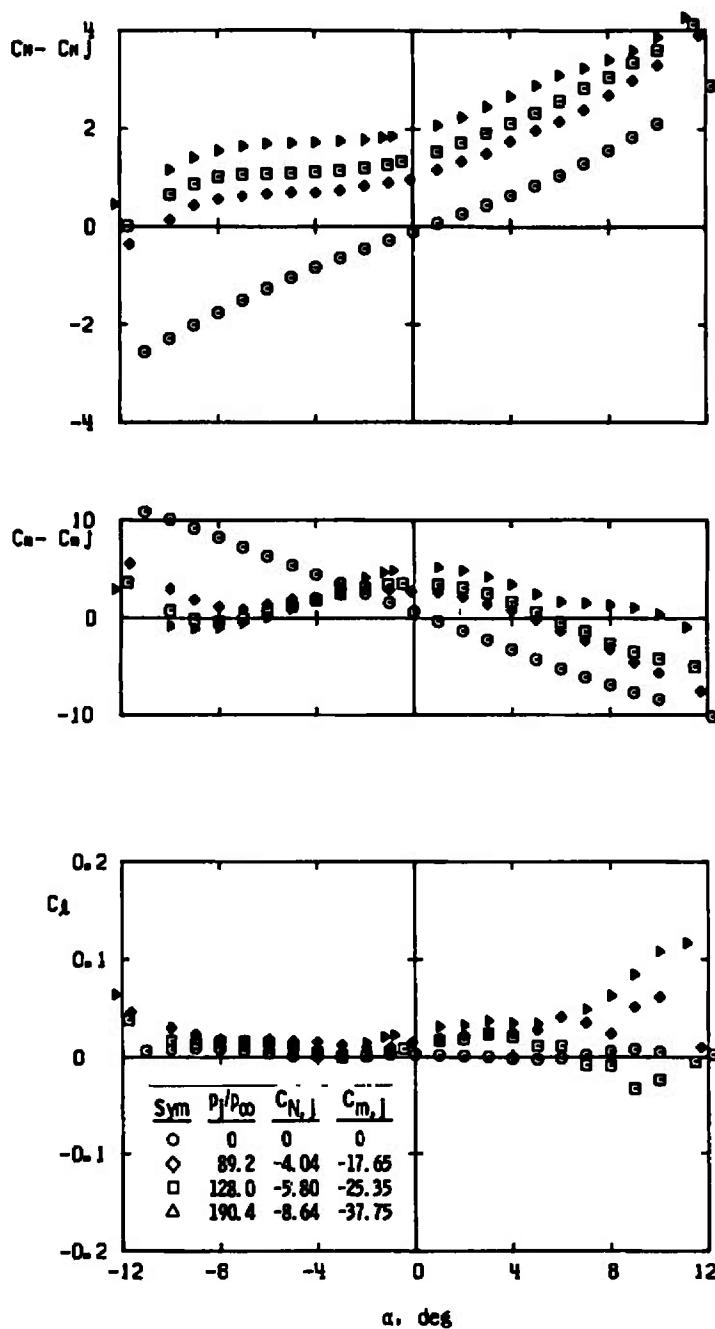
a. $\phi = 0$, $M_\infty = 2.0$, $Re_\ell = 5.1 \times 10^6$

Fig. I-3 Control Jet Effects on the ATR Missile with the Nozzle Jets at $x_j/D = 4.37$ and Rolled 45 deg from the Missile Fins

Sym	p_j/p_∞	$C_{N,j}$	$C_{m,j}$
○	0	0	0
◇	92.4	-4.19	-18.29
□	125.8	-5.70	-24.92
△	191.3	-8.68	-37.93
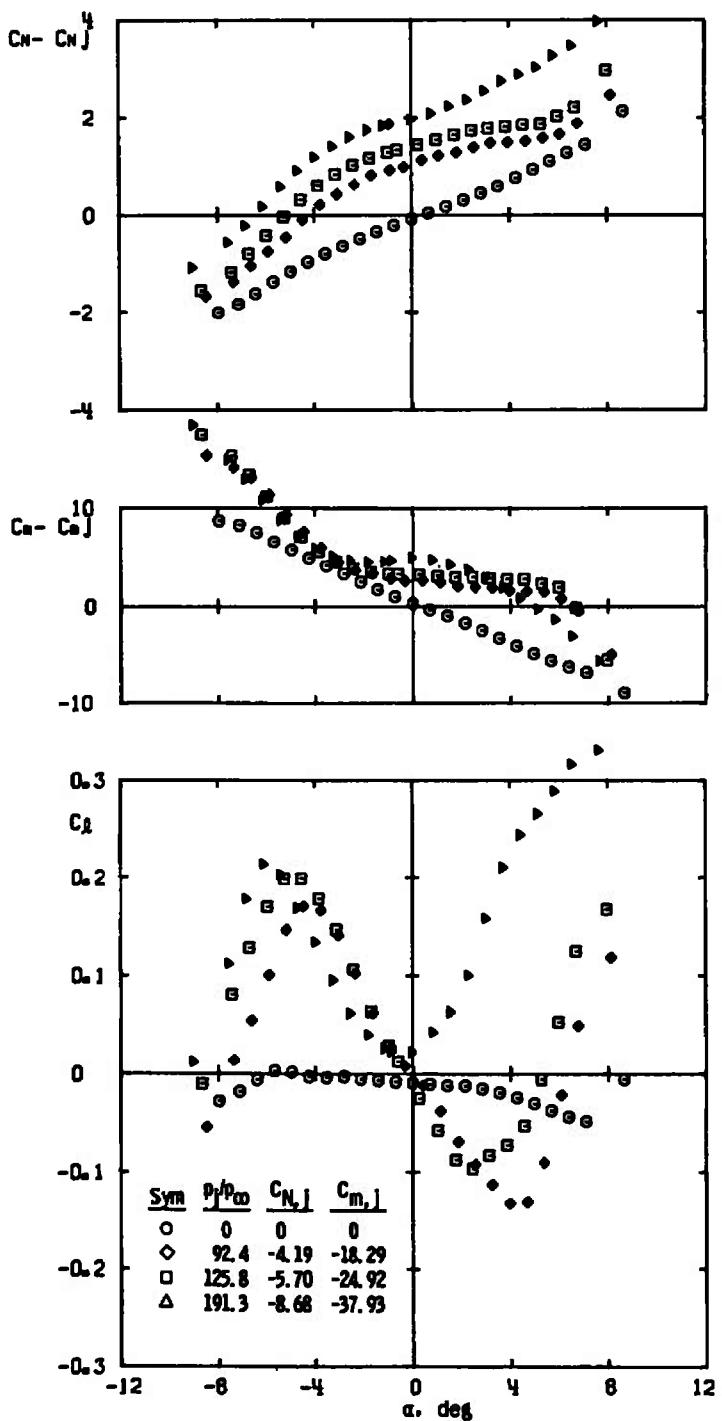
b. ϕ = -45 deg, M_∞ = 2.0, $Re\ell$ = 5.1 x 10⁶
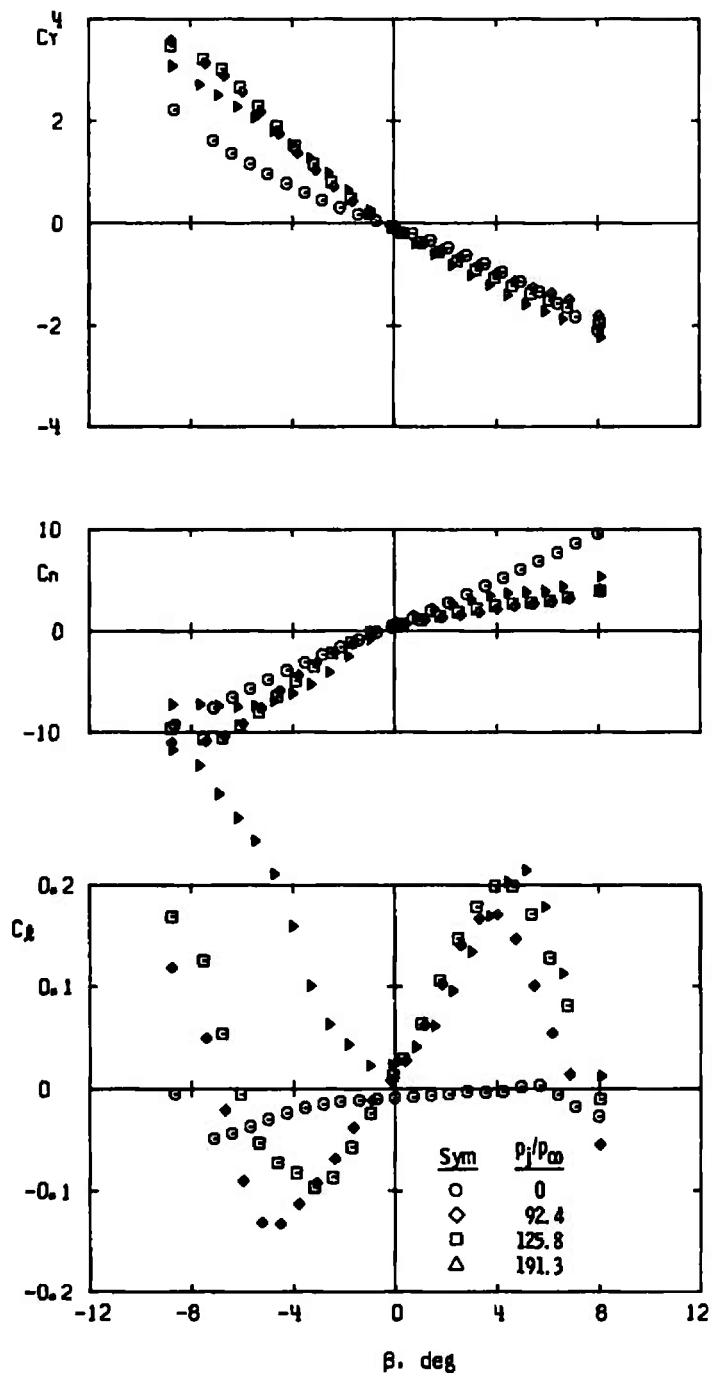
Fig. I-3 Continued

b. Concluded
Fig. I-3 Continued

c. ϕ = -90 deg, M_∞ = 2.0, Re_ℓ = 5.1 x 10^6

Fig. I-3 Continued

d. $\phi = 0$, $M_\infty = 3.0$, $Re_\ell = 12.5 \times 10^6$
Fig. I-3 Continued

Sym	p_j/p_∞	C_{N_j}	C_{m_j}
○	0	0	0
◇	122.8	-2.43	-10.63
□	209.3	-4.15	-18.15
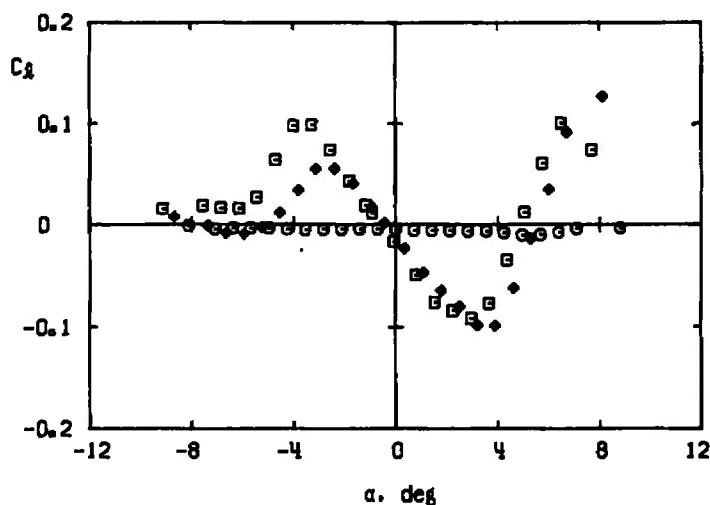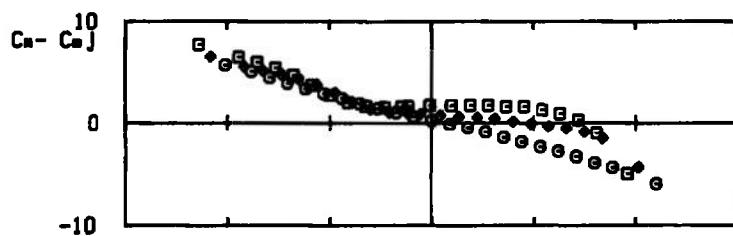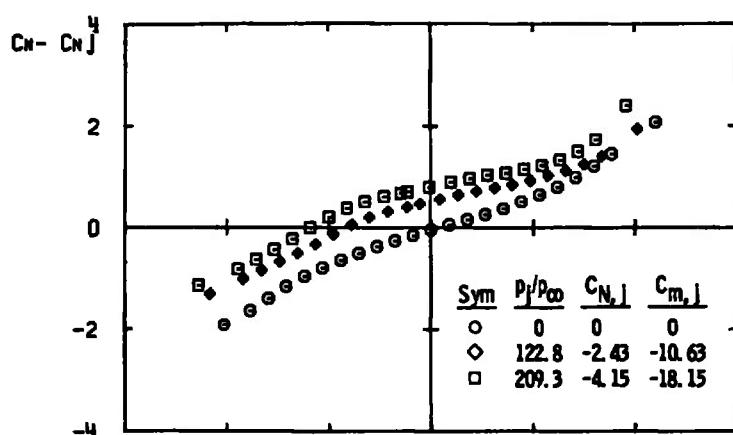
e. ϕ = -45 deg, M_∞ = 3.0, Re_ℓ = 12.5 x 10^6
Fig. I-3 Continued

e. Concluded
Fig. I-3 Concluded
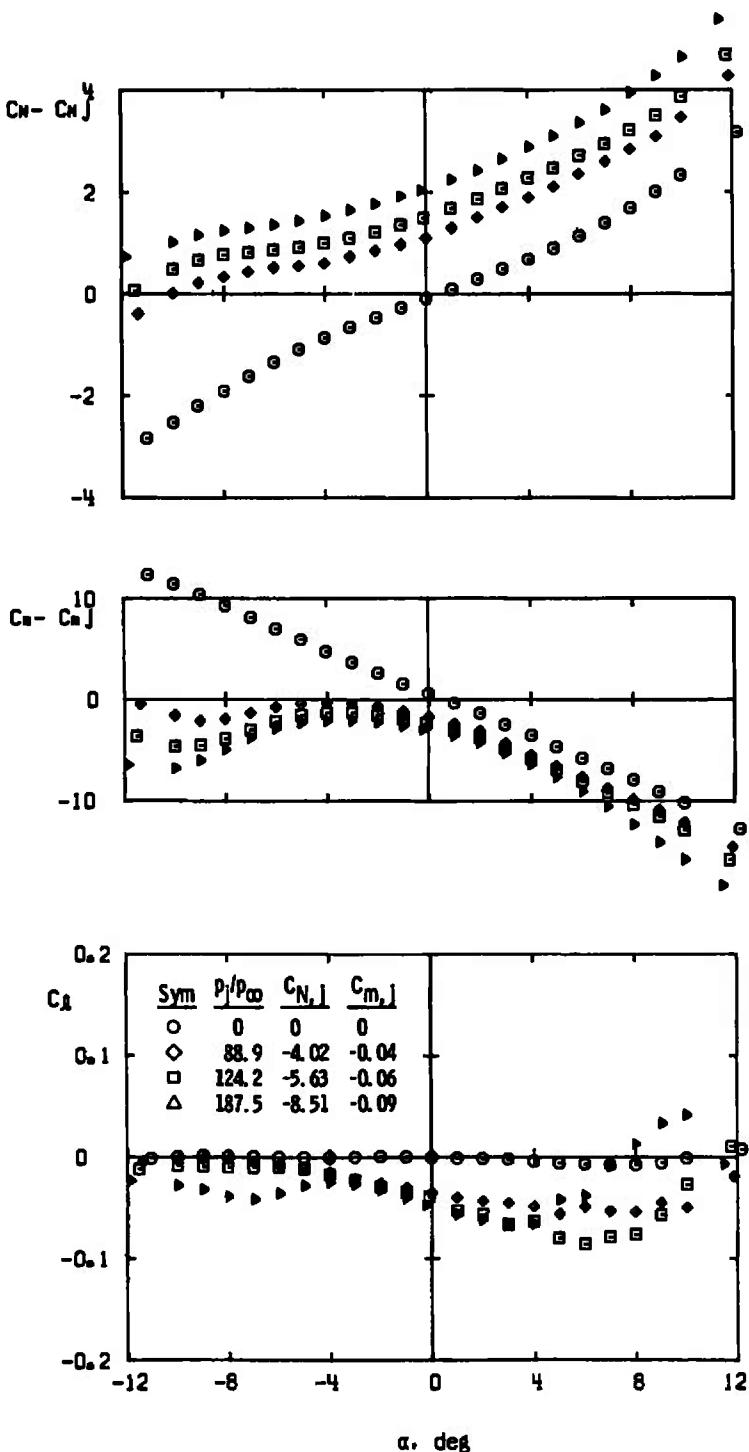
a. $\phi = 0$, $M_\infty = 2.0$, $Re_\ell = 5.1 \times 10^6$

Fig. I-4 Control Jet Effects on the ATR Missile with the Nozzle Jets at $x_j/D = 0.0$ and Aligned with the Fins
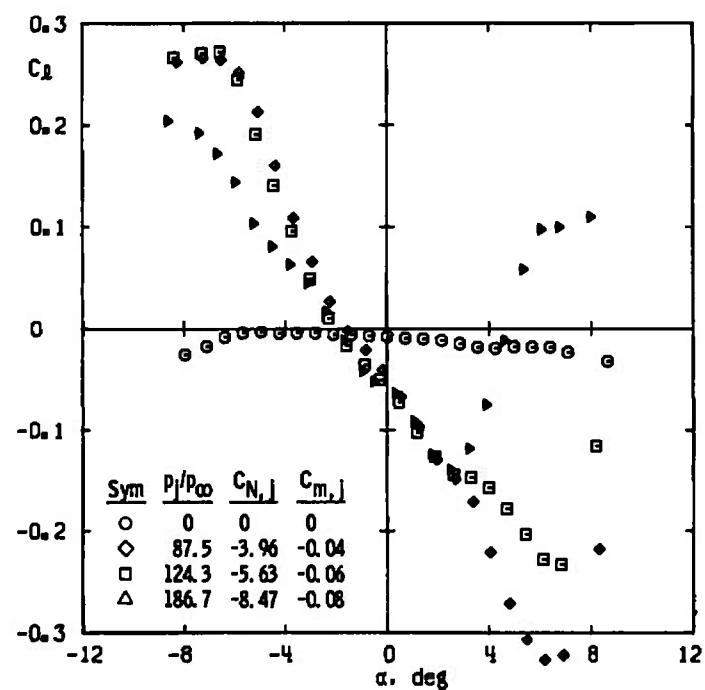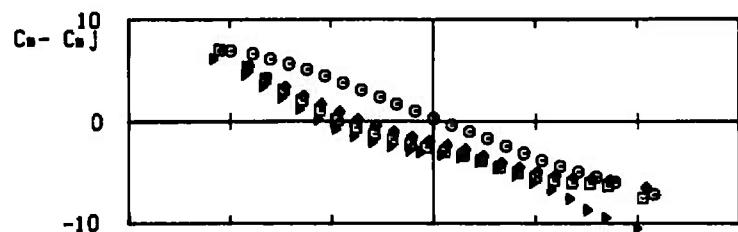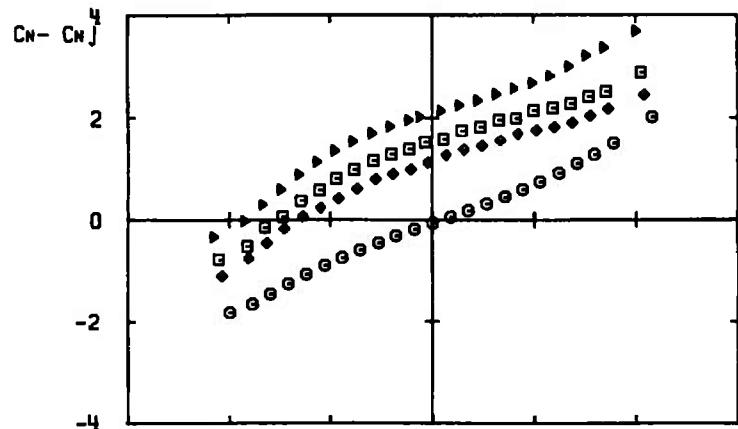
b. ϕ = -45 deg, M_∞ = 2.0, Re_ℓ = 5.1 x 10^6
Fig. I-4 Continued
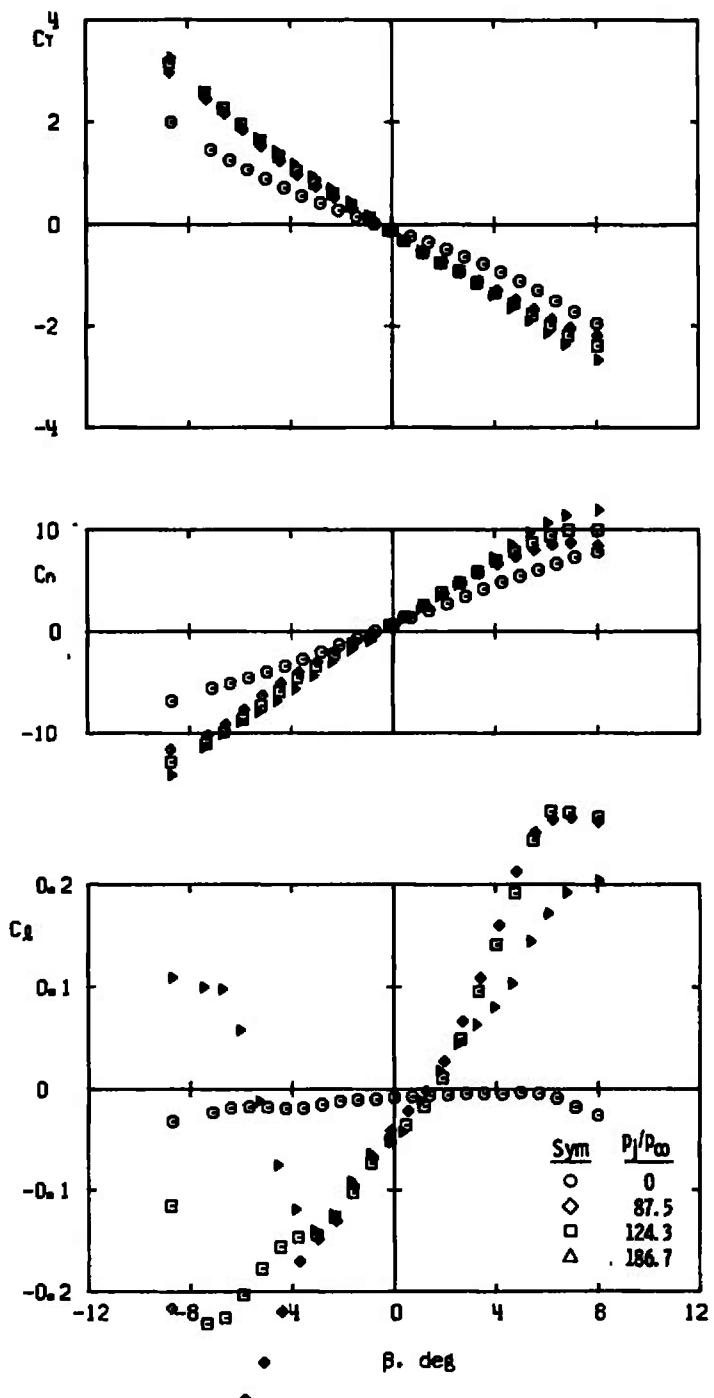
b. Concluded
Fig. I-4 Continued

c. ϕ = -90 deg, M_∞ = 2.0, Reℓ = 5.1 x 10^6
Fig. I-4 Continued

83
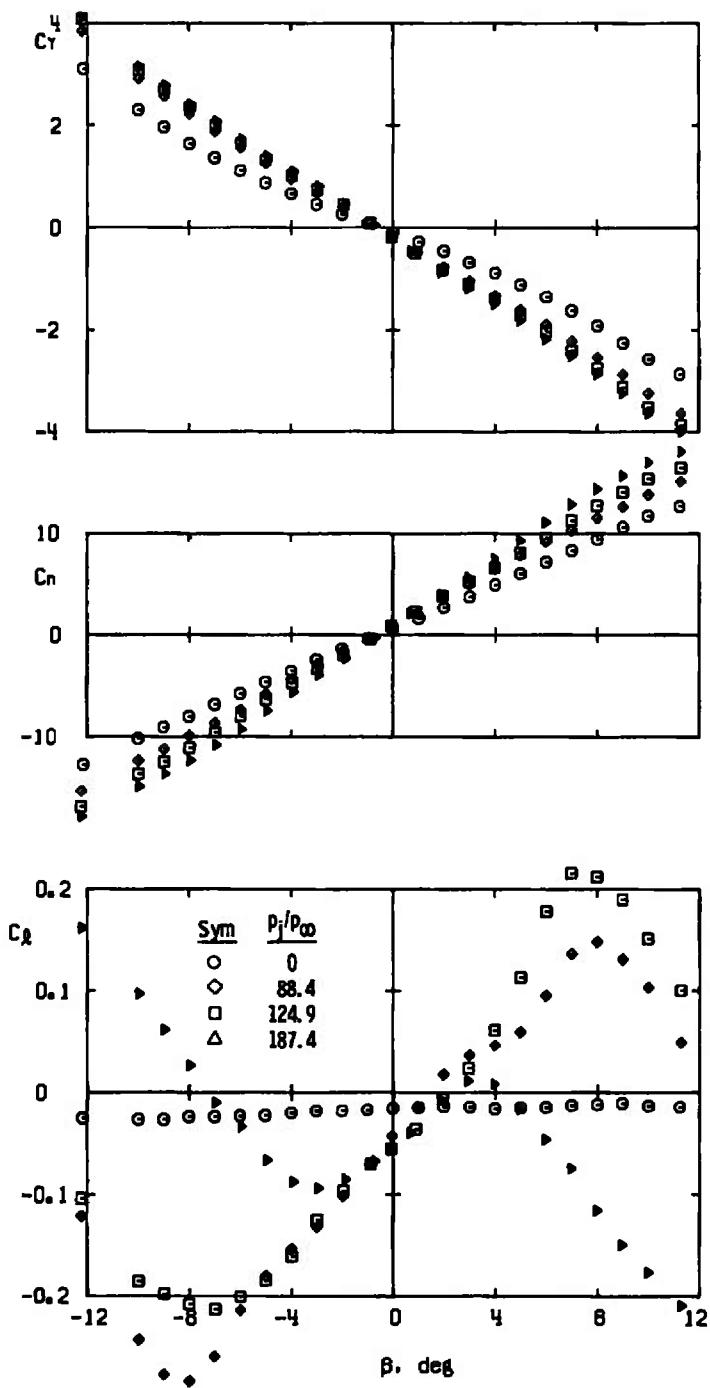
d. $\phi = 0$ and -90 deg, $M_\infty = 2.0$, $Re_\ell = 10.4 \times 10^6$
Fig. I-4 Continued

Sym	p_j/p_∞
□	0
△	93.3
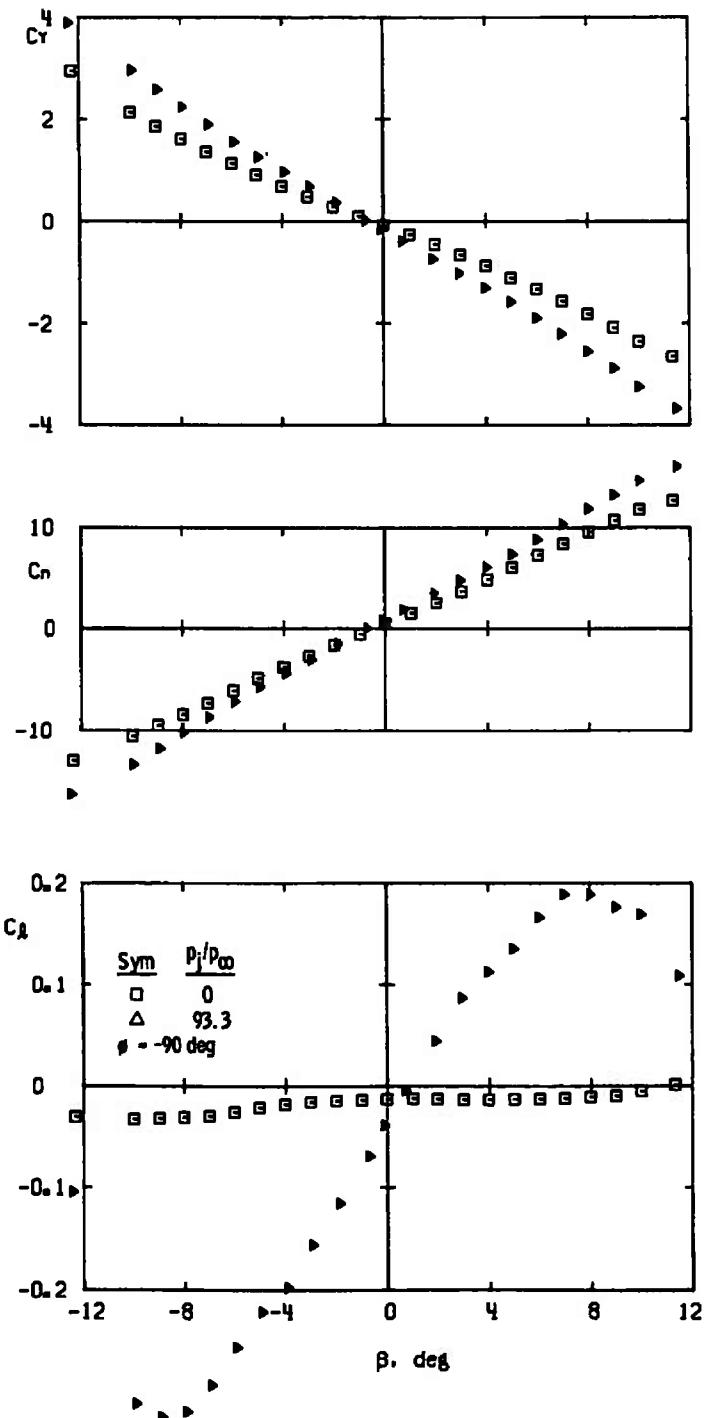
$\phi = -90$ deg

d. Concluded
Fig. I-4 Continued
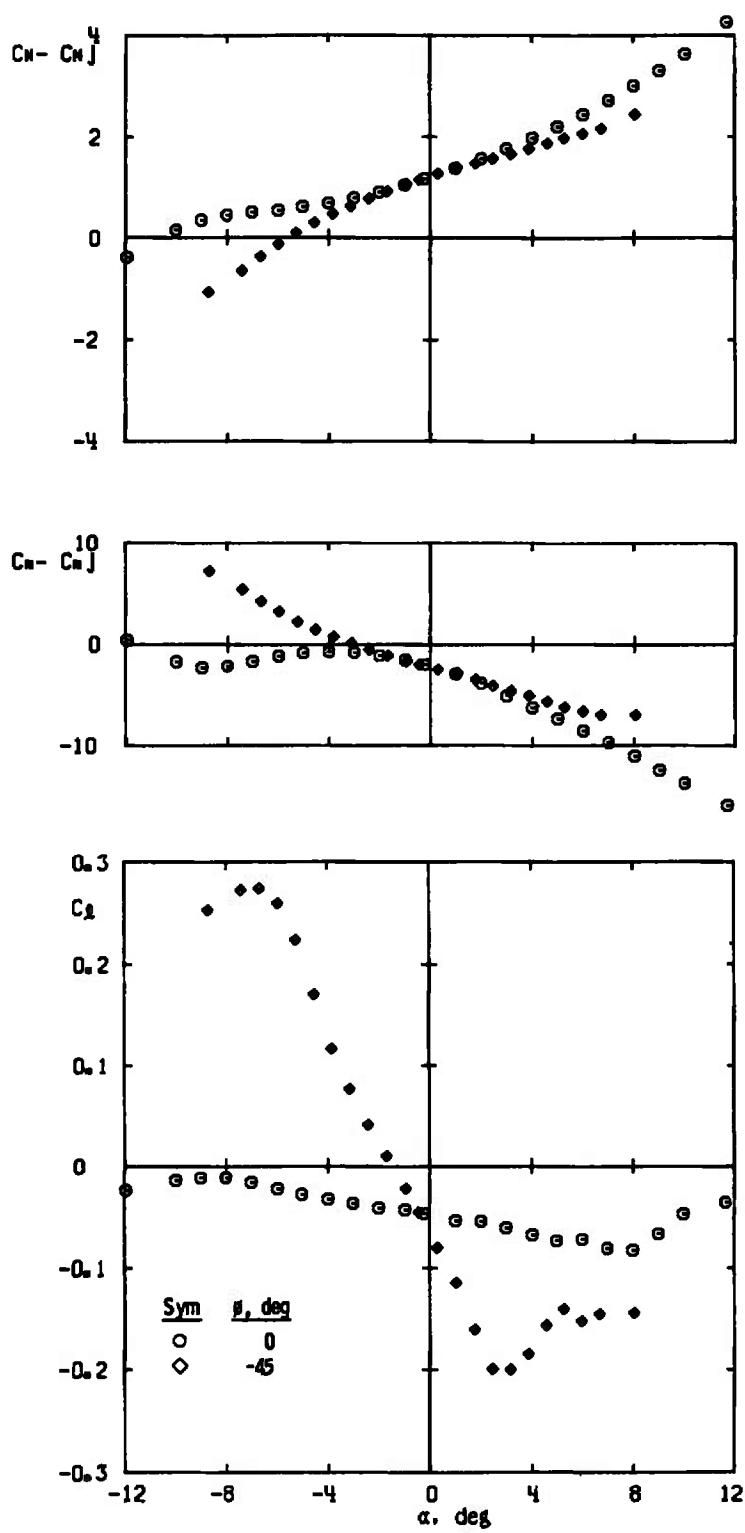
e. Variable ϕ, $p_j/p_\infty = 93.5$, $M_\infty = 2.0$, $Re\ell = 10.4 \times 10^6$
Fig. I-4 Continued
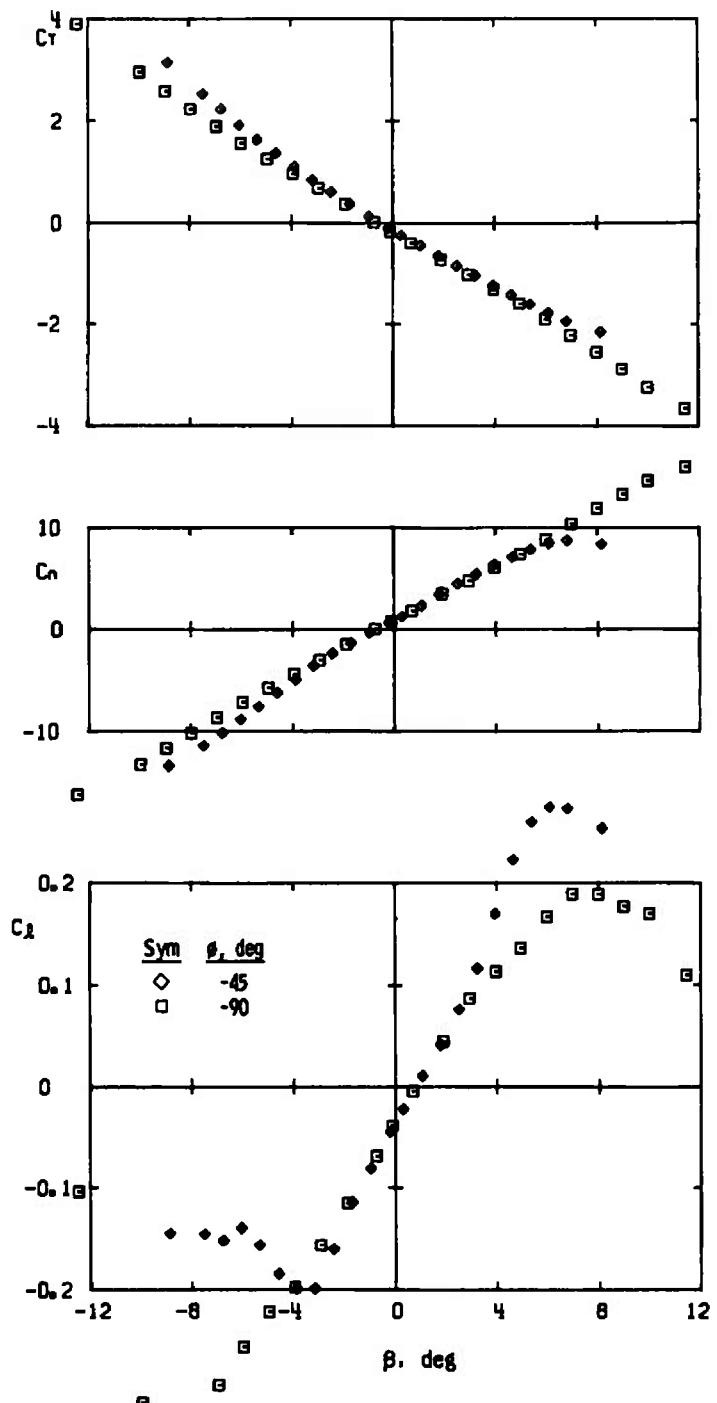
e. Concluded
Fig. I-4 Continued
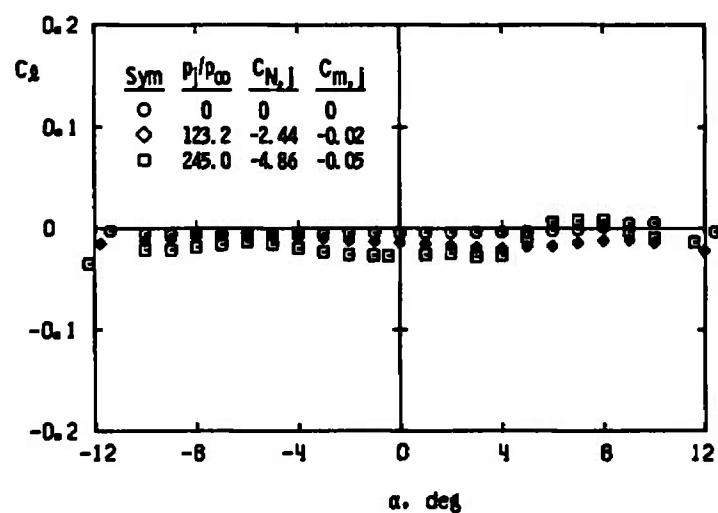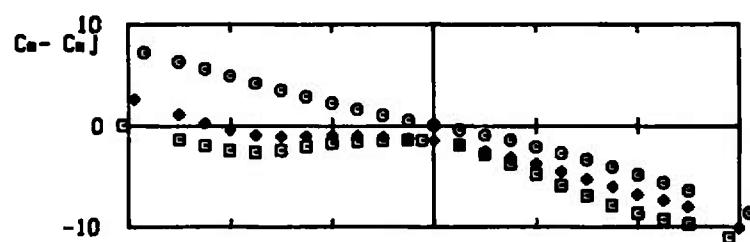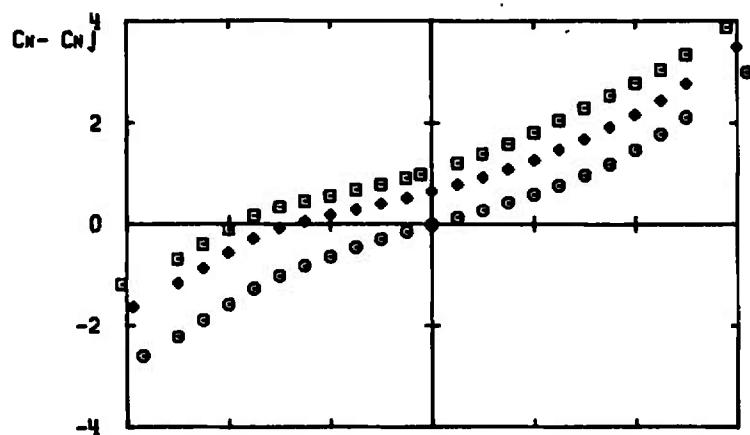
f. $\phi = 0$, $M_\infty = 3.0$, $Re_\ell = 12.5 \times 10^6$
Fig. I-4 Continued
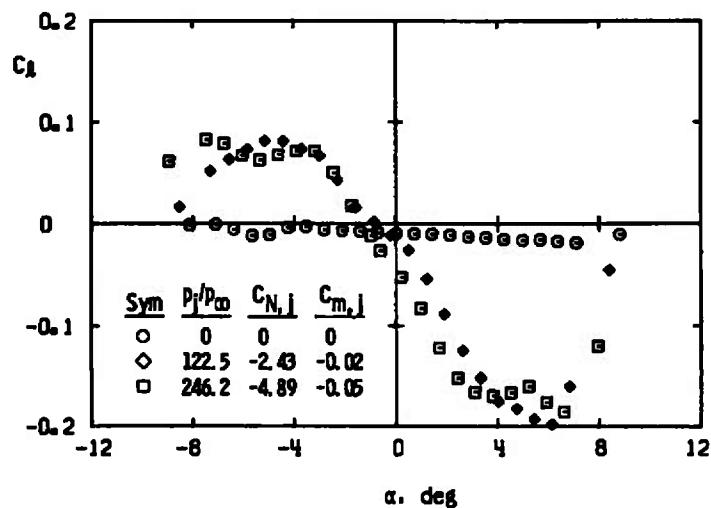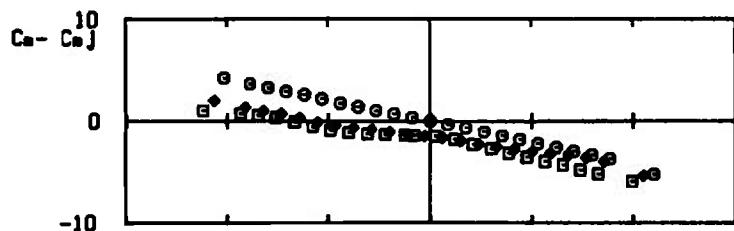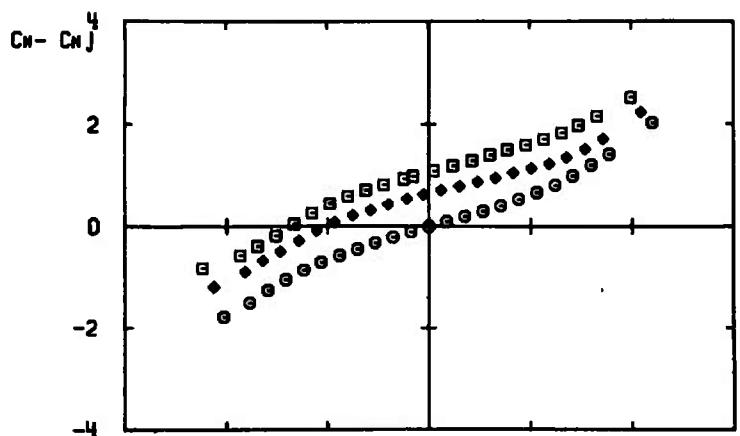
g. ϕ = -45 deg, M_∞ = 3.0, Re$_\varrho$ = 12.5 x 10^{6}
Fig. I-4 Continued
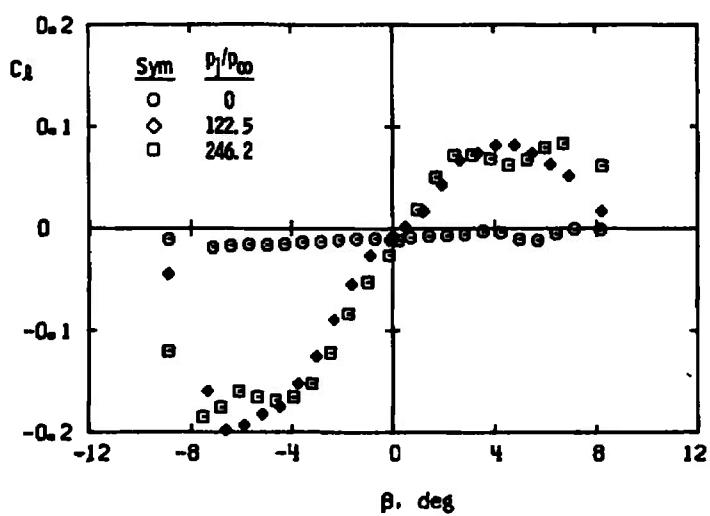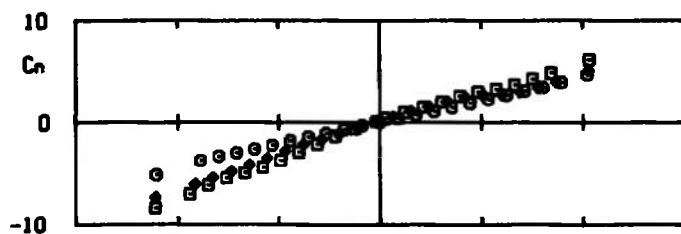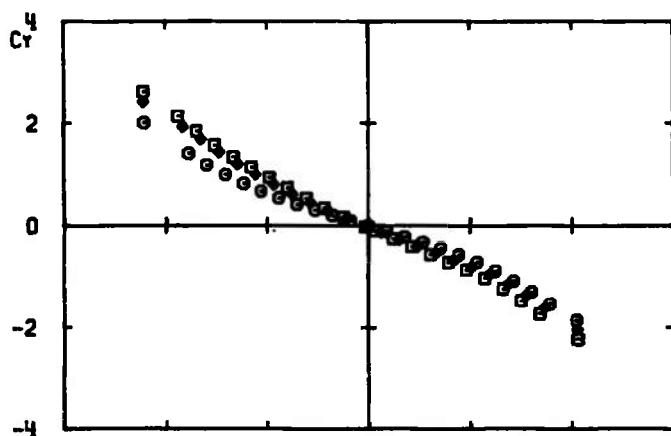
g. Concluded
Fig. I-4 Continued
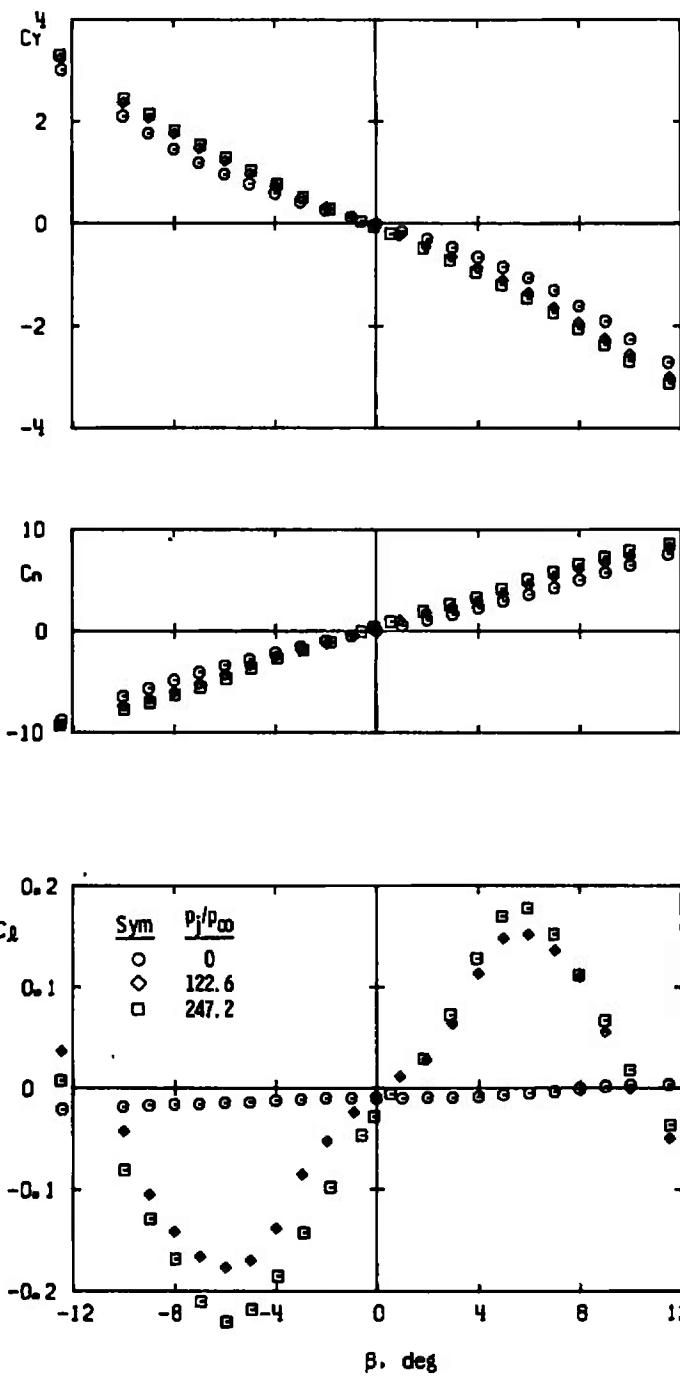
h. $\phi = -90$ deg, $M_\infty = 3.0$, $Re_\ell = 12.5 \times 10^6$
Fig. I-4 Concluded
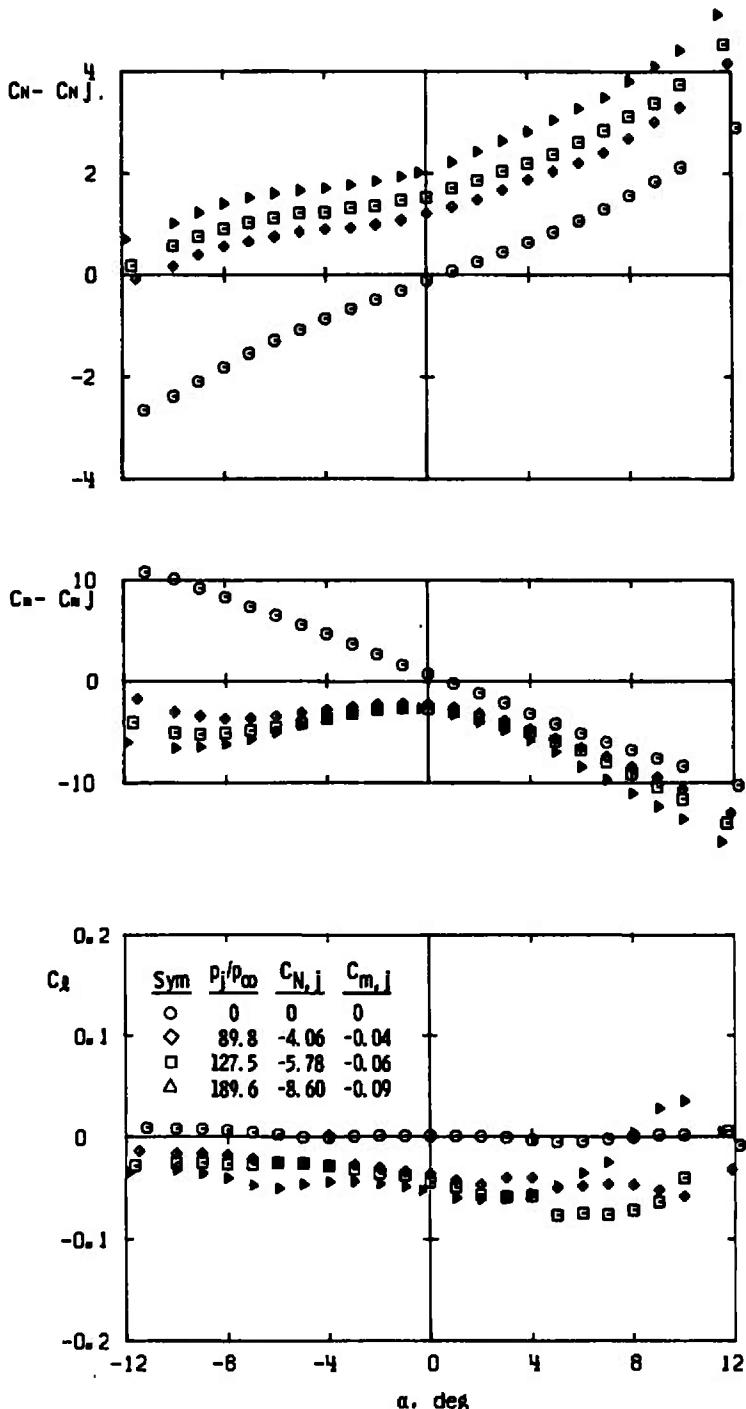
a. $\phi = 0$, $M_\infty = 2.0$, $Re_\ell = 5.1 \times 10^6$

Fig. I-5 Control Jets on the ATR Missile with the Nozzle Jets at $x_j/D = 0.0$ and Rolled 45 deg from the Missile Fins

Sym	p_j/p_∞	$C_{N,j}$	$C_{m,j}$
O	0	0	0
◇	90.0	-4.07	-0.04
□	126.4	-5.73	-0.06
△	189.7	-8.61	-0.09

b. ϕ = -45 deg, M_∞ = 2.0, Re_ℓ = 5.1 x 10^6

Fig. I-5 Continued

b. Concluded
Fig. I-5 Continued
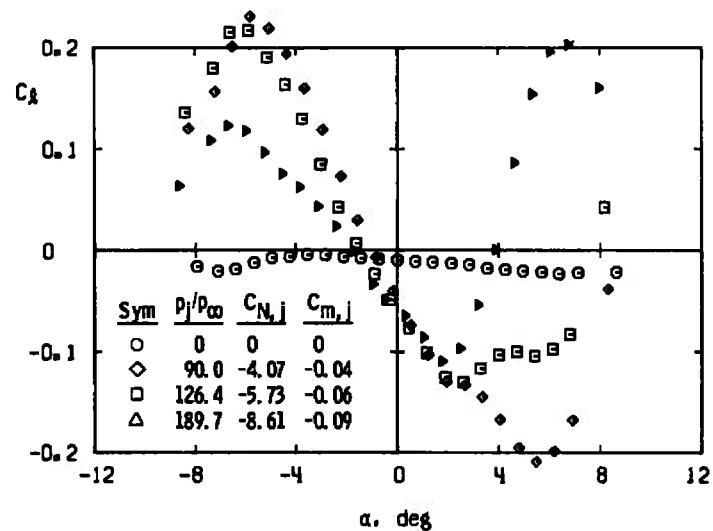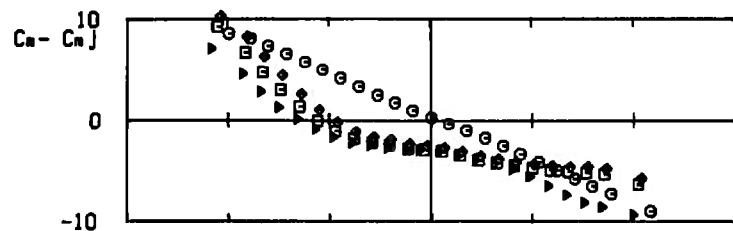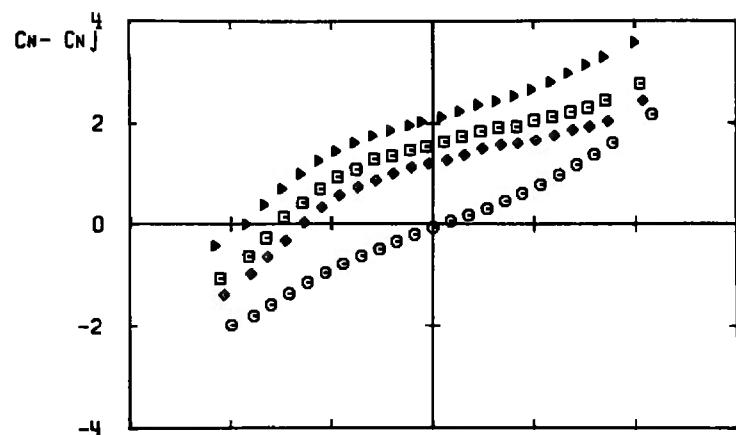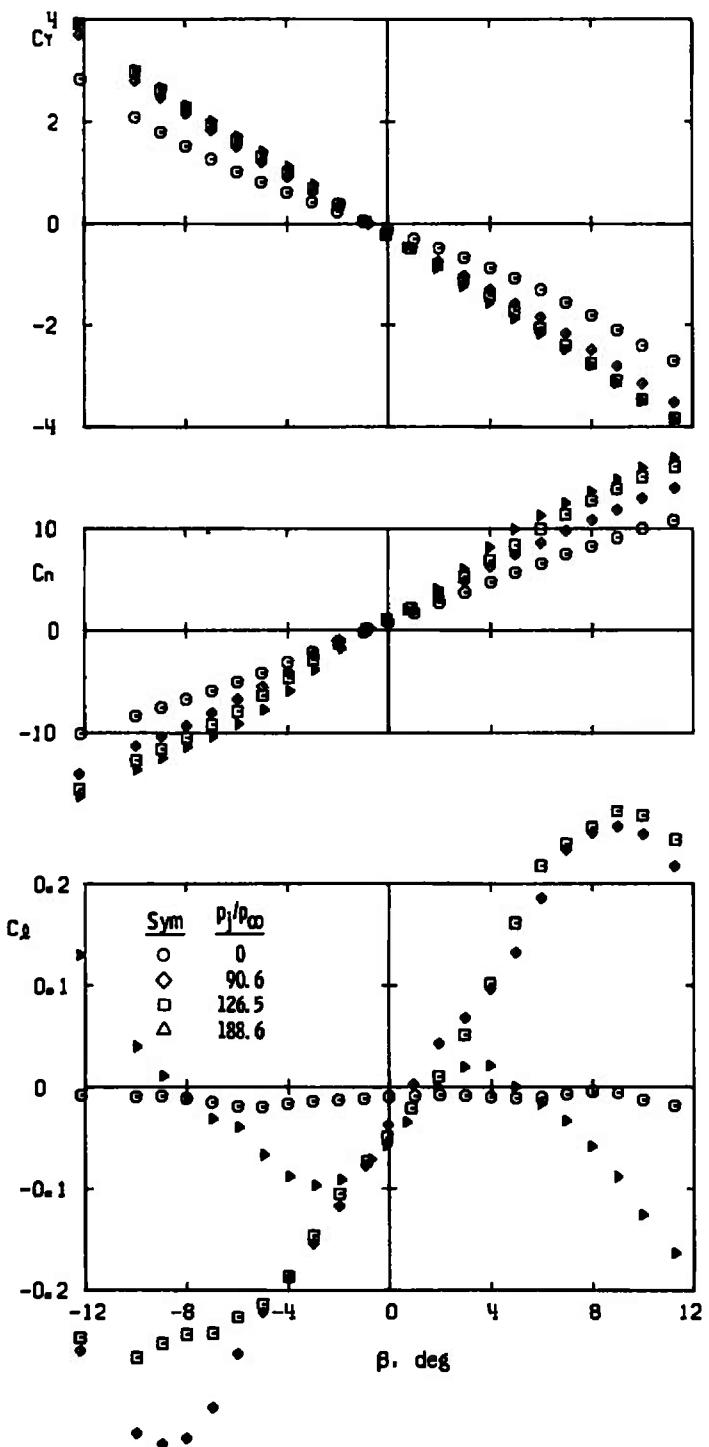
c. $\phi = -90$ deg, $M_\infty = 2.0$, $Re_\ell = 5.1 \times 10^6$
Fig. I-5 Continued
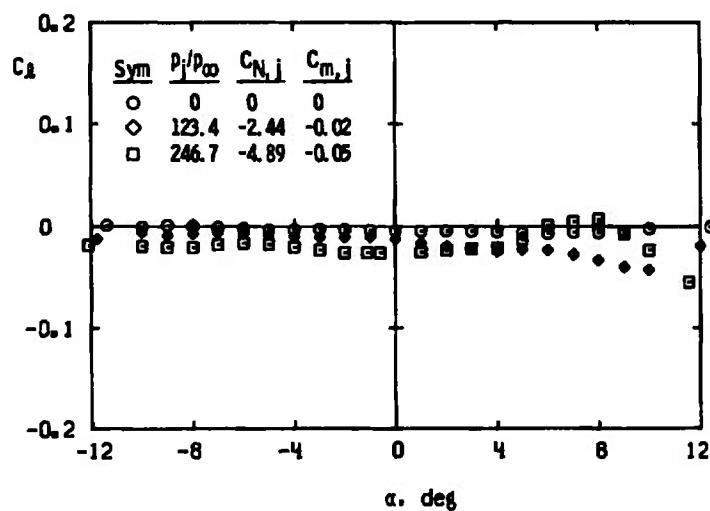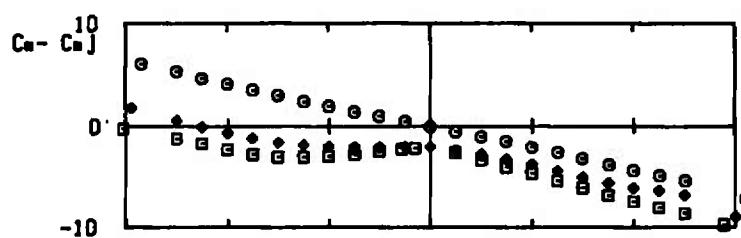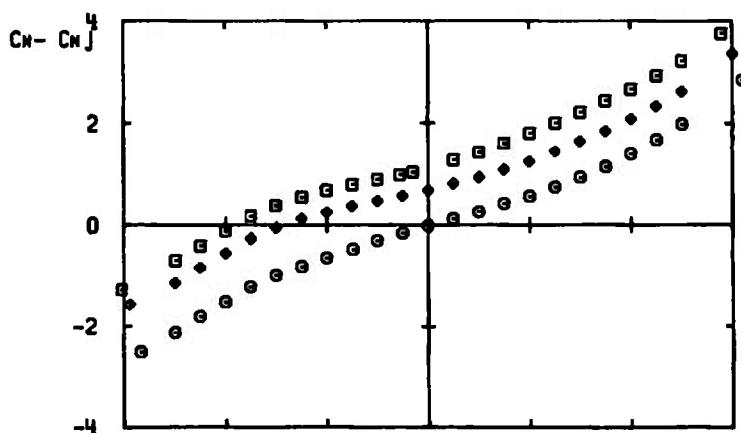
d. $\phi = 0$, $M_\infty = 3.0$, $Re_\ell = 12.5 \times 10^6$
Fig. I-5 Continued
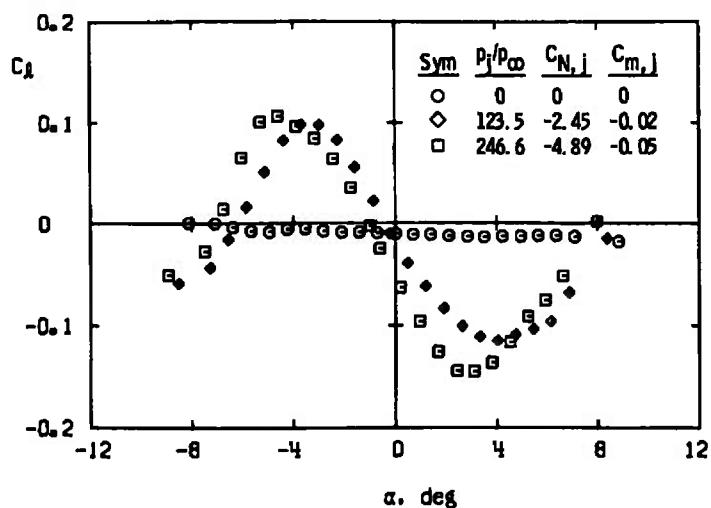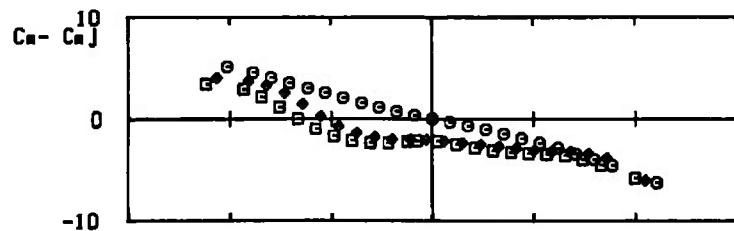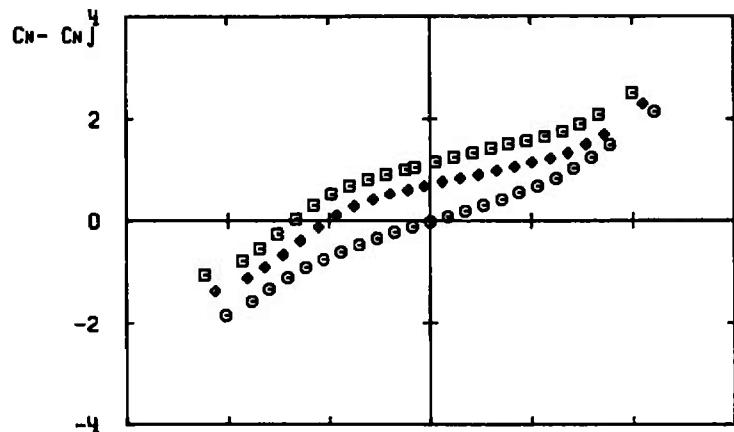
e. $\phi = -45$ deg, $M_\infty = 3.0$, $Re_\ell = 12.5 \times 10^6$
Fig. I-5 Continued
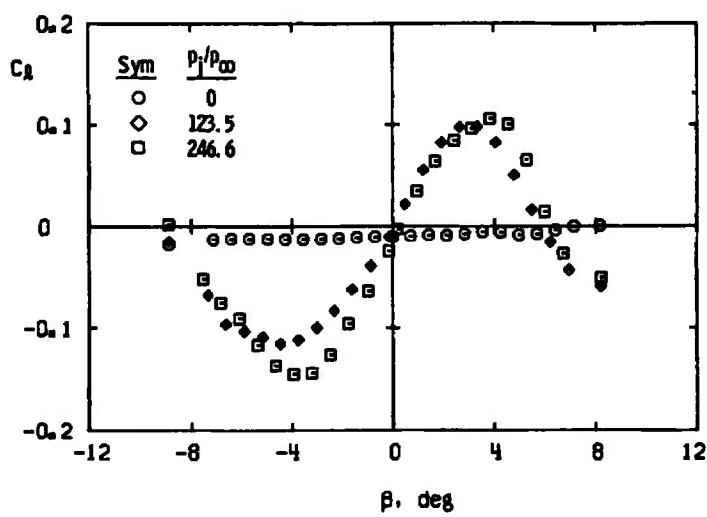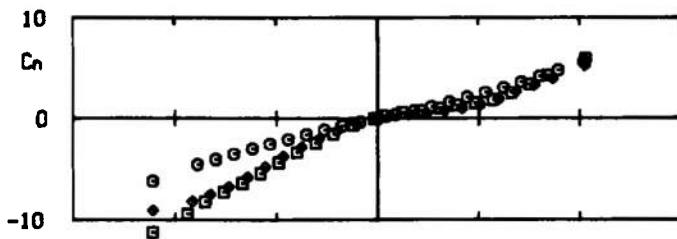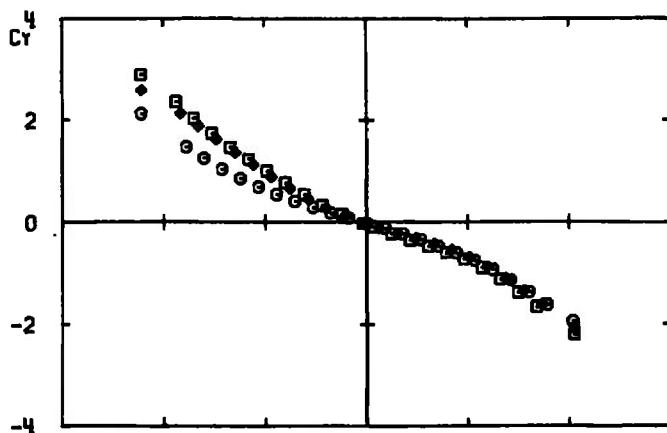
e. Concluded
Fig. I-5 Continued

98
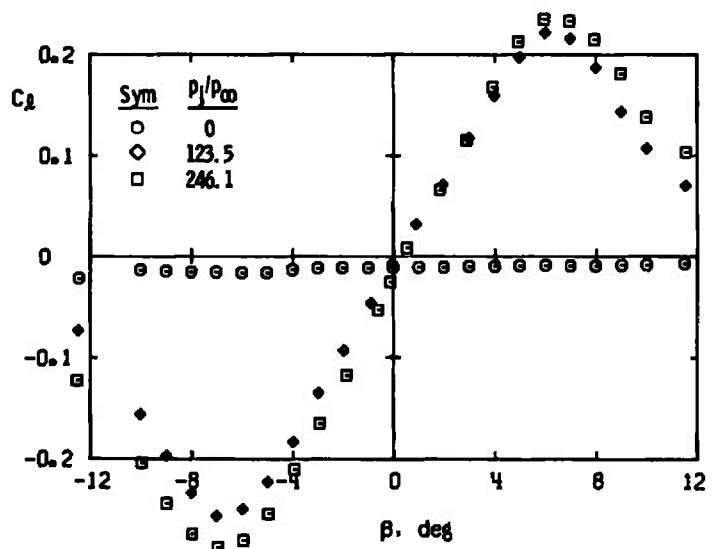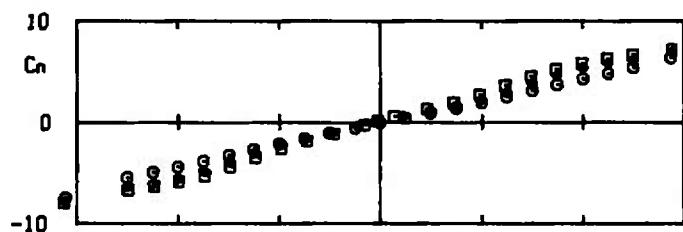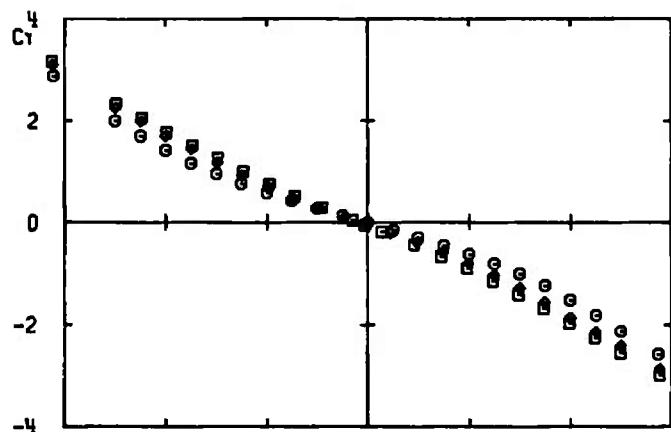
f. $\phi = -90$ deg, $M_\infty = 3.0$, $Re_\ell = 12.5 \times 10^6$
Fig. I-5 Concluded

99

APPENDIX II
TYPICAL SET OF SHADOWGRAPH PICTURES OF THE
FLOW-FIELD DISTURBANCE PRODUCED BY THE
RCS JET PLUMES

$\alpha = 0.1$ deg $\alpha = -0.3$ deg

$\alpha = -5.4$ deg $\alpha = -5.3$ deg

$\alpha = -10.3$ deg $\alpha = -10.7$ deg

a. $Re_\ell = 5.1 \times 10^6$,   b. $Re_\ell = 10.4 \times 10^6$,
    $p_j/p_\infty = 0.0$ $p_j/p_\infty = 0.0$
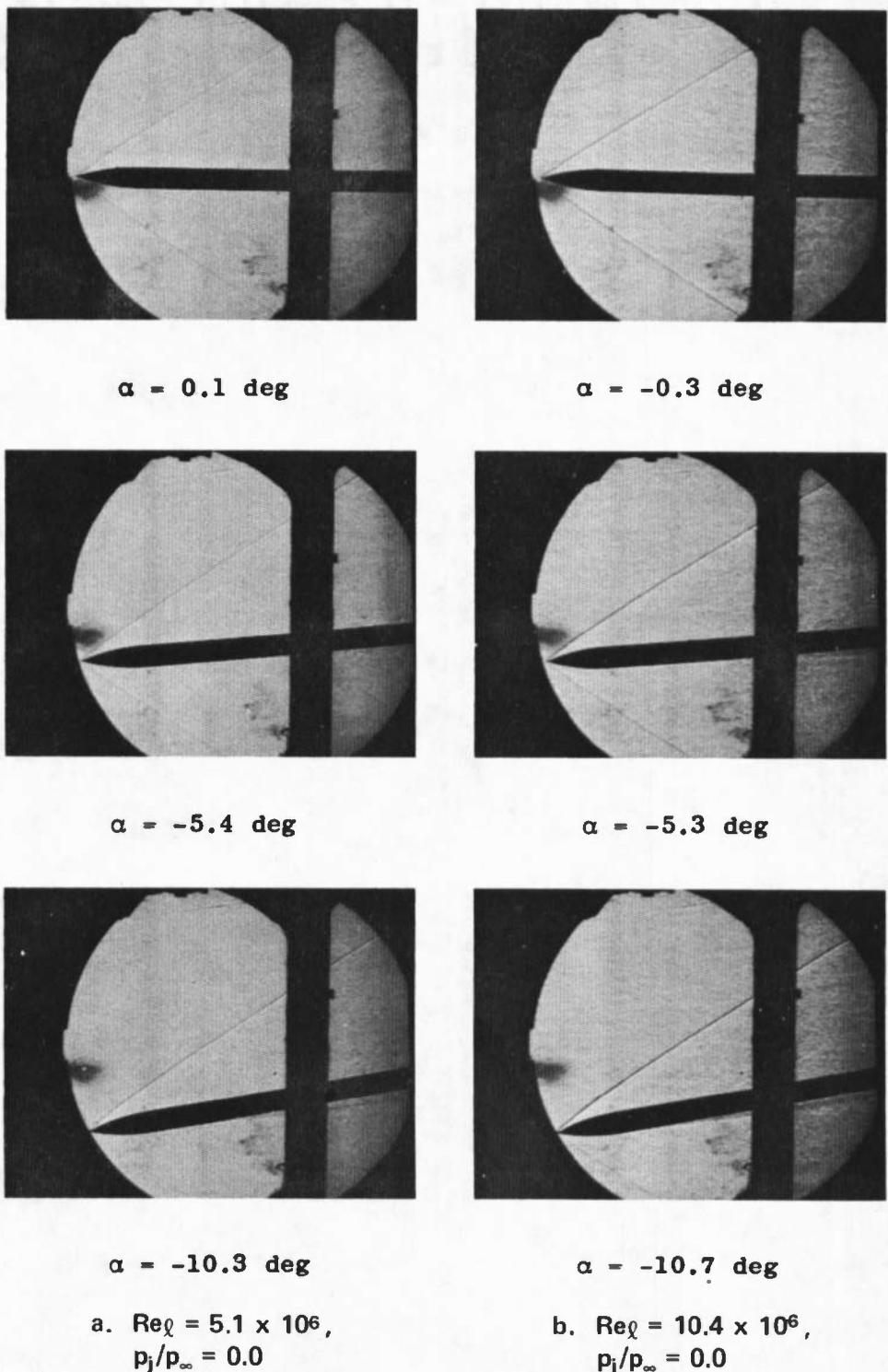
Fig. II-1 Flow Field Generated by the ATR Missile and by the Wake from
the RCS Located at $x_j/D = 4.37$ on the Missile, $M_\infty = 2.0$

103
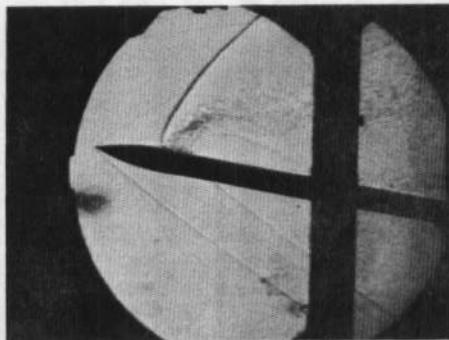
α = 9.3 deg
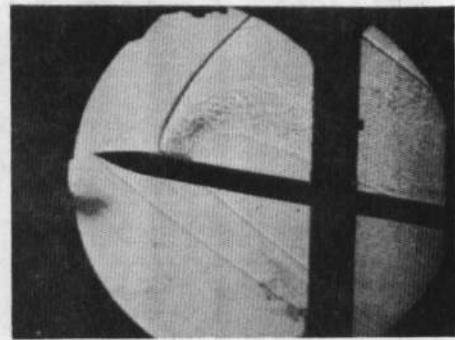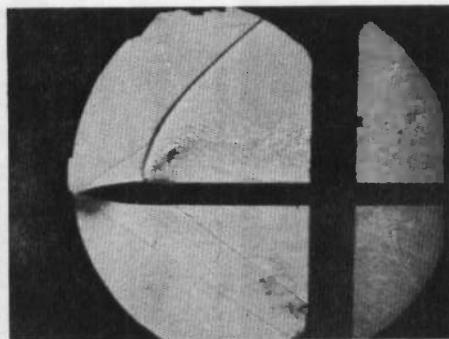
α = 9.0 deg

α = 0.7 deg
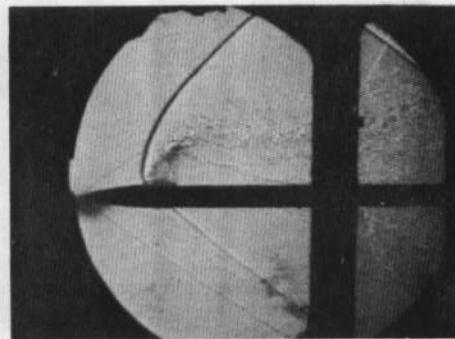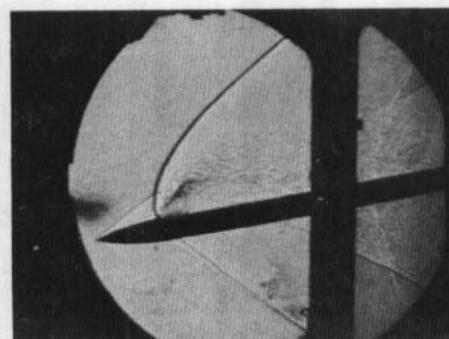
α = 1.0 deg

α = -11.0 deg
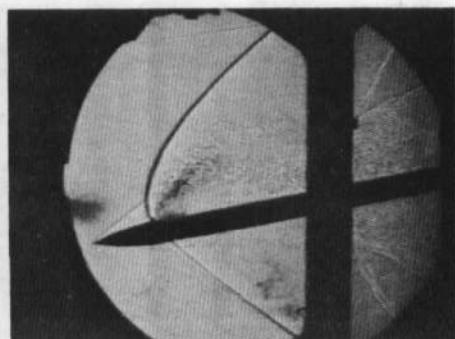
α = -11.3 deg

c. Re$_\ell$ = 5.1 x 10^6, ϕ = 0,
    p$_j$/p$_\infty$ = 127, C$_{N,j}$ = -5.75

d. Re$_\ell$ = 5.1 x 10^6, ϕ = 0,
    p$_j$/p$_\infty$ = 189, C$_{N,j}$ = -8.58

Fig. II-1 Continued
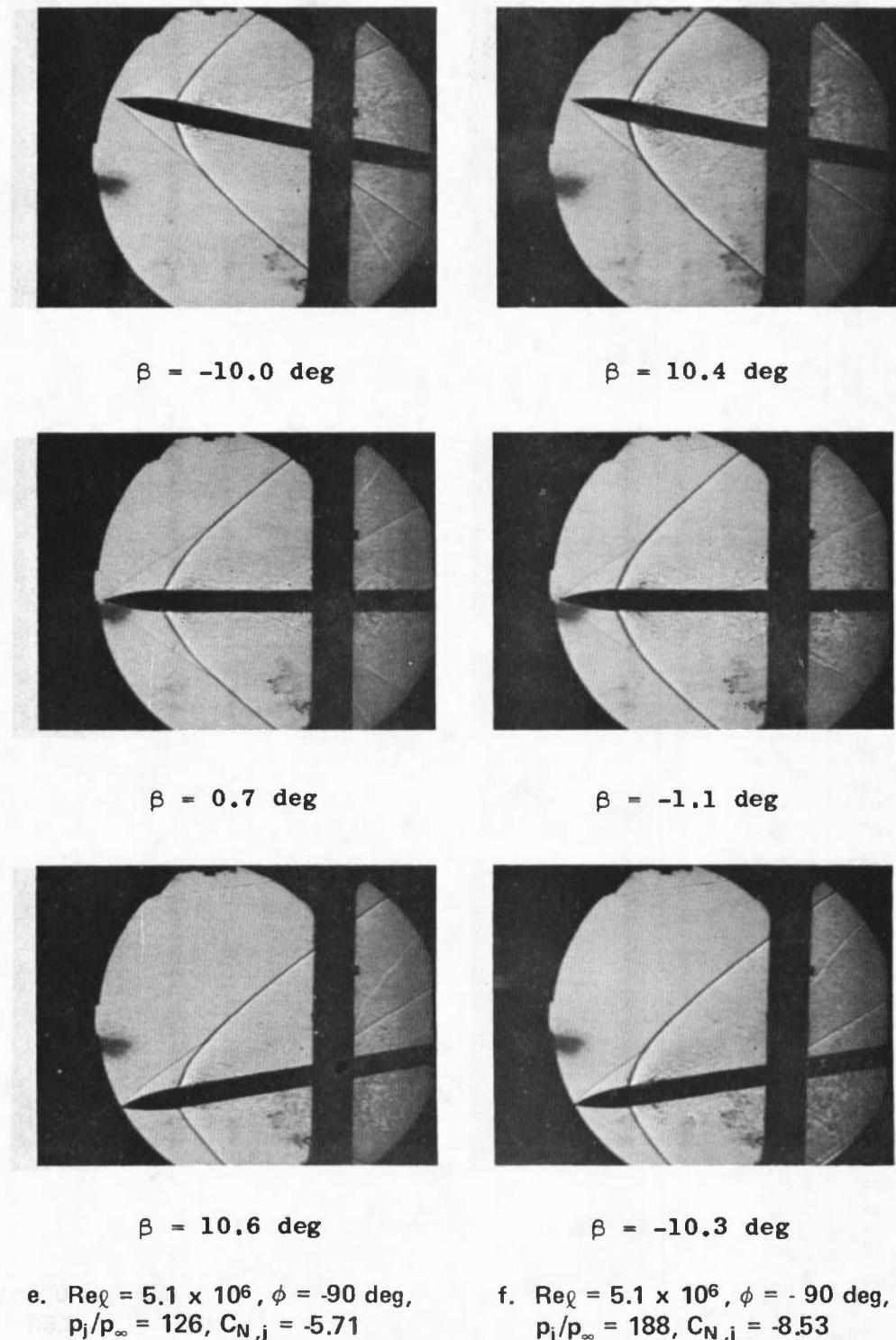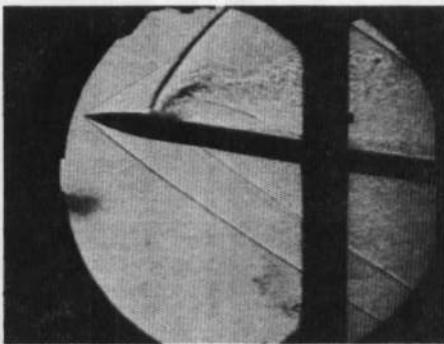
$\beta = -10.0$ deg

$\beta = 10.4$ deg

$\beta = 0.7$ deg

$\beta = -1.1$ deg

$\beta = 10.6$ deg

$\beta = -10.3$ deg

e. $Re_{\ell} = 5.1 \times 10^6$, $\phi = -90$ deg,
$p_j/p_{\infty} = 126$, $C_{N,j} = -5.71$

f. $Re_{\ell} = 5.1 \times 10^6$, $\phi = -90$ deg,
$p_j/p_{\infty} = 188$, $C_{N,j} = -8.53$

Fig. II-1 Continued

α = 10.5 deg

β = -10.6 deg

α = -1.0 deg

β = 1.1 deg

α = -10.8 deg

β = 10.6 deg

g. Re_ℓ = 10.4 x 10^6, ϕ = 0,
    p_j/p_∞ = 93, $C_{N,j}$ = -4.2
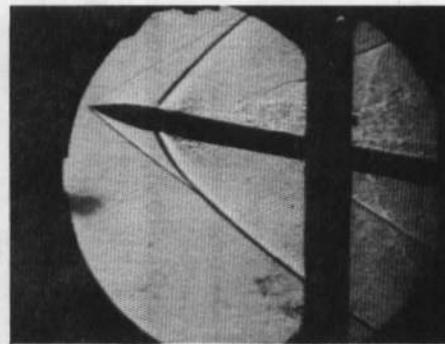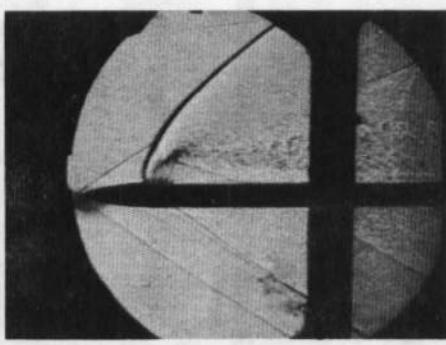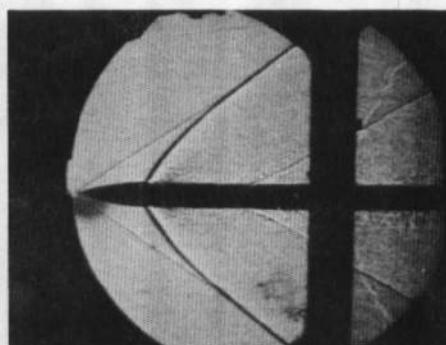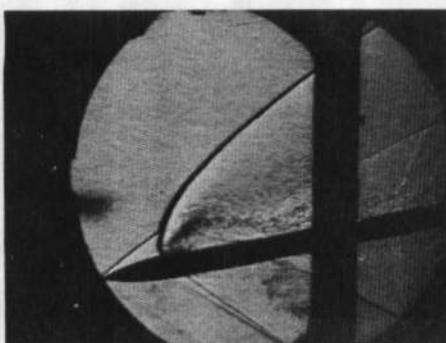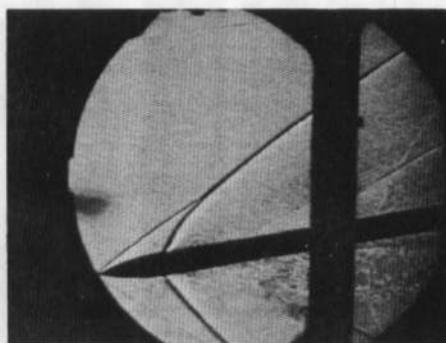
h. Re_ℓ = 10.4 x 10^6, ϕ = -90 deg,
    p_j/p_∞ = 94, $C_{N,j}$ = -4.2

Fig. II-1 Concluded
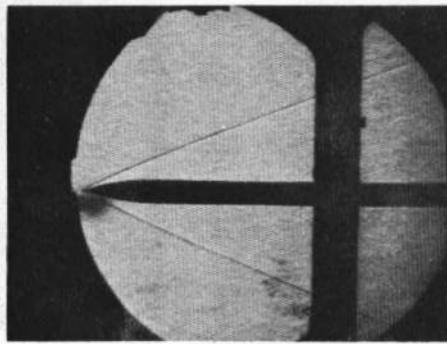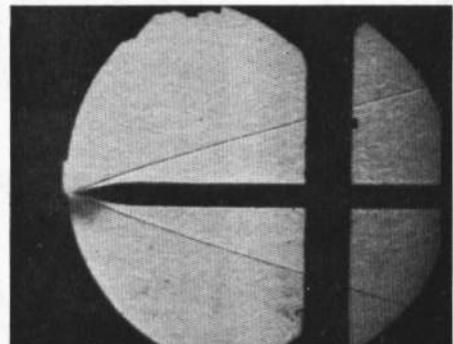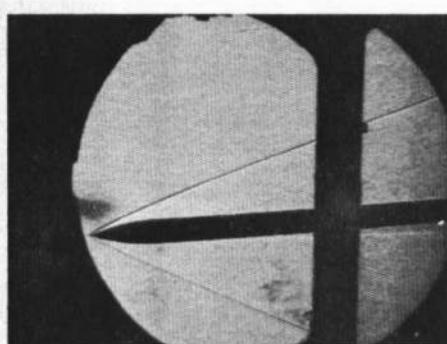
α = -0.4 deg

α = -0.4 deg

α = -5.1 deg
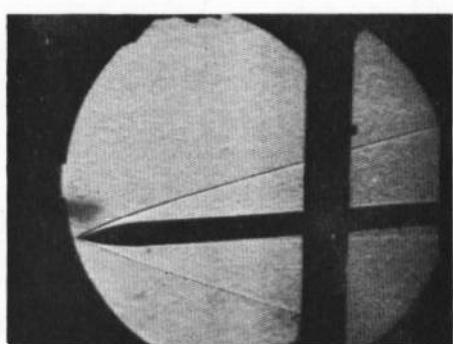
α = -5.4 deg
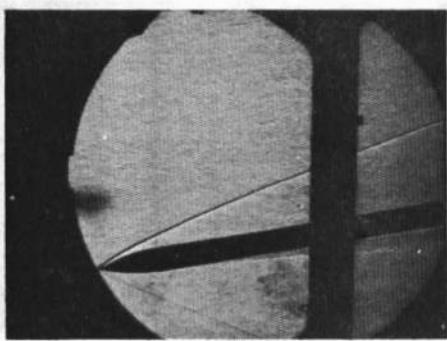
α = -10.6 deg
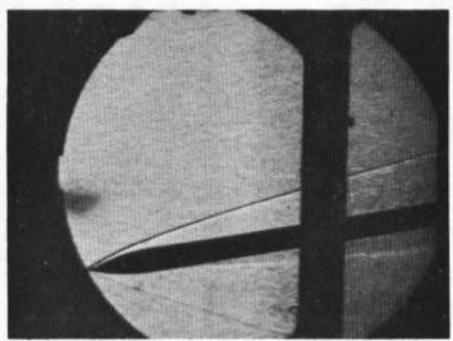
α = -10.4 deg

a. $M_\infty = 3.0$, $Re\ell = 12.5 \times 10^6$ b. $M_\infty = 4.0$, $Re\ell = 17.1 \times 10^6$

Fig. II-2 Flow Field Generated by the ATR Missile at Mach Numbers 3, 4, and 5 without the RCS ($p_j/p_\infty = 0$)
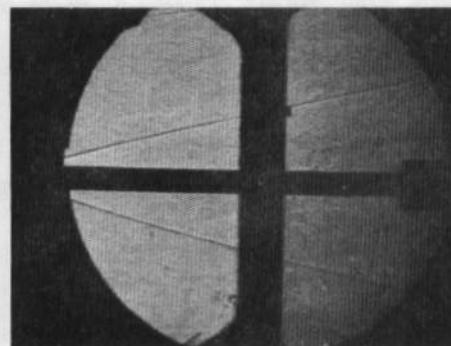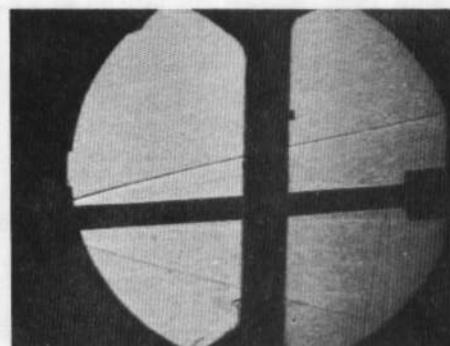
$\alpha = -0.3$ deg

$\alpha = -5.3$ deg
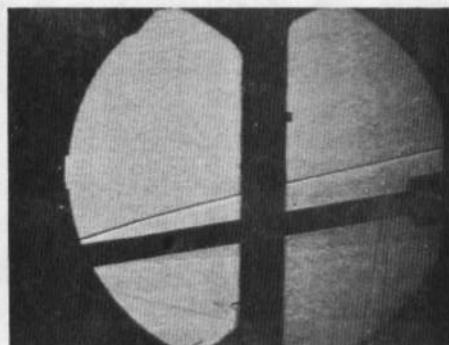
$\alpha = -10.3$ deg

c. $M_\infty = 5.0$, $Re\ell = 19.3 \times 10^6$
Fig. II-2 Concluded
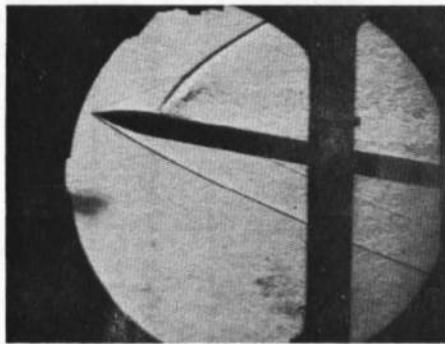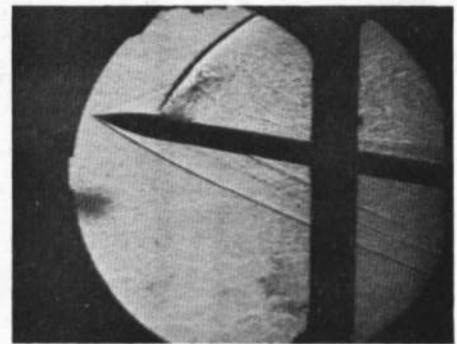
$\alpha = 9.7$ deg $\qquad\qquad$ $\alpha = 9.0$ deg
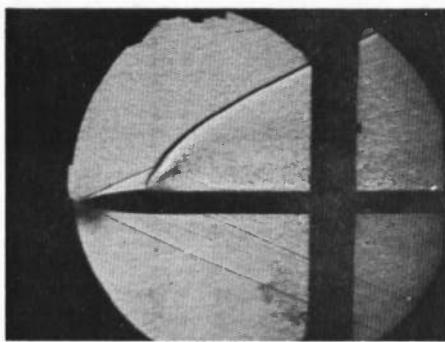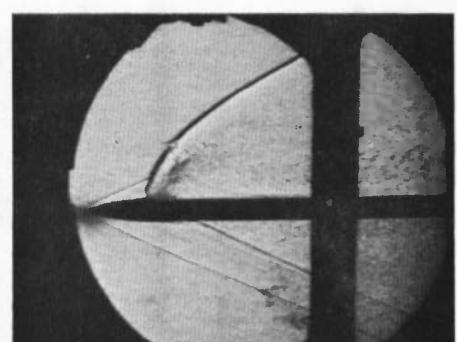
$\alpha = -0.9$ deg $\qquad\qquad$ $\alpha = -1.5$ deg
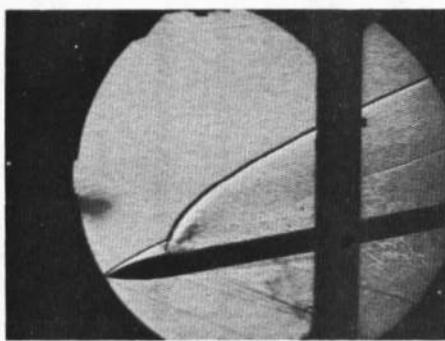
$\alpha = -11.2$ deg $\qquad\qquad$ $\alpha = -11.6$ deg
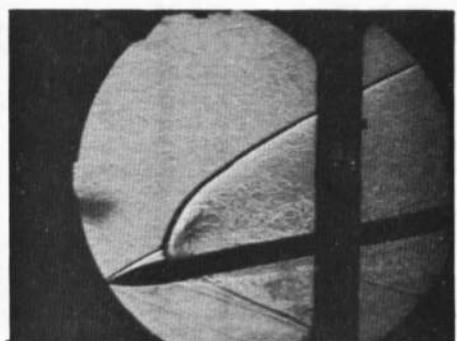
a. $\phi = 0$, $p_j/p_\infty = 124$, $\qquad$ b. $\phi = 0$, $p_j/p_\infty = 246$,
$\quad$ $C_{N,j} = -2.45$ $\qquad\qquad\qquad$ $C_{N,j} = -4.88$

Fig. II-3 Flow Field Generated by the Wake from the RCS Located at
$x_j/D = 4.37$ on the ATR Missile, $M_\infty = 3.0$, $Re_\ell = 12.5 \times 10^6$
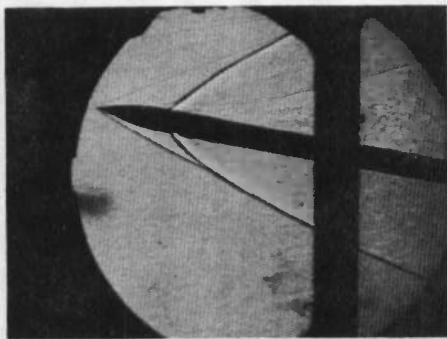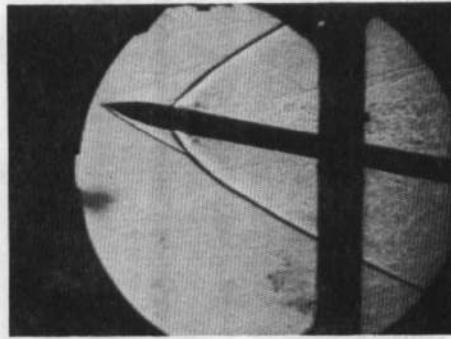
β = -10.5 deg

β = -10.5 deg
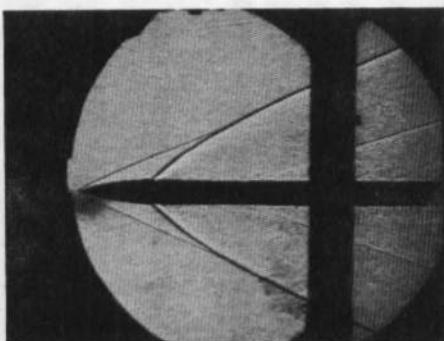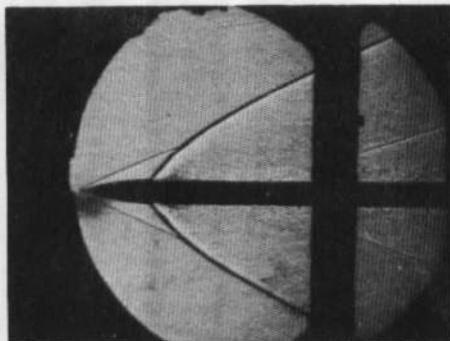
β = 0.7 deg

β = 1.2 deg
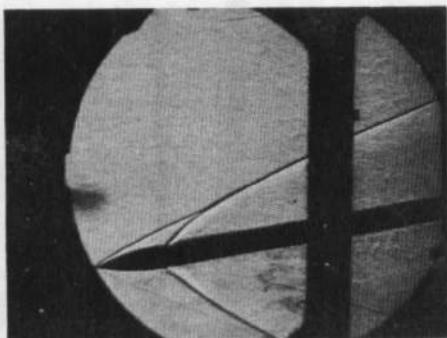
β = 10.7 deg
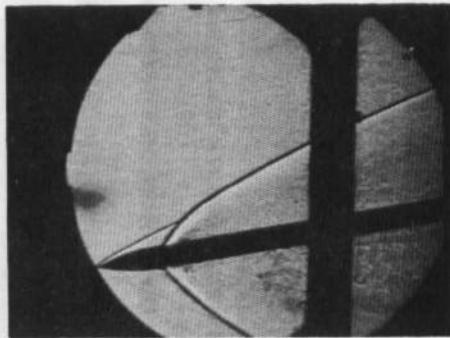
β = 10.9 deg

c. φ = -90 deg, p_j/p_∞ = 123,
    $C_{N,j}$ = -2.43

d. φ = -90 deg, p_j/p_∞ = 246,
    $C_{N,j}$ = -4.87

Fig. II-3 Concluded
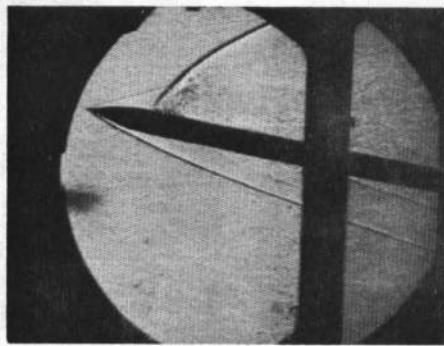
α = 9.5 deg
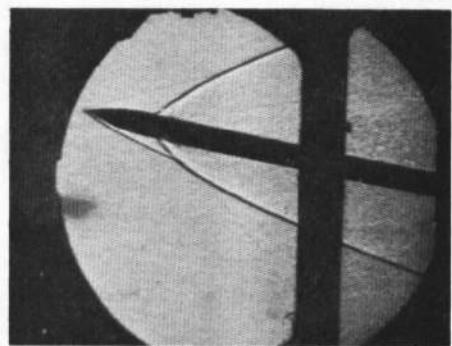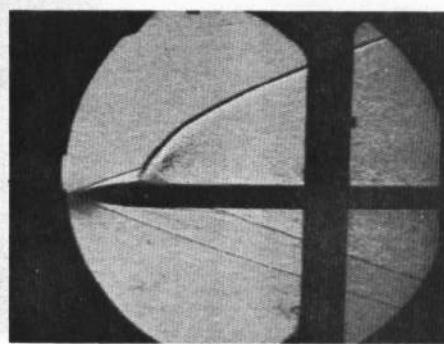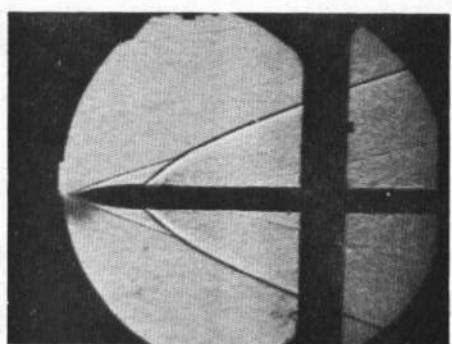
β = -10.4 deg
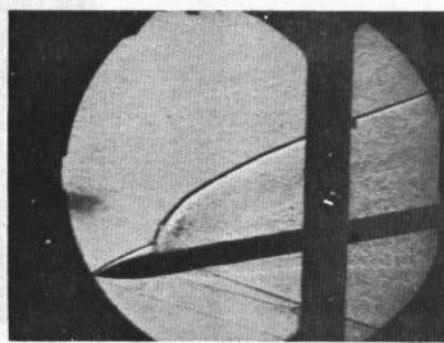
α = -1.1 deg

β = 0.8 deg

α = -11.1 deg
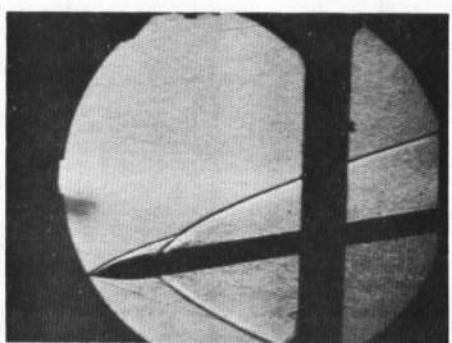
β = 10.4 deg

a. $\phi = 0$, $p_j/p_\infty = 265$,
$C_{N,j} = -2.93$

b. $\phi = -90$ deg, $p_j/p_\infty = 268$,
$C_{N,j} = -2.95$

Fig. II-4 Flow Field Generated by the Wake from the RCS Located at
$x_j/D = 4.37$ on the ATR Missile, $M_\infty = 4.0$, $Re_\ell = 17.1 \times 10^6$

111
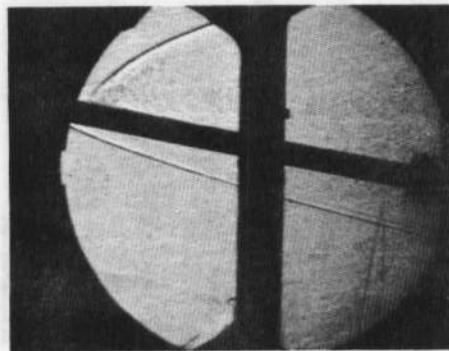
$\alpha = 9.7$ deg
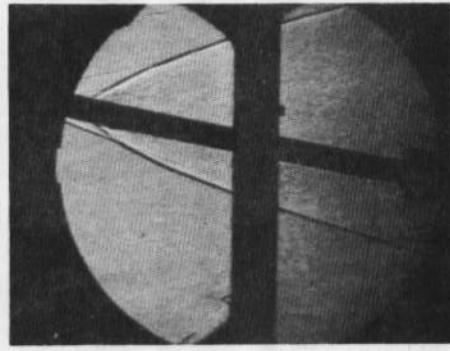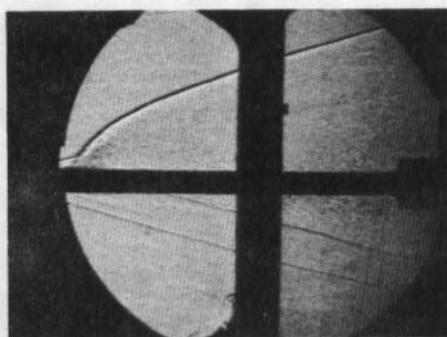
$\beta = -10.3$ deg

$\alpha = -0.8$ deg
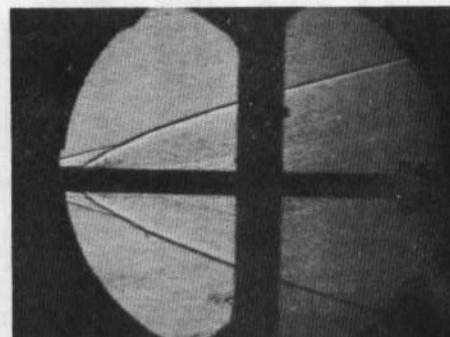
$\beta = 0.6$ deg
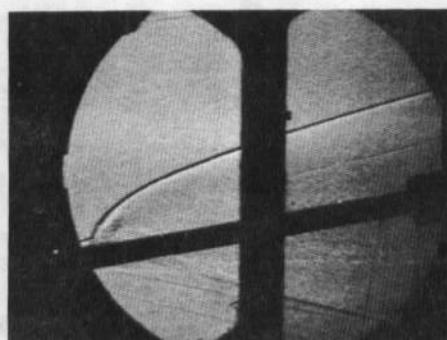
$\alpha = -10.8$ deg

$\beta = 10.3$ deg

a. $\phi = 0$, $p_j/p_\infty = 265$,
   $C_{N,j} = -1.88$
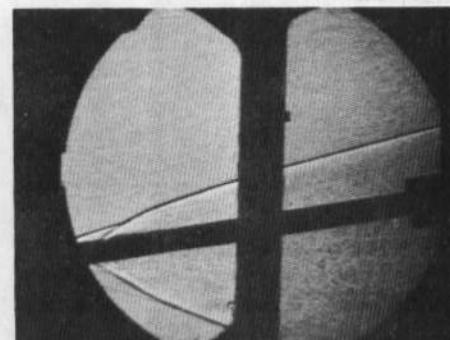
b. $\phi = -90$ deg, $p_j/p_\infty = 268$,
   $C_{N,j} = -1.90$

Fig. II-5 Flow Field Generated by the Wake from the RCS Located at
$x_j/D = 4.37$ on the ATR Missile, $M_\infty = 5.0$, $Re_\ell = 19.3 \times 10^6$

DOCUMENT CONTROL DATA - R & D

(Security classification of title, body of abstract and indexing annotation must be entered when the overall report is classified)

1 ORIGINATING ACTIVITY (Corporate author)	2a. REPORT SECURITY CLASSIFICATION
Arnold Engineering Development Center Arnold Air Force Station, Tennessee 37389	UNCLASSIFIED
	2b. GROUP N/A

3 REPORT TITLE

REACTION JET CONTROL EFFECTS ON THE AIR FORCE ADVANCED TACTICAL ROCKET AT MACH NUMBERS 2, 3, 4, AND 5

4 DESCRIPTIVE NOTES (Type of report and inclusive dates)

Final Report -- April 16 through 17, 1973

This document has been approved for public release
its distribution is unlimited. [handwritten notes]

5 AUTHOR(S) (First name, middle initial, last name)

W. T. Strike, Jr.

6 REPORT DATE	7a. TOTAL NO. OF PAGES	7b. NO OF REFS
September 1973	120	5

8a. CONTRACT OR GRANT NO	9a. ORIGINATOR'S REPORT NUMBER(S)
b. PROJECT NO	AEDC-TR-73-157 AFATL-TR-73-178
c. Program Element 63601F	9b. OTHER REPORT NO(S) (Any other numbers that may be assigned this report)
d. System 670D	ARO-VKF-TR-73-97

10. DISTRIBUTION STATEMENT Distribution limited to U. S. Government agencies only; this report contains information on test and evaluation of military hardware; September 1973; other requests for this document must be referred to Air Force Armament Laboratory (DLTI), Air Force Systems Command.

11. SUPPLEMENTARY NOTES	12. SPONSORING MILITARY ACTIVITY
Eglin AFB, FL 32542. Available in DDC.	AFATL/DLTI Eglin AFB, FL 32542

13. ABSTRACT This program is part of a study to provide the Advanced Tactical Rocket (ATR) under development by the Air Force Armament Laboratory with a jet reaction control system (RCS). This control system, consisting of four sets of six supersonic nozzle jets, will be used to make final corrections to the ATR trajectory. The wind tunnel study was conducted at Mach numbers 2, 3, 4, and 5 using a 4/7-scale model of the ATR with a set of six sonic nozzles to simulate, with air, the jet wake disturbance produced by the full-scale RCS. The tests were conducted with the RCS placed at two different axial positions along the model axis and at roll angles of 0 and -45 deg with respect to the vertical tail fins. The data consisted of 5-component force (excluding axial force) and moment data. The model angle of attack was varied from -12 to 12 deg, and model roll angle was varied from 0 to -90 deg. The disturbance generated by the RCS simulation produced significant rolling moments when the model was in a combined pitch and roll attitude. Also, the slope of the aerodynamic coefficients with angle of attack varied depending on the RCS jet conditions and model roll position.

Distribution limited to U. S. Government agencies only; this report contains information on test and evaluation of military hardware; September 1973; other requests for this document must be referred to Air Force Armament Laboratory (DLTI), Air Force Systems Command, Eglin AFB, FL 32542.

DD FORM 1473 1 NOV 65

14. KEY WORDS	LINK A		LINK B		LINK C	
	ROLE	WT	ROLE	WT	ROLE	WT
missiles						
aircraft rockets						
aerodynamic characteristics						
supersonic flow						
control jets						

AFSC
Arnold AFS Tenn